THE ASTROPHYSICAL JOURNAL

AN INTERNATIONAL REVIEW OF SPECTROSCOPY AND ASTRONOMICAL PHYSICS

VOLUME 100 SEPTEMBER 1944 NUMBER 2

ON THE RADIATIVE EQUILIBRIUM OF A STELLAR ATMOSPHERE. III

S. CHANDRASEKHAR
Yerkes Observatory

Received May 31, 1944

ABSTRACT

In this paper the method described in an earlier paper (*Ap. J.*, **100**, 76, 1944) is applied to solving the equation of transfer

$$\mu \frac{dI}{d\tau} = I(\tau, \mu) - \tfrac{3}{16}\left[(3-\mu^2)\int_{-1}^{+1} I(\tau, \mu)d\mu + (3\mu^2-1)\int_{-1}^{+1} I(\tau, \mu)\mu^2 d\mu\right],$$

which incorporates Rayleigh's law of scattering. The general solution in the nth approximation is explicitly worked out, and the numerical forms of the first four approximations found.

1. *Introduction.*—In an earlier paper[1] we have shown how, basing on an idea originally due to G. Wick, it is possible to solve all the standard problems of radiative transfer in the theory of stellar atmospheres by a systematic and rapid method of approximation. However, the applications of the method are not limited to the standard problems considered. The field of application is much wider; and, as an illustration of the further possibilities of the method, we shall consider in this paper a typical problem in the theory of radiative transfer which involves a "phase function," i.e., a function which describes the anisotropy of the scattered radiation. More specifically we shall consider the case of Rayleigh's law of scattering, according to which the probability of a pencil of radiation being scattered into a direction inclined at an angle Θ to the incident direction and confined to an element of solid angle $d\omega'$ is

$$\tfrac{3}{4}(1+\cos^2\Theta)\frac{d\omega'}{4\pi}. \qquad (1)$$

Apart from the fact that the consideration of this problem will make a first advance in the systematic solving of radiative problems involving phase functions, it has also an independent interest for astrophysical theory. For example, it is now being generally recognized that the Thomson scattering of free electrons is a principal, if not a dominant, source of continuous opacity in the early-type stars.[2] And, as is well known, the Thomson

[1] *Ap. J.*, **100**, 76, 1944. This paper will be referred to as "II," while the still earlier paper, *Ap. J.*, **99**, 180, 1944, will be referred to as "I."

[2] V. A. Ambarzumian, *Pub. Astr. Obs. U. Leningrad*, No. 22, Issue 4, 13, 1938; A. Unsöld, *Zs. f. Ap.*, **21**, 229, 1942; M. Rudkjøbing, *Zs. f. Ap.*, **21**, 254, 1942.

scattering takes place according to the law (1). Again, the resonance line scattering by atoms (in the absence of collision broadening) also follows Rayleigh's law.[3] Thus, Rayleigh's law of scattering appears in a fundamental way in several problems in the theory of stellar atmospheres. We shall, accordingly, devote this paper to the solving of the equation of transfer which incorporates this law of scattering.

2. *The equation of transfer with Rayleigh's law of scattering.*—Considering as usual the case of a plane-stratified atmosphere, we have quite generally (for the notation regarding the angular co-ordinates see Fig. 1)

$$\cos\vartheta\,\frac{dI}{d\tau} = I(\tau,\vartheta) - \frac{1}{4\pi}\int_0^{\pi}\int_0^{2\pi} I(\tau,\vartheta')\,\gamma(\vartheta',\varphi';\vartheta)\sin\vartheta'd\vartheta'd\varphi', \qquad (2)$$

where $\gamma(\vartheta',\varphi';\vartheta)/4\pi$ denotes the phase function governing the probability of the scattering of a pencil of radiation in the direction (ϑ',φ') into the direction $(\vartheta,0)$. (Note that in writing equation (2) we have utilized the symmetry of the problem about the axis $\vartheta = 0$). For Rayleigh's law of scattering equation (2) takes the explicit form

$$\left.\begin{aligned}\cos\vartheta\,\frac{dI}{d\tau} = I(\tau,\vartheta) - \frac{3}{16\pi}\int_0^{\pi}\int_0^{2\pi} I(\tau,\vartheta') \\ \times\,[1+(\cos\vartheta\cos\vartheta'+\sin\vartheta\sin\vartheta'\cos\varphi')^2]\sin\vartheta'd\vartheta'd\varphi'\,.\end{aligned}\right\} \qquad (3)$$

The integration over φ' is readily performed, and we are left with

$$\cos\vartheta\,\frac{dI}{d\tau} = I(\tau,\vartheta) - \frac{3}{8}\int_0^{\pi} I(\tau,\vartheta')\,[1+\cos^2\vartheta\cos^2\vartheta'+\tfrac{1}{2}\sin^2\vartheta\sin^2\vartheta']\sin\vartheta'd\vartheta'. \qquad (4)$$

Writing μ for $\cos\vartheta$, and after some minor rearranging of the terms, equation (4) takes the form

$$\mu\,\frac{dI}{d\tau} = I - \frac{3}{16}\left[(3-\mu^2)\int_{-1}^{+1} I(\tau,\mu)\,d\mu + (3\mu^2-1)\int_{-1}^{+1} I(\tau,\mu)\,\mu^2 d\mu\right]. \qquad (5)$$

This is the equation to be solved.

In the theory of stellar atmospheres it is customary to introduce the quantities J and K defined by

$$J(\tau) = \frac{1}{2}\int_{-1}^{+1} I(\tau,\mu)\,d\mu \qquad \text{and} \qquad K(\tau) = \frac{1}{2}\int_{-1}^{+1} I(\tau,\mu)\,\mu^2 d\mu\,. \qquad (6)$$

In terms of these quantities the equation of transfer (5) can be written as

$$\mu\,\frac{dI}{d\tau} = I - \tfrac{3}{8}\left[(3-\mu^2)J + (3\mu^2-1)K\right], \qquad (7)$$

which shows that in the usual Eddington-Milne approximation $K = \frac{1}{3}J$ our present problem is not different from the standard one considered in I and II.

3. *The general solution of the equation of transfer* (5) *in the* n*th approximation.*—As in II, we replace the integrals on the right-hand side of equation (5) by a sum according to Gauss's formula for numerical quadratures. This enables the replacement of the integro-differential equation (5) by a system of linear equations which in the nth approximation is (cf., II, eq. [6])

$$\mu_i\,\frac{dI_i}{d\tau} = I_i - \tfrac{3}{16}\left[(3-\mu_i^2)\Sigma a_j I_j + (3\mu_i^2-1)\Sigma a_j\mu_j^2 I_j\right] \qquad (i = \pm 1, \ldots, \pm n), \qquad (8)$$

[3] Cf. H. Zanstra, *M.N.*, **101**, 250, 273, 1942.

where, as in II, we have used I_j to denote $I(\tau, \mu_j)$. Further, in equation (8) the μ_j's are the zeros of the Legendre polynomial of order $2n$ and the a_j's are the appropriate Gaussian weights.

An alternative form of equation (8) which we shall find more convenient is

$$\mu_i \frac{dI_i}{d\tau} = I_i - \tfrac{3}{16}\left[\Sigma a_j (3-\mu_j^2)\, I_j + \mu_i^2 \Sigma a_j (3\mu_j^2 - 1)\, I_j\right] \qquad (i = \pm 1, \ldots, \pm n). \quad (9)$$

We shall now find the different linearly independent solutions of the system (9) and later, by combining these, obtain the general solution.

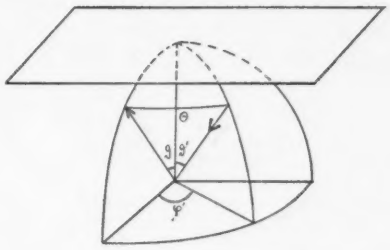

FIG. 1

First we seek a solution of (9) of the form

$$I_i = g_i e^{-k\tau} \qquad (i = \pm 1, \ldots, \pm n), \quad (10)$$

where the g_i's and k are constants, for the present unspecified. Substituting this form for I_i in equation (9), we obtain

$$(1 + \mu_i k)\, g_i = \tfrac{3}{16}\left[\Sigma a_j (3-\mu_j^2)\, g_j + \mu_i^2 \Sigma a_j (3\mu_j^2 - 1)\, g_j\right], \quad (11)$$

which implies that g_i must be expressible in the form

$$g_i = \frac{\alpha + \beta\mu_i^2}{1 + \mu_i k} \qquad (i = \pm 1, \ldots, \pm n), \quad (12)$$

where α and β are certain constants independent of i. Inserting the solution (12) back into equation (11), we find

$$\alpha + \beta\mu_i^2 = \tfrac{3}{16}\left[\Sigma \frac{a_j (3-\mu_j^2)\,(\alpha + \beta\mu_j^2)}{1 + \mu_j k} + \mu_i^2 \Sigma \frac{a_j (3\mu_j^2 - 1)\,(\alpha + \beta\mu_j^2)}{1 + \mu_j k}\right]. \quad (13)$$

Since this equation must be valid for all i's, we must require that

$$\alpha = \tfrac{3}{16} \Sigma \frac{a_j (3-\mu_j^2)\,(\alpha + \beta\mu_j^2)}{1 + \mu_j k} \quad (14)$$

and

$$\beta = \tfrac{3}{16} \Sigma \frac{a_j (3\mu_j^2 - 1)\,(\alpha + \beta\mu_j^2)}{1 + \mu_j k}. \quad (15)$$

Remembering that

$$a_j = a_{-j} \quad \text{and} \quad \mu_{-j} = -\mu_j \quad (16)$$

we can re-write equations (14) and (15) alternatively in the forms

$$\alpha = \tfrac{3}{8}\sum_{j=1}^{n}\frac{a_j(3-\mu_j^2)\ (\alpha+\beta\mu_j^2)}{1-\mu_j^2k^2} \tag{17}$$

and

$$\beta = \tfrac{3}{8}\sum_{j=1}^{n}\frac{a_j(3\mu_j^2-1)\ (\alpha+\beta\mu_j^2)}{1-\mu_j^2k^2}\,. \tag{18}$$

The constants α and β are thus seen to satisfy a system of homogenous linear equations. The determinant of the system must therefore vanish; and this leads, as we shall presently see, to an equation for k.

First we observe that equations (17) and (18) can be simplified considerably by writing

$$D = \sum_{j=1}^{n}\frac{a_j}{1-\mu_j^2k^2} \tag{19}$$

and expressing the two other series

$$\sum_{j=1}^{n}\frac{a_j\mu_j^2}{1-\mu_j^2k^2} \quad \text{and} \quad \sum_{j=1}^{n}\frac{a_j\mu_j^4}{1-\mu_j^2k^2} \tag{20}$$

in terms of D. We have

$$\left.\begin{aligned}\sum_{j=1}^{n}\frac{a_j\mu_j^2}{1-\mu_j^2k^2} &= \frac{1}{k^2}\sum_{j=1}^{n}a_j\left(\frac{1}{1-\mu_j^2k^2}-1\right)\\ &= \frac{1}{k^2}(D-1)\,.\end{aligned}\right\} \tag{21}$$

Similarly,

$$\left.\begin{aligned}\sum_{j=1}^{n}\frac{a_j\mu_j^4}{1-\mu_j^2k^2} &= \frac{1}{k^2}\sum_{j=1}^{n}a_j\mu_j^2\left(\frac{1}{1-\mu_j^2k^2}-1\right)\\ &= \frac{1}{k^4}(D-1)-\frac{1}{3k^2}.\end{aligned}\right\} \tag{22}$$

Using the foregoing relations, it is verified that equations (17) and (18) become

$$\tfrac{8}{3}\alpha = \alpha\left\{3D-\frac{1}{k^2}(D-1)\right\}+\beta\left\{\frac{1}{k^2}(3D-\tfrac{8}{3})-\frac{1}{k^4}(D-1)\right\} \tag{23}$$

and

$$\tfrac{8}{3}\beta = \alpha\left\{-D+\frac{3}{k^2}(D-1)\right\}+\beta\left\{-\frac{D}{k^2}+\frac{3}{k^4}(D-1)\right\}. \tag{24}$$

These equations can be further reduced to the forms

$$\alpha\left\{(9D-8)-\frac{3}{k^2}(D-1)\right\}+\beta\left\{\frac{1}{k^2}(9D-8)-\frac{3}{k^4}(D-1)\right\}=0 \tag{25}$$

and

$$\alpha\left\{-3D+\frac{9}{k^2}(D-1)\right\}+\beta\left\{-8-3\frac{D}{k^2}+\frac{9}{k^4}(D-1)\right\}=0\,. \tag{26}$$

Hence,

$$\left.\begin{aligned}\left\{(9D-8)-\frac{3}{k^2}(D-1)\right\}\left\{-8-3\frac{D}{k^2}+\frac{9}{k^4}(D-1)\right\}\\ +\left\{\frac{1}{k^2}(9D-8)-\frac{3}{k^4}(D-1)\right\}\left\{3D-\frac{9}{k^2}(D-1)\right\}=0.\end{aligned}\right\} \quad (27)$$

On multiplying out the factors and collecting the various terms in equation (27), we find that we are finally left with

$$\frac{1}{k^2}(D-1)=\tfrac{1}{3}(9D-8); \quad (28)$$

or, according to equations (19) and (21), we have

$$\sum_{j=1}^{n}\frac{a_j\mu_j^2}{1-\mu_j^2k^2}=3\sum_{j=1}^{n}\frac{a_j}{1-\mu_j^2k^2}-\frac{8}{3}. \quad (29)$$

In other words, k^2 must be a root of the equation

$$\frac{8}{3}=\sum_{j=1}^{n}\frac{a_j(3-\mu_j^2)}{1-\mu_j^2k^2}. \quad (30)$$

Equation (30) is of order n in k^2. But $k^2=0$ is a solution of this equation.[4] Hence, equation (30) admits of only $(2n-2)$ distinct nonvanishing roots for k, which must occur in pairs as

$$\pm k_\alpha \qquad (\alpha=1,\ldots,n-1). \quad (31)$$

Returning to equations (25) and (26), we now verify that the first of these is identically satisfied, in virtue of equation (28), while the second reduces to

$$\alpha+3\beta=0; \quad (32)$$

and hence (cf. eq. [12])

$$g_i=\text{constant}\,\frac{3-\mu_i^2}{1+\mu_ik} \qquad (i=\pm1,\ldots,\pm n). \quad (33)$$

We have thus proved that the system of equations (9) allows $(2n-2)$ linearly independent solutions of the form

$$I_i=\text{constant}\,\frac{3-\mu_i^2}{1\pm\mu_ik_\alpha}\,e^{\mp k_\alpha\tau}\left\{\begin{matrix}(i=\pm1,\ldots,\pm n),\\(\alpha=1,\ldots,n-1).\end{matrix}\right\} \quad (34)$$

To complete the solution, we verify that, as in II, equation (9) also admits the solution

$$I_i=b(\tau+\mu_i+Q) \qquad (i=\pm1,\ldots,\pm n), \quad (35)$$

where b and Q are arbitrary constants.

Combining the solutions (34) and (35), we see that the general solution of the system of equations (9) can be written in the form

$$\left.\begin{aligned}I_i=b\left\{\sum_{\alpha=1}^{n-1}(3-\mu_i^2)\left(\frac{L_\alpha e^{-k_\alpha\tau}}{1+\mu_ik_\alpha}+\frac{L_{-\alpha}e^{+k_\alpha\tau}}{1-\mu_ik_\alpha}\right)+\tau+\mu_i+Q\right\}\\ (i=\pm1,\ldots,\pm n),\end{aligned}\right\} \quad (36)$$

where $L_{\pm\alpha}$, $(\alpha=1,\ldots,n-1)$, b, and Q are the $2n$ constants of integration.

[4] Note that $\sum_{j=1}^{n}a_j(3-\mu_j^2)=3-\frac{1}{3}=\frac{8}{3}$.

4. *The solution satisfying the necessary boundary conditions.*—The boundary conditions for the astrophysical problem on hand are that none of the I_i's increase exponentially as $\tau \to \infty$ and that there is no radiation incident on the surface $\tau = 0$. The first of these conditions imply that in the general solution (36) we omit all the terms in exp $(+ k_a\tau)$. We are thus left with

$$I_i = b\left\{\sum_{a=1}^{n-1}(3-\mu_i^2)\frac{L_a e^{-k_a\tau}}{1+\mu_i k_a} + \tau + \mu_i + Q\right\} \quad (i = \pm 1, \ldots, \pm n). \quad (37)$$

Next the nonexistence of any radiation incident on $\tau = 0$ requires that

$$I_{-i} = 0 \quad \text{at} \quad \tau = 0 \quad \text{and for} \quad i = 1, \ldots, n, \quad (38)$$

or, according to equation (37),

$$\sum_{a=1}^{n-1}\frac{3-\mu_i^2}{1-\mu_i k_a}L_a + Q - \mu_i = 0 \qquad (i = 1, \ldots, n). \quad (39)$$

These are the n equations which determine the n constants L_a, $a = 1, \ldots, n-1$, and Q. The constant b is left arbitrary and is related to the constant net flux of radiation in the atmosphere.

For, defining the net flux in terms of F, where

$$F = 2\int_{-1}^{+1} I\mu\, d\mu\,, \quad (40)$$

we have in our present approximation

$$F = 2\Sigma a_i\mu_i I_i\,. \quad (41)$$

Using the solution (37) for I_i, we have

$$F = 2b\left\{\sum_{a=1}^{n-1}L_a e^{-k_a\tau}\sum_i\frac{a_i\mu_i(3-\mu_i^2)}{1+\mu_i k_a} + \Sigma a_i\mu_i^2 + (\tau+Q)\Sigma a_i\mu_i\right\}. \quad (42)$$

But

$$\left.\begin{aligned}\sum_i\frac{a_i\mu_i(3-\mu_i^2)}{1+\mu_i k_a} &= \frac{1}{k_a}\sum_i(3-\mu_i^2)\,a_i\left(1-\frac{1}{1+\mu_i k_a}\right)\\ &= \frac{1}{k_a}\left(\frac{16}{3} - \sum_i\frac{(3-\mu_i^2)\,a_i}{1+\mu_i k_a}\right),\end{aligned}\right\} \quad (43)$$

and this vanishes according to equation (30). Hence,

$$F = \tfrac{4}{3}b = \text{constant}\,. \quad (44)$$

We can therefore re-write the solution (37) in the form

$$I_i = \tfrac{3}{4}F\left\{\sum_{a=1}^{n-1}\frac{(3-\mu_i^2)L_a e^{-k_a\tau}}{1+\mu_i k_a} + \tau + \mu_i + Q\right\} \quad (i = \pm 1, \ldots, \pm n). \quad (45)$$

In terms of the foregoing solution for the I_i's we can obtain convenient formulae for J and K, defined as in equation (6).

Considering first J, we have

$$\left.\begin{aligned} J &= \tfrac{1}{2}\Sigma a_i I_i \\ &= \tfrac{3}{8}F\left\{\sum_{a=1}^{n-1} L_a e^{-k_a\tau}\sum_i \frac{a_i(3-\mu_i^2)}{1+\mu_i k_a} + 2(\tau+Q)\right\}, \end{aligned}\right\} \tag{46}$$

or, according to equation (30),

$$J = \tfrac{3}{4}F\left(\tau+Q+\frac{8}{3}\sum_{a=1}^{n-1} L_a e^{-k_a\tau}\right). \tag{47}$$

Considering next K, we have

$$\left.\begin{aligned} K &= \tfrac{1}{2}\Sigma a_i\mu_i^2 I_i \\ &= \tfrac{3}{8}F\left\{\sum_{a=1}^{n-1} L_a e^{-k_a\tau}\sum_i \frac{a_i(3-\mu_i^2)\mu_i^2}{1+\mu_i k_a} + \tfrac{2}{3}(\tau+Q)\right\}. \end{aligned}\right\} \tag{48}$$

On the other hand,

$$\left.\begin{aligned} \sum_i \frac{a_i(3-\mu_i^2)\mu_i^2}{1+\mu_i k_a} &= 2\sum_{i=1}^{n}\frac{a_i(3-\mu_i^2)\mu_i^2}{1-\mu_i^2 k_a^2} \\ &= \frac{2}{k_a^2}\sum_{i=1}^{n} a_i(3-\mu_i^2)\left(\frac{1}{1-\mu_i^2 k_a^2}-1\right) \\ &= \frac{2}{k_a^2}\left[\sum_{i=1}^{n}\frac{a_i(3-\mu_i^2)}{1-\mu_i^2 k_a^2} - \frac{8}{3}\right], \end{aligned}\right\} \tag{49}$$

which vanishes in virtue of equation (30). Hence,

$$K = \tfrac{1}{4}F(\tau+Q). \tag{50}$$[5]

Now from the equation of transfer in the form (7) it is evident that the rate of emission of radiant energy by the material at τ in the direction μ is given in terms of the source function

$$\mathcal{J}(\tau,\mu) = \tfrac{3}{8}[(3-\mu^2)J + (3\mu^2-1)K]. \tag{51}$$

Substituting for J and K from equations (47) and (50), we find that

$$\mathcal{J}(\tau,\mu) = \tfrac{3}{4}F\left[(3-\mu^2)\sum_{a=1}^{n-1} L_a e^{-k_a\tau} + \tau + Q\right]. \tag{52}$$

The law of darkening can now be derived from the relation

$$I(0,\mu) = \int_0^\infty \mathcal{J}(\tau,\mu)\, e^{-\tau/\mu}\frac{d\tau}{\mu}; \tag{53}$$

or, with $\mathcal{J}(\tau,\mu)$ given as in equation (52), we have

$$I(0,\mu) = \tfrac{3}{4}F\left[\mu+Q+(3-\mu^2)\sum_{a=1}^{n-1}\frac{L_a}{1+k_a\mu}\right]. \tag{54}$$

This completes the solution of the problem in the nth approximation.

[5] This equation is really an expression of the "K-integral" (cf. I, p. 182), which exists also in our present problem.

Finally, some remarks concerning the equations which determine the constants of integration L_a ($a = 1, \ldots, n-1$) and Q may be made. Considering the function

$$S(\mu) = \sum_{a=1}^{n-1} \frac{(3-\mu^2) L_a}{1-\mu k_a} + Q - \mu , \tag{55}$$

it follows from equation (39) that

$$S(\mu_i) = 0 \qquad (i = 1, \ldots, n). \tag{56}$$

This fact enables us to determine $S(\mu)$ explicitly (cf. II, § 6). For, multiplying equation (55) by the function

$$R(\mu) = (1-\mu k_1)(1-\mu k_2)\ldots(1-\mu k_{n-1}), \tag{57}$$

we obtain a polynomial of degree n in μ which vanishes for $\mu = \mu_i$, $i = 1, \ldots, n$. Accordingly, $S(\mu)R(\mu)$ cannot differ from the polynomial

$$P(\mu) = (\mu-\mu_1)(\mu-\mu_2)\ldots(\mu-\mu_n) \tag{58}$$

by more than a constant factor. This factor can be determined by comparing the coefficients of the highest power of μ (namely, μ^n) in $P(\mu)$ and $S(\mu)R(\mu)$. In the former it is unity, while in the latter it is

$$(-1)^n k_1 k_2 \ldots k_{n-1} \left(1 - \sum_{a=1}^{n-1} \frac{L_a}{k_a}\right). \tag{59}$$

Hence,

$$S(\mu) = (-1)^n k_1 k_2 \ldots k_{n-1} \left(1 - \sum_{a=1}^{n-1} \frac{L_a}{k_a}\right) \frac{P(\mu)}{R(\mu)}. \tag{60}$$

On the other hand, from equation (55) it follows that, if we multiply the right-hand side of this equation by $(1-\mu k_a)$ and then set $\mu = 1/k_a$, we are left with

$$\left(3 - \frac{1}{k_a^2}\right) L_a . \tag{61}$$

Hence,

$$\left(3 - \frac{1}{k_a^2}\right) L_a = \lim_{\mu = 1/k_a} (1-\mu k_a) S(\mu) ; \tag{62}$$

or, using equation (60) for $S(\mu)$, we have

$$\left(3 - \frac{1}{k_a^2}\right) L_a = (-1)^n k_1 k_2 \ldots k_{n-1} \left(1 - \sum_{\beta=1}^{n-1} \frac{L_\beta}{k_\beta}\right) \frac{P(1/k_a)}{R_a(1/k_a)}, \tag{63}$$

where R_a differs from R in the omission of the factor $(1-\mu k_a)$ on the right-hand side of equation (57). According to equation (63), the L_a's, apart from a constant multiplicative factor, can all be determined without going through an explicit solution of the linear equations (39). The multiplicative factor and the remaining constant Q can then be determined from any two of the n equations represented by (39). This procedure for evaluating the constants of integration is likely to be advantageous in the explicit working-out of the solutions in their numerical forms.

Again, according to equations (55), (58), and (60), we have

$$3\sum_{a=1}^{n-1} L_a + Q = S(0) = k_1 k_2 \ldots . k_{n-1}\mu_1\mu_2 \ldots . \mu_n \left(1 - \sum_{a=1}^{n-1} \frac{L_a}{k_a}\right). \tag{64}$$

On the other hand, it is readily verified that equation (30), when written out in full, has the form

$$(-1)^{n-1} 8\mu_1^2\mu_2^2 \ldots . \mu_n^2 k^{2n-2} + \ldots . + \tfrac{1}{5}^2 = 0 \tag{65}$$

and that, therefore,

$$\mu_1\mu_2 \ldots . \mu_n k_1 k_2 \ldots . k_{n-1} = \sqrt{\tfrac{1}{5}^2 \times \tfrac{1}{8}} = \sqrt{0.3}. \tag{66}$$

Equation (64) now becomes

$$3\sum_{a=1}^{n-1} L_a + Q = \sqrt{0.3}\left(1 - \sum_{a=1}^{n-1} \frac{L_a}{k_a}\right), \tag{67}$$

a relation which will be useful for checking a derived set of constants.

5. *The numerical forms of the solution in the first four approximations.*—According to equation (47), we can write, quite generally,

$$J(\tau) = \tfrac{3}{4}F(\tau + q[\tau]), \tag{68}$$

where

$$q(\tau) = Q + \frac{8}{3}\sum_{a=1}^{n-1} L_a e^{-k_a\tau}. \tag{69}$$

Hence,

$$q(0) = Q + \frac{8}{3}\sum_{a=1}^{n-1} L_a \quad \text{and} \quad q(\infty) = Q. \tag{70}$$

The first four approximations to the solution have been numerically evaluated, and the results are given below:

i) *First approximation.*—

$$q(\tau) = \frac{1}{\sqrt{3}}, \tag{71}$$

and

$$I(0, \mu) = \tfrac{3}{4}F\left(\mu + \frac{1}{\sqrt{3}}\right). \tag{72}$$

It is therefore seen that in this approximation the solution is identical with that considered in II (cf. eqs. [35] and [36]). This is, however, to be expected, in view of what has already been noted, that in the $K = \frac{1}{3}J$ approximation the equation of transfer incorporating the Rayleigh law of scattering is no different from the case of isotropic scattering.

ii) *Second approximation.*—

$$q(\tau) = 0.69539 - 0.11959e^{-\sqrt{3.5}\tau}, \tag{73}$$

$$q(0) = 0.57580\,; \qquad q(\infty) = 0.69539\,, \tag{74}$$

and

$$I(0, \mu) = \tfrac{3}{4}F\left[\mu + 0.69539 - (3 - \mu^2)\frac{0.044845}{1 + 1.87083\mu}\right]. \tag{75}$$

iii) *Third approximation.*—

$$q(\tau) = 0.70509 - 0.10073\,e^{-3.08624\tau} - 0.028831\,e^{-1.20629\tau}, \tag{76}$$

$$q(0) = 0.57553\,; \qquad q(\infty) = 0.70509\,, \tag{77}$$

and

$$I(0,\mu) = \tfrac{3}{4}F\left[\mu + 0.70509 - (3-\mu^2)\left(\frac{0.037773}{1+3.08624\mu} + \frac{0.010812}{1+1.20629\mu}\right)\right]. \tag{78}$$

iv) *Fourth approximation.*—

$$\left.\begin{aligned} q(\tau) = 0.70802 - 0.082361\,e^{-4.337235\tau} - 0.038611\,e^{-1.56218\tau} \\ - 0.011598\,e^{-1.09612\tau}, \end{aligned}\right\} \tag{79}$$

$$q(0) = 0.57545\,; \qquad q(\infty) = 0.70802\,, \tag{80}$$

and

$$\left.\begin{aligned} I(0\ \mu) = \tfrac{3}{4}F\left[\mu + 0.70802 - (3-\mu^2)\left(\frac{0.030885}{1+4.337235\mu}\right.\right. \\ \left.\left. + \frac{0.014479}{1+1.56218\mu} + \frac{0.0043493}{1+1.09612\mu}\right)\right]. \end{aligned}\right\} \tag{81}$$

The functions $q(\tau)$ and the laws of darkening in the various approximations are tabulated in Tables 1 and 2. Comparing these tables with the corresponding ones in II, we observe that the incorporation of Rayleigh's phase function in the equation of transfer does not introduce any essential modifications. However, the interest in the calculations

TABLE 1

THE FUNCTION $q(\tau)$ DERIVED ON THE BASIS OF THE SECOND, THIRD, AND FOURTH APPROXIMATIONS (EQS. [73], [76], AND [79])

τ	$q(\tau)$			τ	$q(\tau)$		
	Second Approximation	Third Approximation	Fourth Approximation		Second Approximation	Third Approximation	Fourth Approximation
0.00	0.5758	0.5755	0.5755	0.90	0.6732	0.6891	0.6926
.05	.5865	.5916	.5950	1.0	.6770	.6919	.6950
.10	.5962	.6056	.6112	1.2	.6827	.6958	.6985
.15	.6051	.6176	.6247	1.4	.6867	.6984	.7010
.20	.6131	.6281	.6359	1.6	.6894	.7002	.7028
.25	.6205	.6372	.6452	1.8	.6913	.7014	.7041
.30	.6272	.6451	.6531	2.0	.6926	.7023	.7050
.35	.6333	.6520	.6597	2.2	.6934	.7030	.7057
.40	.6388	.6580	.6653	2.4	.6940	.7034	.7063
.50	.6485	.6678	.6742	2.6	.6945	.7038	.7067
.60	.6565	.6753	.6808	2.8	.6948	.7041	.7070
.70	.6631	.6811	.6857	3.0	.6950	.7043	.7072
0.80	0.6686	0.6856	0.6896	∞	0.6954	0.7051	0.7080

TABLE 2

THE LAWS OF DARKENING GIVEN BY THE SECOND, THIRD, AND FOURTH APPROXIMATIONS (EQS. [75], [78], AND[81])

μ	$I(0, \mu)/F$		
	Second Approximation	Third Approximation	Fourth Approximation
0	0.4206	0.4195	0.4192
0.1	0.5118	0.5175	0.5208
0.2	0.5991	0.6076	0.6119
0.3	0.6839	0.6937	0.6981
0.4	0.7669	0.7773	0.7815
0.5	0.8488	0.8593	0.8633
0.6	0.9297	0.9402	0.9440
0.7	1.0100	1.0203	1.0240
0.8	1.0897	1.0998	1.1033
0.9	1.1691	1.1789	1.1822
1.0	1.2481	1.2576	1.2607

is far more in illustrating the feasibility of solving problems of radiative transfer involving phase functions in an entirely satisfactory manner.

In conclusion, I wish to record my indebtedness to Miss Frances Herman for her assistance with the numerical work.

EFFECT OF TEMPERATURE ON THE WAVE LENGTH OF A TRANSMISSION BAND OF THE INTERFERENCE POLARIZING MONOCHROMATOR*

EDISON PETTIT
Mount Wilson Observatory
Received May 15, 1944

ABSTRACT

The shift due to temperature change of a transmission band of the interference polarizing monochromator has been computed from the known value of the birefringence of quartz. Direct observation with two specimen prisms shows agreement for temperatures above 25° C, but smaller shifts than theory requires for lower temperatures.

The wave length of a transmission band of the interference polarizing monochromator[1] is

$$\lambda = d_0(\mu_e - \mu_o), \tag{1}$$

where $(\mu_e - \mu_o)$ is the birefringence and d_0 the thickness of a crystal plate which will produce a difference of one wave length in the light-paths of the extraordinary and ordinary rays. Since the birefringence varies with the temperature, d_0 is calculated for some temperature t. For any temperature change, dt, the wave length of the transmission band will shift a small amount $d\lambda$, although this fact has been mentioned only briefly in the literature.[2] Moreover, it can be shown that $d\lambda/dt$ is itself a function of the temperature. We may determine $d\lambda/dt$ from direct or indirect experimental evidence. We shall examine the indirect evidence first.

The value of $d\lambda/dt$ is the differential of equation (1):

$$\frac{d\lambda}{dt} = d_0 \frac{d}{dt}(\mu_e - \mu_o) + \frac{dd_0}{dt}(\mu_e - \mu_o). \tag{2}$$

The quantity dd_0/dt may also be written d_0C, where C is the coefficient of linear expansion of the quartz plate perpendicular to the axis. R. B. Sosman[3] gives several determinations of C. If we reject the measures of Buisson, which seem to refer to a peculiar specimen of quartz, the remaining measures (by Benoît, Fizeau, and Lindman) are consistent with the formula

$$C = (0.1325 + 0.00012t) \times 10^{-4}, \tag{3}$$

which expresses the expansion coefficient over the range of approximately 0°–100° C.

The birefringence may be calculated from Sosman's empirical equation,[4] which represents a long series of measures by Macé de Lépinay (1891). The equation may be stated as follows:

$$\left.\begin{aligned}(\mu_e - \mu_o) = {} & 8.86027 \times 10^{-3} + 0.10785 \times 10^{-3}\lambda^{-2} + 0.002136 \times 10^{-3}\lambda^{-4} \\ & - 0.16667 \times 10^{-3}\lambda^2 - 10^{-6}t(1 + 1.111 \times 10^{-3}t)\,(1.01 + 0.2\lambda^2),\end{aligned}\right\} \tag{4}$$

* *Contributions from the Mount Wilson Observatory, Carnegie Institution of Washington,* No. 694.

[1] E. Pettit, *Pub. A.S.P.*, **53**, 171, 1941.

[2] *Ibid.*; see also J. W. Evans, *Pub. A.S.P.*, **52**, 305, 1940.

[3] *The Properties of Silica*, p. 387, New York, 1927.

[4] *Ibid.*, p. 642.

where λ is in microns and t is in degrees centigrade. The differential of this equation with respect to t is

$$\left.\begin{aligned}\frac{d}{dt}(\mu_e-\mu_o)=-[&0.21570\times10^{-3}\lambda^{-3}+0.008544\times10^{-3}\lambda^{-5}+0.33333\\&\times10^{-3}\lambda+0.4\times10^{-6}\lambda t(1+1.111\times10^{-3}t)]\frac{d\lambda}{dt}-10^{-6}(1+2.222\\&\times10^{-3}t)\,(1.01+0.2\lambda^2).\end{aligned}\right\}\quad(5)$$

Since the monochromator is used with temperatures well below 100° C and for wave lengths between 0.4 and 0.7 μ, we have calculated the coefficient of $d\lambda/dt$ in equation (5) for these values and find 0.0044 for $\lambda = 0.4\ \mu$ and 0.00094 for $\lambda = 0.7\ \mu$. For $H\alpha$ we shall, therefore, use 0.001.

To compute $d\lambda/dt$ the properties of two monochromator prisms will be used. The first consists of 7 blocks of quartz for which $H\alpha$ is centered on the transmission band at 41.3° C; the second of 6 blocks for which $H\alpha$ is centered on the transmission band at 45.0° C. They have, therefore, the following properties:

$$d_0 = 0.072895 \text{ mm (No. 1)},\quad 0.072931 \text{ mm (No. 2)},$$

$$\frac{dd_0}{dt} = (9.65859+0.00875t)\times10^{-7} \text{ mm (No. 1)},$$

$$\frac{dd_0}{dt} = (9.66336+0.00875t)\times10^{-7} \text{ mm (No. 2)},$$

$$(\mu_e-\mu_o) = 9.05039\times10^{-3}-1.0961\times10^{-6}t-1.2178\times10^{-9}t^2,$$

$$\frac{d}{dt}(\mu_e-\mu_o) = -\left(1.0961\times10^{-6}+2.4356\times10^{-9}t+0.001\,\frac{d\lambda}{dt}\right),$$

$$\frac{d\lambda}{dt} = -(0.71158+0.00171t)\text{ A (No. 1)},\quad(6)$$

$$\frac{d\lambda}{dt} = -(0.71192+0.00171t)\text{ A (No. 2)}.\quad(7)$$

Since the coefficients are negligible, the terms in the second and third[5] powers of t disappear.

As a laboratory test of equations (6) and (7) each monochromator prism was mounted in turn on a movable platform within a temperature-controlled paper box. The temperature was read with a thermometer having known calibration errors. Sunlight passing through windows in the box was transmitted by the prism to the slit of a 1-meter concave-grating spectroscope used in the first order. The value of one division on the head of the wave-length screw was found to be nearly constant at 1.352 A over the region $\lambda\lambda$ 6550–6590. The probable error of six settings on the transmission band is about 0.1 division, or 0.14 angstroms, indicating that the graduations are somewhat too coarse.

Prism No. 1 (at the beginning of the test, 10° below its normal operating temperature) required 25 minutes after the air temperature was raised to normal for the sunlight passing through the center of the prism to show $H\alpha$ in the middle of the transmission band; prism No. 2 required 90 minutes. In actual observation, the time interval between the changes in temperature and the wave-length readings on the transmission band was 1 hour and 2 hours for the two prisms, respectively.

[5] $-(2\times10^{-8}t^2+10^{-11}t^3)$A for either prism.

After the wave-length scale was read for light transmitted by the center of the prism, the prism was shifted laterally and another reading made on light transmitted near one side. If an appreciable difference was observed, time was allowed to elapse, and then other readings were made until it was found that the prism as a whole had reached the temperature indicated by the thermometer. The prism was then shifted to one side, and settings were made on $H\alpha$. The difference, reduced to angstroms, gave the displacement, $\Delta\lambda$, of the band from $H\alpha$ for that temperature, the procedure eliminating temperature-effects on the zero of the wave-length dial of the spectroscope.

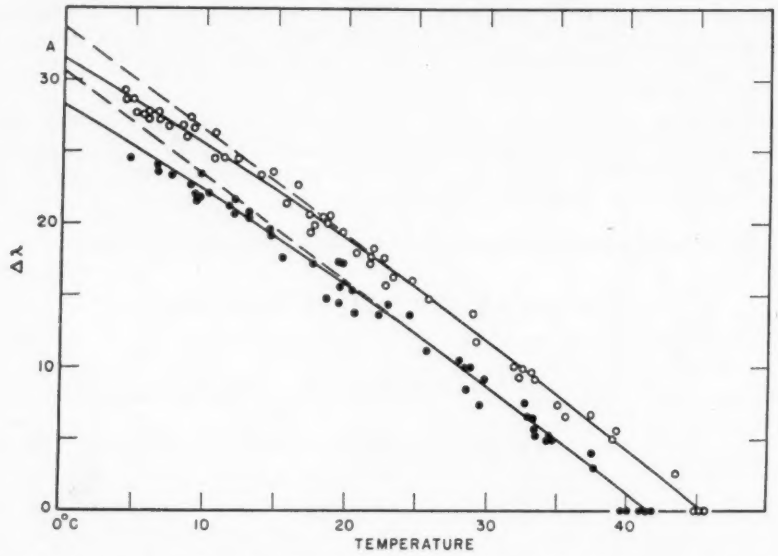

FIG. 1.—Displacement $\Delta\lambda$ from the $H\alpha$ line, of the transmission band of two quartz interference polarizing monochromators for various temperatures; prism No. 1 below, No. 2 above. Solid lines show means of observed points and dashed lines the corresponding curves computed from the known birefringence of quartz perpendicular to the axis.

When a series of readings was to be made, the box was allowed to cool off overnight. An hour before sunrise it was covered with a thick cloth to prevent further changes of temperature of more than a half-degree until measurements began. These were started shortly after sunrise and were continued with definite temperature changes under thermostatic control at intervals depending on which prism was being studied.

Figure 1 shows the observed displacements of the band from $H\alpha$ plotted against temperature. Part of the scattering of the observations is due to the operating range of the thermostat—about 0.7° C. Some stratification of temperature may have taken place in the prism, since the fan stirred the air in the box only when the electrical heating unit was operating. The settings of the spectroscope may have been subject to some correction because of tooth-errors in the gearing of the wave-length dial, but the inaccuracy is supposed to be negligible.

We may compute $\Delta\lambda$ from equations (6) and (7). Integrating, we have[6]

$$\Delta\lambda = -[0.71158(t_0 - t) + 0.000855(t_0^2 - t^2)]\ \text{A (No. 1)}, \qquad (8)$$

$$\Delta\lambda = -[0.71192(t_0 - t) + 0.000855(t_0^2 - t^2)]\ \text{A (No. 2)}, \qquad (9)$$

[6] The higher-power terms, $-[7 \times 10^{-9}(t_0^3 - t^3) + 25 \times 10^{-13}(t_0^4 - t^4)]$ A for either prism, are negligible.

where t_0 is the normal operating temperature of the prism and $\Delta\lambda$ is the displacement of the transmission band due to the change of temperature $(t_0 - t)$.

The curves representing equations (8) and (9) are shown as dashed lines in Figure 1. The observed and computed curves agree well for temperatures higher than about 25° C, but the computed $\Delta\lambda$ is definitely too great for lower temperatures. No reason for this departure is patent. If the second terms of equations (8) and (9) could be eliminated, the resulting straight line would fit the observations of Figure 1 reasonably well throughout, but no reason for this elimination exists. In any event, the plot of $\Delta\lambda$ in Figure 1, or equations (6) and (7), or (8) and (9), give

$$\frac{d\lambda}{dt} = -0.782 \text{ A/°C (No. 1)} \qquad \text{or} \qquad -0.789 \text{ A/°C (No. 2)}$$

at the operating temperatures of the prisms, 41.3° and 45° C, respectively.

DOUBLY IONIZED RARE EARTHS IN α^2 CANUM VENATICORUM*

P. SWINGS
Mount Wilson Observatory
Received May 26, 1944

ABSTRACT

The strongest lines of *Eu* III, *Gd* III, *Ce* III, *Sa* III, and *La* III in the region λλ 3070–3300 are identified in the spectrum of α^2 CVn. Their intensities and radial velocities undergo changes parallel to those of the lines of the corresponding singly ionized elements. Several unidentified lines in the blue-violet region are probably due to *Dy* III.

Several recent papers[1] have provided many new observational data regarding α^2 Canum Venaticorum, and attempts have been made to relate the spectroscopic anomalies of this star to those of a number of other peculiar A-type stars.[2] But a convincing interpretation of the spectroscopic variations and of the anomalous intensities of the rare-earth lines in α^2 CVn has not yet been found, although definite progress has been made. One of the difficulties lies in the fact that very few metals show lines of both the neutral and the ionized atom; and, moreover, all unblended arc lines are very weak and can hardly serve for a discussion of the ionization conditions and of their variations with phase. Yet it has been shown conclusively that the elementary theory of ionization fails to explain the observed variations in line intensities. As a consequence, an attempt has been made to attribute the abnormally high intensity of the *Eu* II lines as well as the abnormally low intensity of the *Ca* II line and other similar phenomena either to a reduced or to an enhanced ionization of the corresponding atoms in a field of radiation that is not of the black-body type. Within the spectrum of a specific atom there is no observed effect suggestive of a geometrical dilution of the exciting radiation. Hence a possible effect of the Lyman lines (in absorption or emission), of the Lyman continuum, and of other strong atomic lines around λ 1000 was mentioned. For thermodynamic equilibrium the ionization of *Eu* II in α^2 CVn should be far advanced, and the *Eu* II lines should be weak, while those of *Eu* III should be strong. Moreover, at first thought one would be tempted to expect that a maximum intensity of *Eu* II lines should be associated with a minimum of *Eu* III and vice versa, regardless of the type of ionization equilibrium. Unfortunately, no spectrum of a doubly ionized rare earth (except *Ce* III) was available until recently; hence the various possibilities could not be discussed thoroughly, although it was felt that any progress in the understanding of α^2 CVn would have a direct application to the general problem of the peculiar A stars.

The only spectroscopic data on a doubly ionized rare earth previously published concern *Ce* III.[3] The published lines of *Ce* III lie in the region $\lambda < 3550$ A; and, although several of them were identified[4] in α^2 CVn with a fair degree of certainty, their behavior with

* *Contributions from the Mount Wilson Observatory, Carnegie Institution of Washington*, No. 695.

[1] Struve and Swings, *Observatory*, **64**, 291, 1942, and *Ap. J.*, **98**, 361, 1943; O. Struve, *Proc. Amer. Phil. Soc.*, **85**, 349, 1942; W. S. Tai, *M.N.*, **100**, 94, 1939, and *Ap. J.*, **96**, 218, 1942; W. W. Morgan, *Pub. Yerkes Obs.*, **7**, Part III, 1935; Nikonov and Brodskaja, *Bull. Acad. Sci. Georgian S.S.R.*, **3**, No. 7, 657, 1942.

[2] The author has in view such A stars as were previously called "manganese stars" (α And), "strontium stars" (73 Dra), etc., also the A stars which show abnormally weak lines of *Ca* II.

[3] A. S. and R. B. King, *Mt. W. Contr.*, No. 441; *Ap. J.*, **75**, 40, 1932; P. N. Kalia, *Indian J. Phys.*, **8**, 137, 1933; T. L. de Bruin, *Proc. Amsterdam Academy of Sciences*, **40**, 334, 1937; Russell, King, and Lang, *Phys. Rev.*, **52**, 456, 1937.

[4] Struve and Swings, *Ap. J.*, **98**, 361, 1943.

phase was unknown. Recently Dr. A. S. King has re-examined his spectrograms of the spark of rare earths with a view to detecting lines of doubly ionized elements; and he has generously put at my disposal unpublished lists of measured wave lengths of *Eu* III, *Gd* III, *Sa* III, *Nd* III, and *Pr* III in the ultraviolet region. The upper wave-length limits of Dr. King's tables are: for *Eu* III, 3194.3; *Gd* III, 3176.6; *Sa* III, 3398.4; *Nd* III, 3431.4; *Pr* III, 3568.4. It is in this ultraviolet region that the lines of these doubly ionized rare earths are most conspicuous, although other lines appear at longer wave lengths. No strong *Dy* III line appears in the *Dy* spark in the ultraviolet region around λ 3200. We shall also include in the present study *La* III, which has the two strong $6s^2S-6p^2P^o$ lines 3171.68 (lab. int. 300) and 3517.14 (lab. int. 200).[5] Lanthanum is a chemical analogue of scandium and yttrium and immediately precedes the group of the fourteen "rare earths." But the atom-building process accounting for the rare-earth elements is actually anticipated in the electron configurations of *La;* hence certain ionization properties of *La* are closely related to those of the rare earths, rendering logical the inclusion of *La* in the present study.

The previously published spectroscopic data on α^2 CVn in the region $\lambda < 3400$ A are still insufficient for a discussion of the doubly ionized rare earths, since they were based on spectrograms of dispersion about 20 A/mm, which is definitely insufficient for α^2 CVn on account of the complexity of the spectrum. Three coudé spectrograms taken by W. S. Adams with the 100-inch reflector were kindly placed at my disposal. These plates (dispersion 2.91 A/mm) are excellent, being well exposed as far toward the ultraviolet as λ 3070. The dates and phases are 1944, April 10, phase 0^d44 (0.08 per.); 1943, March 26, phase 1^d91 (0.35 per.); and 1943, March 28, phase 3^d28 (0.60 per.). The lines of the singly ionized rare earths are very strong on the first two plates and absent (or much weaker) on the third.

It would have been desirable to measure the spectrograms completely from λ 3070 to λ 3600, where adequate published data begin, but lack of time—due to the pressure of war research—prevented. Only those lines or groups of lines near the wave lengths of the strongest laboratory lines of the doubly ionized rare earths were measured. The identifications were based not only on wave-length coincidences but also, in blends, on the known intensity behavior with phase of the various singly ionized elements.

It was at once apparent that the absorption lines due to doubly ionized rare earths are definitely of class A, i.e., they reach their intensity maximum at the same time as *Eu* II. The lines of *Eu* III are absent at phase 3^d28^m, while the lines of *Gd* III behave similarly but have a slightly smaller range in intensity, and the lines of *Sa* III and *Ce* III have a much smaller range. The lines were measured for wave length and radial velocity for phases 0^d44 and 1^d91 only, with results summarized in Table 1. The lines which proved to be heavily blended are not included. The changes in radial velocity are given only for well-defined lines. On account of the uncertainty of the laboratory wave lengths[6] the *changes* in radial velocity have more meaning than the absolute values, except in the case of *Ce* III. There is no definite identification of *Nd* III or *Pr* III.

From Table 1 it is apparent that the identification of *Eu* III, *Gd* III, *Ce* III, *Sa* III, and *La* III is as reliable as can be expected in the present state of our laboratory knowledge of these spectra, although it would have been more satisfactory had the whole spectrograms been measured. Yet, even before any actual measurement, simple examination with a hand magnifier of the high-dispersion plates had definitely convinced the author that the doubly ionized elements are indeed present. This illustrates an obvious advantage of very high dispersion.

[5] A. S. King and Edna Carter, *Mt. W. Contr.*, No. 326; *Ap. J.*, **65**, 86, 1927; Russell and Meggers, *Bur. Standards J. Res.*, **9**, 625, 1932.

[6] The lines of *Eu* III, *Gd* III, and *Sa* III are usually wide and diffuse in the heavy-current spark generally used by Dr. King; a weaker spark would narrow them, thus providing better wave lengths; but such laboratory work has to be postponed.

The mean ranges in radial velocity given in Table 1 are very similar to those of the corresponding singly ionized elements. A previous investigation[4] has shown that the changes in radial velocity from phase 0^d44 to phase 1^d91 have approximately the following values:

Eu II: + 11 km/sec; *Ce* II: + 9 km/sec (somewhat uncertain);
Gd II: + 4 km/sec; *Sa* II: + 4 km/sec.

TABLE 1

ESSENTIAL OBSERVATIONAL DATA ON LINES OF DOUBLY IONIZED RARE EARTHS

Element	Laboratory		Stellar Intensities			Stellar Wave Length		Radial Velocity		Change in Radial Velocity between Phases 0^d44 and 1^d91		Notes
	λ	Int.	Phase 1^d91	Phase 3^d28	Phase 0^d44	Phase 0^d44	Phase 1^d91	Phase 0^d44	Phase 1^d91	Individual	Mean	
								km/sec	km/sec	km/sec	km/sec	
Eu III	3170.97	150	3	Abs.	3	70.97	71.10	+ 0.0	+12.3	+12.3	+12.3	1
	3183.77	100	1	Abs.	1	83.7	83.9	.....	.....	.....		2
Gd III	3118.01	1000	5	0	5	18.06	18.11	+ 4.8	+ 9.6	+ 4.8	+ 4.3	3
	3176.64	200	3	1	3	76.67	76.71	+ 2.8	+ 6.6	+ 3.8		4
Ce III	3106.97	200	4	2	4	06.93	07.05	− 3.9	+ 7.7	+11.6		.....
	3121.55	400	4	1	4	21.53	21.60	− 1.9	+ 4.8	+ 6.7		5
	3141.25	250	6	2	6	41.25	41.37	.....	.....	.....	+ 8.6	6
	3143.96	200	6	1	6	43.93	44.01	− 2.9	+ 4.8	+ 7.7		7
	3228.56	400	5	2	5	28.53	28.62	− 2.8	+ 5.6	+ 8.4		8
Sa III	3098.57	250	3	1	4	98.68	98.64	.....	.....	.....	Very small	9
	3100.64	200	1	0	1	00.8	00.8	.....	.....	.....		10
	3269.39	400	2	Abs.	2	69.43	69.42	.....	.....	.....		.....
La III	3171.68	.....	1	Abs.	1	71.46	71.54	−19.9	−12.3	+ 7.6	+ 7.6	.....

NOTES TO TABLE 1

1. *Dy* II 70.75 (40), *Gd* II 71.09 (125), and *Eu* II 70.96 (10) have only minor effect.
2. Too faint for reliable radial velocity.
3. *Eu* II 17.99 (15) and *Gd* II 17.97 (40) have only minor effect.
4. *Eu* II 76.60 (8) has no effect.
5. *Gd* II 21.76 (80), *Ti* II 21.60 (20), and *Eu* II 21.78 (6) have only minor effect.
6. *Dy* II 41.13 (200) may have appreciable effect.
7. *Eu* II 44.21 (15), *Ti* II 43.76 (125), and *Dy* II 43.83 (50) may have a slight effect.
8. *Ti* II 28.60 (100) and *Gd* II 28.64 (15) may have slight effect.
9. *Gd* II 98.65 (800) has appreciable effect.
10. Too near strong *Gd* II 00.51 (10,000) for accurate measurement.

We may thus at least say that the changes in radial velocity for the doubly ionized rare earths are in the same direction and of very nearly the same amount as those of the singly ionized rare earths. In fact, if we consider the uncertainties of the laboratory and stellar wave lengths, the radial velocities of *Eu* III, *Gd* III, and *Ce* III at phases 0^d44 and 1^d91 agree very well indeed in absolute value with the radial velocities of the lines of the cor-

responding singly ionized elements. It seems logical to assume that the changes in radial velocity which are found to be the same for the singly and the doubly ionized rare earths between phases 0^d44 and 1^d91 will also be the same for other phases, but this point has not been checked.

The ranges in line intensity of the doubly ionized rare earths also parallel those of the singly ionized elements. Among the latter, *Eu* II has the largest intensity range; this is also true of *Eu* III among the doubly ionized elements. Similarly, *Ce* III has a much smaller intensity range, just as *Ce* II does.

Hence it appears justifiable to conclude that, in a general way, singly and doubly ionized rare earths behave alike both in intensity and in radial velocity.

The next step consists in examining whether or not some of the strong unidentified lines measured in α^2 CVn are also attributable to doubly ionized rare earths. In the blue-violet region there are about a dozen unidentified lines which reach an intensity of 3 or more at certain phases.[4] Dr. King kindly examined his spectrograms of sparks of rare earths with a view to deciding whether spark lines, absent in the arc (hence presumably due to doubly ionized elements), appeared near the α^2 CVn wave lengths. Three of the α^2 CVn lines—λ 4447.6, λ 4621.2, and λ 4621.6—cannot be examined because they are too near *N* II lines, which are very strong on Dr. King's spectrograms. No coincidence was found with the sparks of *Eu* and *Gd;* but a strong *Dy* spark[7] revealed two diffuse lines of fair strength not present in the arc—hence probably due to *Dy* III—at λ 4410.0 and λ 4572.9, which are strong (maximum intensity 5) unidentified lines in α^2 CVn. These two α^2 CVn lines have a similar intensity behavior with phase and are definitely of class A.

Next a list was prepared of all the unidentified lines of α^2 CVn which reach an intensity of at least 2 at a given phase, from λ 3800 to λ 4723. While very few coincidences with *Eu* III or *Gd* III lines can be observed,[8] approximately 60 of the 90 unidentified lines coincide reasonably well with spark lines of *Dy*. Considering that a number of identifications are simply impossible on account of the presence of lines of *O* I, *O* II, *N* II, *Dy* I, and *Dy* II in the spark, the percentage of coincidences—about 75 per cent—appears rather convincing. Practically all the corresponding α^2 CVn lines behave with phase more or less like λ 4572.9; at any rate, very few intensity behaviors among the 60 coincidences indicate a different origin.

Because laboratory wave lengths are not very accurate, individual radial velocities have little if any meaning. But here again, as in the ultraviolet region, it is found that in a general way the radial velocities of the lines tentatively attributed to *Dy* III behave with phase exactly as the *Dy* II lines do. For lack of time, publication of the details of coincidences must be postponed.

Whether or not lines of doubly ionized rare earths appear in stellar spectra without the simultaneous presence of the singly ionized elements cannot be ascertained quite conclusively from the observational data available at present. The ultraviolet lines of *Eu* III, *Gd* III, *Ce* III, and *Sa* III are not found with certainty in the published lists of lines of α Cygni[9] and of the B stars,[10] while an unidentified line measured in 55 Cygni at λ 3517.15 is probably due to *La* III. On the other hand, many of the strongest unidentified lines of α^2 CVn in the violet-blue region coincide reasonably well with wholly or partly unidentified lines in the table of B-star lines published by H. Kühlborn.[11] This table is very com-

[7] The lines which appear to be due to *Dy* III are much stronger in the violet region than around λ 3200.

[8] The two unidentified α^2 CVn lines λ 4182.0 and λ 4422.2 coincide with *Eu* III lines.

[9] J. H. Rush, *Ap. J.*, **95**, 213, 1942; O. Struve, *Ap. J.*, **90**, 699, 1939; A. B. Wyse, *Lick Obs. Bull.*, **18**, No. 492, 129, 1938.

[10] Adams and Dunham, *Mt. W. Contr.*, No. 583; *Ap. J.*, **87**, 102, 1938; Struve, *loc. cit.*

[11] *Veröff. Univ.-Sternw. Berlin-Babelsberg*, **12**, 1, 1938.

plete, and, although the reality of some of the tabulated faint lines may be doubted, the very large percentage of excellent wave-length coincidences favors the conclusion that lines of doubly ionized rare earths are actually observed in the normal B-type stars, especially γ Pegasi.

The observations of α^2 CVn point thus to the following conclusions:

a) *Eu* III, *Gd* III, *Ce* III, *Sa* III, and *La* III are observed in the ultraviolet region.

b) The variations in intensity and radial velocity of these doubly ionized elements with phase are very similar to those of the singly ionized atoms.

c) Several unidentified lines in the blue-violet region are very probably due to *Dy* III and are probably present in ordinary B-type stars.

We do not know the values of the third ionization potentials of the rare earths except cerium, for which it is probably 19.5 v. The ultraviolet region corresponding to approximately 20 v. (λ 617 A) does not contain lines or continua that can be thought of as capable of affecting strongly the ionization in a stellar atmosphere, although certain *Ne* I, *Ne* I, and metallic lines may possibly have some effect.

At any rate the new observational data indicate that a number of previous suggestions concerning the abnormal intensities of lines of *Eu* II, *Gd* II, etc., have to be revised, since singly and doubly ionized elements behave exactly alike. In a search for an explanation of the spectroscopic anomalies of α^2 CVn and related stars, we shall possibly have to return eventually to a modernized version of the stratification phenomena first suggested by A. Fowler in 1913,[12] possibly combined with considerations of nonblack-body exciting radiation.

My cordial thanks are due to Dr. W. S. Adams and Dr. A. S. King for their generous help and encouragement.

[12] *Observatory*, **36**, 440, 1913.

THE RESOLUTION OF MESSIER 32, NGC 205, AND THE CENTRAL REGION OF THE ANDROMEDA NEBULA*

W. BAADE
Mount Wilson Observatory
Received April 27, 1944

ABSTRACT

Recent photographs on red-sensitive plates, taken with the 100-inch telescope, have for the first time resolved into stars the two companions of the Andromeda nebula—Messier 32 and NGC 205—and the central region of the Andromeda nebula itself. The brightest stars in all three systems have the photographic magnitude 21.3 and the mean color index +1.3 mag. Since the revised distance-modulus of the group is $m - M = 22.4$, the absolute photographic magnitude of the brightest stars in these systems is $M_{pg} = -1.1$.

The Hertzsprung-Russell diagram of the stars in the early-type nebulae is shown to be closely related to, if not identical with, that of the globular clusters. This leads to the further conclusion that the stellar populations of the galaxies fall into two distinct groups, one represented by the well-known H-R diagram of the stars in our solar neighborhood (the slow-moving stars), the other by that of the globular clusters. Characteristic of the first group (type I) are highly luminous O- and B-type stars and open clusters; of the second (type II), short-period Cepheids and globular clusters. Early-type nebulae (E–Sa) seem to have populations of the pure type II. Both types seem to coexist in the intermediate and late-type nebulae.

The two types of stellar populations had been recognized among the stars of our own galaxy by Oort as early as 1926.

In contrast to the majority of the nebulae within the local group of galaxies which are easily resolved into stars on photographs with our present instruments, the two companions of the Andromeda nebula—Messier 32 and NGC 205—and the central region of the Andromeda nebula itself have always presented an entirely nebulous appearance. Since there is no reason to doubt the stellar composition of these unresolved nebulae—the high frequency with which novae occur in the central region of the Andromeda nebula could hardly be explained otherwise—we must conclude that the luminosities of their brightest stars are abnormally low, of the order of $M_{pg} = -1$ or less compared with $M_{pg} = -5$ to -6 for the brightest stars in our own galaxy and for the resolved members of the local group. Although these data contain the first clear indication that in dealing with galaxies we have to distinguish two different types of stellar populations, the peculiar characteristics of the stars in unresolved nebulae remained, in view of the vague data available, a matter of speculation; and, since all former attempts to force a resolution of these nebulae had ended in failure, the problem was considered one of those which had to be put aside until the new 200-inch telescope should come into operation.

It was therefore quite a surprise when plates of the Andromeda nebula, taken at the 100-inch reflector in the fall of 1942, revealed for the first time unmistakable signs of incipient resolution in the hitherto apparently amorphous central region—signs which left no doubt that a comparatively small additional gain in limiting magnitude, of perhaps 0.3–0.5 mag., would bring out the brightest stars in large numbers.

How to obtain these few additional tenths in limiting magnitude was another question. Certainly there was little hope for any further gain from the blue-sensitive plates hitherto used, because the limit set by the sky fog, even under the most favorable conditions, had been reached. However, the possibility of success with red-sensitive plates remained. From data accumulated in recent years it is known that the limiting red magnitude which can be reached on ammoniated red-sensitive plates at the 100-inch in

* *Contributions from the Mount Wilson Observatory, Carnegie Institution of Washington,* No. 696.

reasonable exposure times is close to $m_{pr} = 20.0$, the limiting photographic magnitude being $m_{pg} = 21.0$. These figures make it clear at once that stars beyond the reach of the blue-sensitive plates can be recorded in the red only if their color indices are larger than +1.0 mag.—the larger, the better. Now there are good reasons to believe that the brightest stars in the unresolved early-type galaxies actually have large color indices. When a few years ago the Sculptor and Fornax systems were discovered at the Harvard Observatory, Shapley introduced these members of the local group of galaxies as stellar systems of a new kind.[1] Shortly afterward, however, Hubble and the writer pointed out that in all essential characteristics, particularly the absence of highly luminous O- and B-type stars, these systems are closely related to the unresolved members of the local group.[2] It was therefore suggested that in dealing with the Sculptor and Fornax systems "we are now observing extragalactic systems which lack supergiants and are yet close enough to be resolved." Since the brightest stars in the Sculptor system, according to later observations by the present writer, have large color indices (suggesting spectral type K), it appeared probable that this would hold true for the brightest stars in the unresolved members of the Andromeda group. Altogether there was good reason to expect that the resolution of these systems could be achieved with the 100-inch reflector on fast red-sensitive plates if every precaution were taken to utilize to the fullest extent the small margin available in the present circumstances.

Since success depended so much upon a careful use of the available light-intensities, it may be surprising that the final tests were made in the light of the narrow band λλ 6300–6700 (on ammoniated Eastman 103E plates behind a Schott RG 2 filter). The reason is the following: It is quite true that nearly twice the speed in the red could have been obtained if a yellow filter, transmitting wave lengths > λ 5000, had been used instead of the red filter. But experience has shown that the benefits to be derived from the larger range of wave lengths are of doubtful value, particularly in long exposures, because the larger range includes two of the strongest emission lines of the night sky—the green aurora line at λ 5577 and the red [*O* I] doublet λ 6300, λ 6364.

The red doublet at λ 6300, λ 6364 has proved to be especially troublesome for astronomical photography, partly because it falls into the region of maximum sensitivity of the E plates, partly because it displays erratic intensity changes from night to night and even in the same night. These changes are large, and it is well known that not infrequently, particularly at the times of sunspot maxima, the intensity of the red doublet surpasses that of the strong green line by a factor 2 or more. Consequently, it is impossible to predict whether on a given night the exposure time for the range λλ 5000–6700 has to be restricted to 1 hour or can be safely extended to several hours. To avoid any difficulties resulting from uncontrolled sky fog, which are especially serious for objects near the plate limit, it was decided to use the narrower range of wave lengths cut out by the RG 2 filter. Although this filter transmits about 24 per cent of the red doublet, no difficulties have thus far been encountered even with exposure times up to 9 hours. It may be remarked here that the plates to be discussed later are practically free from sky fog.

The minimum exposure times required with the RG 2 filter turned out to be 4 hours. Exposures of this length with a large reflector present a number of problems if critical definition is the prime requisite. That only nights with exceptionally fine definition, together with a practically perfect state of the mirror, would do hardly needs mention. Fortunately, these conditions are easily met on Mount Wilson during the fall months when the Andromeda region is in opposition. But real difficulties were presented by changes of focus during the relatively long exposures. On account of the normal drop in temperature during the night these changes are quite large under average conditions; hence repeated refocusing with the knife edge—usually once every hour—is necessary as the ex-

[1] *Nature*, **142**, 715, 1938; *Proc. Nat. Acad.*, **25**, 565, 1939.

[2] *Pub. A.S.P.*, **51**, 40, 1939.

posure proceeds. Although a special, precision-built plateholder arrangement is available for such purposes, its manipulation is always somewhat risky because the change from the field to a suitable focus star and back has to be made in complete darkness. Even if such repeated manipulations are performed without mishap during a prolonged exposure, the method remains a makeshift, since between two settings the plate will gradually move out of focus. To avoid both difficulties it seemed best to use only nights on which the focus-changes at the 100-inch are very small if not entirely negligible. Such conditions are not infrequently met on Mount Wilson during the fall, when, owing to a temperature inversion, the temperature stays practically constant all night. Neither was it difficult in the present case to select the proper nights. Since in the fall the Andromeda region culminates around midnight, a careful watch of the state of the mirror and of the temperature in the early evening hours permits a fair prediction of the focus-changes during the latter part of the night. Eventual small changes in focus during the exposure can then be inferred from changes in the coma of the guiding star. Although this method has fallen into disrepute because of some bad experiences of earlier observers, the writer has found it as good as the knife-edge test if the following conditions are fulfilled: (1) a nearly perfect figure of the mirror; (2) steady and crisp images; and (3) such an adjustment of the guiding eyepiece that small focus-changes produce marked changes in the coma pattern of the guiding star. All exposures discussed in the following pages have been made in this manner. As a control of the correct handling of the focus-changes, the focus was checked with the knife edge at the end of each exposure. In every case the difference between the last actually used focus and the knife-edge setting was well below 0.1 mm.

The plates of the Andromeda nebula, of Messier 32, and of NGC 205, taken in this manner at the 100-inch reflector during the fall months of 1943, led to the expected results. All three systems were resolved into stars. A description of the plates thus far obtained follows. Since the preparation of adequate reproductions would involve time-consuming experiments impossible under present conditions, illustrations will be published later. The plate of NGC 185 in the following *Contribution* will give the reader an idea how far the resolution of the hitherto unresolved systems of the local group has been successful.

I. *Messier 32, the brighter, round companion of the Andromeda nebula (ammoniated 103E plate behind Schott RG 2 filter, λλ 6300–6700; exposure 3^{h}30^m; August 25, 1943).*—The plate was obtained under ideal conditions: a perfect mirror, seeing 5–6, and no change in focus during the whole exposure (which was cut short by the oncoming twilight). As a result, the smallest stellar images on the plate have diameters of less than 0.7″ of arc.

The central part of Messier 32 is completely burned out, but the outer parts have disintegrated into an unbelievable mass of the faintest stellar images. The plate is of special interest because it shows in an instructive manner which features are the first signs of resolution in systems of this type. They are star chains, formed by accidental groupings of some of the brightest members of the system. Clearly resolved into stars on the red exposure, they were indicated on the best blue-sensitive plates taken previously, where they appear as very weak, ill-defined filaments in the otherwise amorphous structure of the nebula.

The extent of Messier 32—i.e., the distance to which its members can be traced—is difficult to ascertain, since a spiral arm of the Andromeda nebula sweeps over the field in such a way that at greater distances from the center of Messier 32 the members of both systems are hopelessly mixed. But there are indications that the situation is even more complicated. To gain more intensity, another 4-hour exposure of Messier 32 was made on August 26, 1943, this time behind a Schott GG11 filter, so that the plate covered the range from λ 5000 to λ 6700. It so happened that the sky began to brighten up after the exposure was started—probably on account of a diffuse aurora—with the result that the plate fog became rather dense. The plate is interesting, however, because it shows that

up to a distance of 17′ south of Messier 32 the field is covered with a stratum of extremely faint stars. Obviously these stars belong to the Andromeda nebula, since their slowly decreasing density in a southward direction follows the contour lines of the nebula. There seems to be little doubt that this mass of faint stars, in luminosity and color index similar to the brightest stars in Messier 32, is identical with the faint extension of the Andromeda nebula first recorded photoelectrically by Stebbins and Whitford.[3] On the plate just mentioned the stars can be traced along the minor axis of the Andromeda nebula to a distance of 32′ from the center, corresponding to the isophote 25.4 mag. per square second of arc (Stebbins and Whitford). Properly centered plates may well shift the limit farther out to lower isophotes.

II. *NGC 205, the fainter elliptical companion of the Andromeda nebula (ammoniated 103E plate behind Schott RG 2 filter, λλ 6300–6700; exposure 4 hours, September 29, 1943).*—During the 4-hour exposure thin haze occasionally drifted over the field, probably reducing the effective exposure time to 3½ hours. The plate was taken under excellent seeing conditions, but with a fast-deteriorating figure of mirror caused by rising temperatures. As a result the otherwise small and crisp images show an irregular flare which may have reduced both resolving-power and limiting magnitude. In spite of these shortcomings, NGC 205 is beautifully resolved up to the very nucleus. It is a much looser aggregation of stars than Messier 32, as was to be expected from its lower surface brightness.

In order to test how far the faint stars revealed on the red exposures are reproduced from one plate to another, a second plate of NGC 205, of only 90 minutes' exposure, was obtained in the larger range λλ 5000–6700 on December 23, 1943. This shorter exposure registers stars as faint as the earlier 4-hour exposure behind the RG 2 filter. The intercomparison of the two plates in the blink comparator showed that the pattern of resolution is identical on both plates, each configuration of faint stellar images on one plate being reproduced on the other. Undoubtedly, a small percentage of the images are still unresolved doubles and accidental groupings of stars, but the majority are certainly single stars. Intercomparison of the two plates led to the discovery of 3 faint variable stars which are undoubtedly members of NGC 205.

Nebulae of the globular type like NGC 205 have always presented the difficulty that their dimensions, as inferred from the extent of the nebulosity, were rather indeterminate. With the resolution of NGC 205 it has become possible to use a definition of the radius which has proved both significant and practical for globular clusters. The radius is defined as the maximum distance from the center up to which the members can be traced. The dimensions of NGC 205 derived in this manner are $2a = 15'.8$, $2b = 9'.1$. The only comparable value is that published by Reynolds,[4] who derived $2a = 12'$ from photometric measures on a plate taken with the Helwan reflector. Reynolds' value should be considered as a lower limit, since his plate was exposed for only 30 minutes.

Because the resolution of NGC 205 proved so easy in red light, a corresponding test on a fast blue-sensitive plate seemed to be of special interest. The nebula was therefore photographed at the 100-inch on the remarkably fast Eastman 103a-0 emulsion. The exposure time was 90 minutes, which represents about the practical limit for plates of this type. The plate reveals incipient resolution of NGC 205 quite unmistakably; but the prevailing pattern is still very soft, and the smallest elements are not yet stars but small-scale fluctuations in the stellar distribution. The resulting impression is very irritating to the eye. The nebulosity has lost its amorphous character, but nothing definite has yet emerged.

III. *The inner amorphous region of the Andromeda nebula (ammoniated 103E plate behind a Schott RG 2 filter, λλ 6300–6700; exposure 4 hours, September 28, 1943).*—The plate was taken under excellent conditions: a perfect mirror, seeing 3–6, focus-changes during the whole 4-hour exposure amounting to less than 0.1 mm. Since it was to be ex-

[3] *Proc. Nat. Acad.*, **20**, 93, 1934.

[4] *M.N.*, **94**, 519, 1933–1934.

pected that the nuclear region of the nebula would be burned out in a 4-hour exposure, the plate was centered on a point of the preceding major axis, 11′ distant from the nucleus. It shows the hitherto amorphous nebulosity disintegrated into a dense sheet of extremely faint stars, all close to the limit of the plate. As expected, the resolution decreases somewhat in the denser parts of the nebulosity but is easily traced to a point 3′.5 from the nucleus where the burnt-out area sets in. Altogether, there is not the slightest doubt that with the proper optical means the Andromeda nebula is resolvable into stars right up to the very nucleus.

The main facts presented in the preceding descriptions can be summarized in the following four statements:

1. By using red-sensitive plates we have recorded the brightest stars in the hitherto unresolved members of the local group of galaxies.
2. The apparent magnitudes of the brightest stars are closely the same in all three systems, a result which was to be expected because the three nebulae form a triple system.
3. At the upper limit of stellar luminosity, stars appear at once in great numbers in these systems. (In what have been termed the resolvable systems, the brightest stars increase very slowly in numbers for the first 1.0–1.5 mag. below the upper limit of luminosity.)
4. With our present instruments early-type nebulae can be resolved on red-sensitive plates if their distance modulus does not exceed that of the Andromeda group.

For an estimate of the apparent magnitude and the color index of the brightest stars in these systems the following data for NGC 205 are available. As mentioned previously, this nebula is not yet clearly resolved into stars on the fast blue-sensitive plate of 90 minutes' exposure, which, according to a comparison with S.A. 68 made on the same night, has a threshold photographic magnitude of $m_{pg} = 21.0$. But the plate leaves no doubt that the step required to reach full resolution is quite small. Comparison with the red plates and experience with the behavior of stellar images near the threshold value suggests that the required gain to bring out the brightest stars is of the order of 0.3–0.4 mag. We adopt, therefore, as photographic magnitude of the brightest stars in these systems $m_{pg} = 21.3$. With this figure fixed, the mean color index of the brightest stars follows at once. Since the threshold red magnitude for the red exposure is $m_{pr} = 20.0$,[5] we obtain for the mean color index of the brightest stars $\overline{CI} = +1.3$ mag. These figures explain why the red-sensitive plates solved our problem: they reached beyond the limits of the blue-sensitive plates because the brightest stars in these systems have color indices in excess of +1.0 mag. But the margin is small indeed, the excess amounting to only 0.3 or 0.4 mag.

With Hubble's distance modulus for the Andromeda group, $m - M = 22.2$, we would obtain as absolute photographic magnitude of the brightest stars $M_{pg} = -0.9$. However, it is now quite certain that Hubble's value of the distance modulus is somewhat too small. Intercomparisons of the Andromeda nebula with S.A. 68, in which a standard sequence of photographic magnitudes on the International System, down to $m_{pg} = 21.0$, has been established by the writer, show that Hubble's magnitudes in Messier 31 require the corrections shown in Table 1.

[5] This value is based on the following data: A 15-minute exposure of the Polar Sequence on an ammoniated 103E plate behind the GG11 filter at the 60-inch reflector shows stars down to $m_{pv} = 17.44$. This value refers to stars of the mean color index +0.86 mag. Since the color scale for the red plates (range λλ 5000–6700) is 1.15 times as wide as that for the photovisual plates, the corresponding red threshold value is $m_{pr} = 17.31$. For the same exposure at the 100-inch the threshold value will be $m_{pr} = 17.31 + 1.10 = 18.41$, and for an exposure time of 90 minutes $m_{pr} = 18.41 + 1.63 = 20.0$, since there is good experimental evidence that the old rule, that increasing the exposure time by a factor 3 results in a gain of 1.0 mag. for threshold values, holds also for the ammoniated 103E plates.

These corrections refer to Hubble's region 4 (48′ south preceding the nucleus), where most of his variables are located. They are probably representative of the whole material. A final discussion will be presented later after all intercomparisons of S.A. 68 with M 31 have been reduced.

Since Hubble used m_{max} instead of m_{med} in the period-luminosity relation and since his values of m_{max} range from 18.1 to 19.3, the scale correction to be applied to the distance modulus turns out to be +0.45 mag. But Hubble's distance modulus is based on the old period-luminosity relation of *Harvard Circular*, No. 280, the zero point of which requires the correction of −0.23 mag. in order to reduce it to the one commonly used in recent years. The distance modulus of the Andromeda nebula on the present system is therefore $m - M = 22.4$. If this value is adopted, the absolute photographic magnitude of the brightest stars in the central region of the Andromeda nebula and in Messier 32 and NGC 205 becomes $M_{pg} = -1.1$.

TABLE 1

m_{pg} (Hubble)	Correction
18.30	+0.35 mag.
18.85	+ .42
19.23	+ .47
19.74	+ .57
20.00	+0.63

With these data at hand we are in the position to draw an important conclusion regarding the Hertzsprung-Russell diagram of the stars in early-type nebulae. As pointed out earlier, it has been known for some time that the highly luminous stars of the main branch (O- and B-type stars), together with the supergiants of types F–M, are absent in these systems; in fact, their absence was the reason why up to now the early-type nebulae have proved to be unresolvable. But neither are the brightest stars which we find in them the common giants of the ordinary H-R diagram, because as a group they are nearly 3 mag. brighter (the average early K-type giant of the H-R diagram has the absolute photographic magnitude $M_{pg} = +1.7$, compared with $M_{pg} = -1.1$ for the mean absolute magnitude of the brightest stars in the early-type nebulae).

It is significant that the same situation is known to exist in the globular clusters. Table 2 serves to illustrate this point. It gives M_{25}—the mean absolute photographic magnitude of the 25 brightest stars in a globular cluster—as a function of M_t, the total brightness (stellar content) of the cluster. Only clusters with distance moduli determined from cluster-type variables have been used. Table 2 shows that for the richest globular

TABLE 2

DATA FOR GLOBULAR CLUSTERS

M_t	M_{25}
−8.12	−1.32
−7.70	−1.21
−7.22	−1.14
−6.70	−1.03
−5.65	−0.55

clusters M_{25} is −1.3, compared with $M_{pg} = -1.1$ for the brightest stars in NGC 205. Now M_{25} in globular clusters and our mean value for the brightest stars in NGC 205 should be closely comparable; for although the value for NGC 205 refers to the several hundred of its brightest stars, it should define nearly the same group of stars as M_{25} in the clusters, because the population of NGC 205, according to its luminosity, exceeds that of the richest globular clusters by a factor 10 to 20. The agreement of the values quoted above is therefore as good as one could expect.

Similarly, there is perfect agreement in the color indices of the brightest stars in early-type nebulae and globular clusters. We derived $CI = +1.3$ mag. for the brightest stars in NGC 205, a value identical with that found by H. Shapley in globular clusters.[6]

We conclude, therefore, that, within the present uncertainties, absolute magnitude and color index of the brightest stars in early-type nebulae are the same as those of the brightest stars in globular clusters. However, the similarity of the stellar populations of early-type nebulae and globular clusters does not end here; for there are strong indications that another, even more unique feature of the H-R diagram of the globular clusters is shared by the stars of the early-type nebulae.

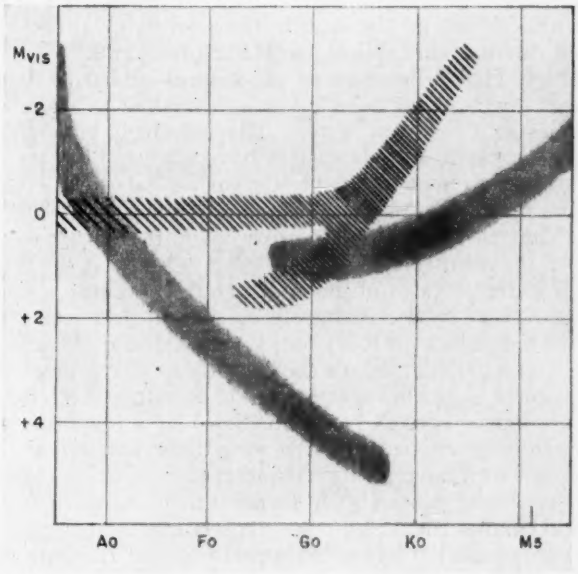

FIG. 1.—Shaded areas: ordinary H-R diagram (type I). Hatched area: H-R diagram of stars in globular clusters (type II).

Figure 1 represents schematically the H-R diagrams of the stars in the neighborhood of the sun (*shaded*) and of those in globular clusters (*hatched*). To conform with the usual practice, photovisual magnitudes have been used for the absolute magnitudes; hence the brightest stars in globular clusters appear now as stars of $M_{pv} = -2.4$. Both the dispersion and the frequency of the stars have been roughly indicated to convey an idea of the distribution of the two groups of stars in the H-R plane.

As already remarked, the H-R diagram for globular clusters begins with early K-type stars of $M_{pv} = -2.4$. On its downward slope the giant branch soon splits into two separate branches, the one continuing more or less in the original direction, the other proceeding nearly horizontally from spectral type G through F and A into the early B's. For our following argument we are concerned with this horizontal branch of the cluster diagram, which is remarkable for two reasons: (1) it sweeps through the well-known Hertzsprung gap of the ordinary H-R diagram; or, to put it differently, stellar states which seem to be excluded in the ordinary H-R diagram for galactic stars in our neighborhood are quite frequent in the H-R diagram of the globular clusters; (2) the short-period Cepheids,

[6] *Star Clusters* ("Harvard Observatory Monographs," No. 2), p. 29, 1930.

which are such a characteristic feature of the globular clusters, are located along this horizontal branch of the cluster diagram.

In a very interesting paper M. Schwarzschild[7] has recently shown that, if the mean absolute magnitudes and the mean color indices of the short-period Cepheids in a cluster are used as co-ordinates, their domain is restricted to a well-defined, exceedingly narrow strip within the horizontal branch. More than that, Schwarzschild produces excellent evidence that any cluster star located within this strip is actually a cluster-type variable. This suggests the following interpretation: Since the short-period Cepheids are localized in a well-defined, narrow strip of the H-R plane, they can be expected in considerable numbers only in stellar populations which possess a high density in this particular region of the H-R plane. This condition is fulfilled by the H-R distribution of the stars in globular clusters.[8] It is not fulfilled by the stars in the solar neighborhood (the slow-moving stars) because their distribution exhibits the Hertzsprung gap.[9]

Obviously, the early-type nebulae are in this respect similar to the globular clusters, for we know at least one globular nebula which, according to all indications, is rich in cluster-type variables—the Sculptor system. This extremely loose globular aggregation of stars and the similarly built Fornax system have already been mentioned in this paper. That both systems are closely related to the early-type nebulae follows at once from the fact that their brightest stars have the same luminosity as the brightest stars in globular clusters,[10] but their unusual structure made it difficult to assign them their proper places among the nebulae. It has since become clear that the Sculptor and Fornax systems are merely extreme cases of globular nebulae, because a continuous series of forms, apparently governed by decreasing stellar content, has been established between the highly concentrated objects of this class, such as Messier 32, and the Sculptor and Fornax structures.[11] As a globular nebula the Sculptor system is of particular interest because it is the only object of its kind near enough to permit a search for cluster-type variables. That they are indeed present has been shown by a preliminary test made a few years ago.[2] Although only one pair of plates were intercompared at that time, some 40 variables were found which have all the characteristics of being cluster-type variables. Undoubtedly a more thorough search will increase their number considerably. Because there is every indication that the Sculptor system is rich in cluster-type variables, we conclude that its stellar population has a high density in the Hertzsprung gap, similar to that observed in the globular clusters.

[7] *Harvard Circ.*, No. 437, 1940.

[8] At first sight, Messier 13, one of the richest globular clusters but exceptionally poor in short-period Cepheids, seems to present difficulties. But the reason why Messier 13 is so deficient in cluster-type variables is quite apparent from its H-R diagram if the accurate distance modulus recently derived by H. Sawyer-Hogg (*Pub. Dunlap Obs.*, Vol. 1, No. 11, 1942) is used. It turns out that the horizontal branch which contains the cluster-type variables is represented in Messier 13 by only a few scattered stars. Obviously, the strength of the horizontal branch varies from cluster to cluster, with Messier 13 and 47 Tucanae at the one extreme, Messier 3 and ω Centauri at the other. The peculiar conditions in Messier 13, therefore, only strengthen our argument.

[9] We have convincing proof that the rich star clouds of the Milky Way do not contribute to the number of the cluster-type variables. In a thorough search for variables in a selected field of the Cygnus cloud (Baade, *A.N.*, **232**, 65, 1928) it was found that, in contrast to all other types of variables which occur in the cloud in large numbers, the cluster-type variables brighter than magnitude 16.0 are represented in exactly the same number (1 variable per 1.6 square degrees) in which they are found in fields near the galactic north pole. The result is conclusive, because recent investigations have shown that for this particular field of the Cygnus region space absorption up to 10 kpc and more is negligible (cf. Oort and Oosterhoff, *B.A.N.*, **9**, 325, 1942).

[10] It should be pointed out that the value for the upper limit of luminosity in the Sculptor system, $M_{pg} = -1.8$, published in the earlier note, and the value derived in the present paper for NGC 205, $M_{pg} = -1.1$, are not contradictory. The former is an attempt to define the brightest member of the Sculptor system, the latter is the mean magnitude of the 100 or more brightest stars in NGC 205.

[11] *Mt. W. Contr.*, No. 697; *Ap. J.*, **100**, 147, 1944.

We thus have two strong arguments which indicate that the H-R diagrams of globular clusters and of early-type nebulae are similar, if not identical:

1. In both populations the brightest stars are K-type stars of $M_{pg} \sim -1.1$.
2. In both populations the distribution in the H-R plane is characterized by high density in the Hertzsprung gap, with the resulting appearance of cluster-type variables.

But we can advance a third argument which explains at the same time why the globular clusters happen to be the prototypes of this peculiar type of stellar population which we will call type II in distinction from populations defined by the ordinary H-R diagram —type I. This is the fact that, as far as the present evidence goes, globular clusters are always associated with stellar populations of type II. A good example is our own galaxy, where the globular clusters clearly have the same spatial distribution as the cluster-type variables which are representative of the stars of the second type. It is also significant that among the nebulae composed solely of stars of type II even the absolutely faintest usually have one or two globular clusters. Examples are NGC 205, the Fornax system, and the two faint globular nebulae NGC 147 and NGC 185, discussed in the following paper. This association suggests that globular clusters are properly regarded as condensations in stellar populations of the second type. Under these circumstances it is hardly surprising that their H-R diagram should be essentially identical with that of the larger populations of which they are members.[12]

Although the evidence presented in the preceding discussion is still very fragmentary, there can be no doubt that, in dealing with galaxies, we have to distinguish two types of stellar populations, one which is represented by the ordinary H-R diagram (type I), the other by the H-R diagram of the globular clusters (type II) (see Fig. 1). Characteristic of the first type are highly luminous O- and B-type stars and open clusters; of the second, globular clusters and short-period Cepheids. Early-type nebulae (E–Sa) seem to have populations of pure type II. Both types coexist, although differentiated by their spatial arrangement, in the intermediate spirals like the Andromeda nebula and our own galaxy.[13] In the late-type spirals and in most of the irregular nebulae the highly luminous stars of type I are the most conspicuous feature. It would probably be wrong, however, to conclude that we are dealing with populations of pure type I, because the occurrence of globular clusters in these late-type systems, for instance, in the Magellanic Clouds, indicates that a population of type II is present too. Altogether it seems that, whereas stars of the second type may occur alone in a galaxy, those of type I occur only in association with type II.

In conclusion it should be pointed out that these same two types of stars were recognized in our own galaxy by Oort as early as 1926.[14] Oort showed that the high-velocity stars of our galaxy (our type II) are of a kind quite different from the slow-moving stars (type I) which predominate in the solar neighborhood. Since his conclusions are based on entirely different material and since they supplement those derived in the present paper, they are worth recalling. They may be summarized as follows: (1) stars belonging to the upper main branch of the ordinary H-R diagram (highly luminous O- and B-type stars) are practically absent among the high-velocity stars; (2) the mean absolute magnitude of dwarfs of a given spectral type seems to be the same for high- and low-velocity stars; (3)

[12] Similarly, we should regard the open clusters as condensations in populations of type I, an interpretation which hardly needs comment in view of the intimate association of open clusters and slow-moving stars in our own galaxy. It is the more acceptable because it would ascribe the curious variations in the composition of open clusters (Trumpler's types) to the large-scale variations in the composition of populations of type I which have been noted not only in our own galaxy but also in several of the nearer extragalactic systems.

[13] The strong concentration of both globular clusters and short-period Cepheids toward the center of our galaxy indicates that the main mass of the stars of type II is located in this region, which, in turn, suggests a structure of our galaxy very similar to that of the Andromeda nebula.

[14] *Groningen Pub.*, No. 40, 1926.

the relative proportion of dwarfs to giants is much higher among the high-velocity stars than among the ordinary stars; (4) the percentage of double stars is two to three times lower among the high-velocity stars.

Conclusion 1 is in perfect agreement with the result derived in the present paper. Of special interest are conclusions 2 and 3, because they contain the first information about the dwarf branch in populations of type II. Obviously, the dwarf branch of stars of type II coincides closely with the dwarf branch of the ordinary H-R diagram. But the number of dwarfs, as we proceed to fainter absolute magnitudes, increases much faster in type II than in type I. It is very probable that this difference between the two populations is the basis for the well-known empirical criterion by which we distinguish globular clusters from open clusters and which may be stated as follows: Of two clusters with the same number of giant stars, the globular cluster has a much richer background of dwarfs than the open cluster.

It must be left to future investigations to fill in the gaps in our present knowledge of populations of type II. What is particularly needed is a representative H-R diagram for stars of this type. For a check of the upper part of the diagram, which at present is based solely on stars in globular clusters, the Sculptor system will be an ideal object. Data about the dwarf branch can be obtained either from an extension of Shapley's earlier investigations of magnitudes and colors in globular clusters or from the high-velocity stars in the solar neighborhood. The structure of the dwarf branch in populations of type II will be of special interest, since recent investigations by G. P. Kuiper[15] and by D. M. Popper[16] have shown that the so-called subdwarfs of our neighborhood are high-velocity stars and hence stars of type II.

Another interesting problem which deserves attention concerns the spectral peculiarities in stars of type II. W. W. Morgan and P. C. Keenan[17] have recently pointed out that for the late-type high-velocity stars α Boo, δ Lep, and Boss 2527 the spectroscopic criteria of luminosity lead to contradictory results. Judged by the weakness of the *CN* break at λ 4215, these stars would be subgiants or dwarfs, whereas the intensity ratio *Fe* I λ 4071:*Sr* II λ 4077 indicates that they are giants. In view of these discrepancies, Morgan and Keenan conclude that "high-velocity stars like Boss 2527, δ Lep, and α Boo appear to be the only stars likely to cause serious trouble in using the method of spectroscopic parallaxes." All three stars, which according to their trigonometric parallaxes are giants, fall in the range from G5 to K1. Other peculiarities may be expected in those stars of type II that lie in the Hertzsprung gap, but little seems to be known about their spectra.

[15] G. P. Kuiper, paper presented at the Colloquium on Novae, Supernovae, and White Dwarfs, Paris, 1939.

[16] D. M. Popper, *Ap. J.*, **95**, 307, 1942; **98**, 209, 1943.

[17] *An Atlas of Stellar Spectra* ("Astrophysical Monographs"), Chicago, 1943.

NGC 147 AND NGC 185, TWO NEW MEMBERS OF THE LOCAL GROUP OF GALAXIES*

W. BAADE
Mount Wilson Observatory
Received May 15, 1944

ABSTRACT

NGC 147 and NGC 185—two elliptical nebulae which form a physical pair—have been resolved into stars at the 100-inch reflector on red-sensitive plates. They are new members of the local group of galaxies, of absolute magnitudes −10.3 and −10.6, respectively. In structure they are intermediate between systems like NGC 205, in which the first departures from the highly concentrated form of the typical E-type nebula are noticeable, and the extremely loose Sculptor and Fornax systems. The addition of NGC 147 and NGC 185 increases the number of recognized members of the local group of galaxies to thirteen. A few features of this nearest sample of galaxies are discussed.

It has been shown in the preceding paper[1] that by means of red-sensitive plates early-type nebulae can be resolved with the 100-inch telescope if their distance does not exceed 300 kpc. Since this distance coincides with the presently adopted outer limit of the local group of galaxies, resolvability into stars provides a convenient criterion by which we may distinguish early-type nebulae within the local group from those outside of it. We are thus able to extend the search for new members of the local group to nebulae of the classes E–Sa.

In the present paper the new criterion is applied to the two elliptical nebulae NGC 147 and NGC 185. Their co-ordinates are shown in the accompanying table. The two systems, with an angular separation of 58 minutes of arc, obviously form a physical pair.

	NGC 147	NGC 185
Right ascension (1900.0)	0^h27^m7	0^h33^m4
Declination (1900.0)	+47°57′	+47°47′
Galactic longitude	87.9°	88.9°
Galactic latitude	−14.0°	−14.2°

Association with the Andromeda nebula is suggested by their small angular distance from this nebula—a little over 7°. Both NGC 147 and NGC 185 are rather inconspicuous objects, with photographic magnitudes of 12.1 and 11.8, respectively, according to the Shapley-Ames *Catalogue*. They were suspected of being members of the local group of galaxies for the following reasons: (1) With both are associated a few globular clusters which have angular diameters comparable to those of the globular clusters in the Andromeda nebula. (2) According to N.U. Mayall, the radial velocity of NGC 185 is −270 km/sec,[2] which, after allowance for galactic rotation, corresponds to a peculiar radial velocity of −50 km/sec. Both facts indicated that NGC 147 and NGC 185 are near-by systems, comparable in distance to the Andromeda group. Red exposures, taken at the 100-inch reflector, fully confirmed this surmise. Both systems were easily resolved into stars. As far as can be judged from these plates, the brightest stars in NGC 147 and NGC

* *Contributions from the Mount Wilson Observatory, Carnegie Institution of Washington*, No. 697.

[1] *Mt. W. Contr.*, No. 696; *Ap. J.*, **100**, 137, 1944.

[2] Unpublished. The writer is greatly obliged to Dr. Mayall not only for calling attention to the low radial velocity of NGC 185 but also for some stimulating discussions about the nature of NGC 147 and NGC 185.

185 are of closely the same apparent magnitude as those in Messier 32, NGC 205, and the inner part of the Andromeda nebula.

NGC 147 (ammoniated 103E plate behind Wratten 29F filter, λλ 6000–6700, 4-hour exposure, October 25, 1943).—This nebula, described in the *N.G.C.* as vF, vL, iR, is one of the most disappointing objects when photographed on ordinary blue-sensitive plates. Even the longest exposures at the Mount Wilson reflectors reveal little more than an ill-defined elongated patch of very faint nebulosity, some $6' \times 3'$ in diameter. The only structural detail to speak of is a semistellar nucleus, of about the nineteenth magnitude, at the center. Close to the nebula and undoubtedly associated with it are two globular clusters, unresolved, but very similar in structure and diameter to those known in the Andromeda nebula. On the basis of these meager data it would obviously be very difficult to assign NGC 147 to any of the known types of nebulae. Elongation and lack of structure might suggest an elliptical nebula, but it would be a very abnormal specimen of this class because of the barely perceptible concentration toward the center. Alternatively, it might be a very faint spiral with abnormally weak spiral arms.

In contrast to the uncertain information provided by the blue-sensitive plates the 4-hour red exposure of NGC 147 is truly revealing. It shows that the nebula is a large star cloud, ellipsoidal in structure and of a density gradient so low that even the central region is fully resolved. The stars can be traced along the major axis to 7.1 minutes of arc from the center, along the minor axis to 4.5 minutes. According to all indications the brightest stars in NGC 147 are of about the same apparent magnitude as those in Messier 32, NGC 205, and the central region of the Andromeda nebula. We can therefore adopt as the provisional distance modulus of NGC 147, $m - M = 22.4$.[3] The resulting absolute magnitude of NGC 147 is $M_{pg} = -10.3$, the faintest thus far observed for a galaxy.

NGC 185 (ammoniated 103E plate behind Wratten 29F filter, λλ 6000–6700, 4-hour exposure, October 23, 1943).—NGC 185, considerably brighter than NGC 147, has been classified by E. P. Hubble[4] as Ep, the peculiarity being the abnormally slow increase in intensity toward the center. It is intermediate in this respect between NGC 205, similarly classified by Hubble as Ep, and NGC 147. NGC 185 is one of the few elliptical nebulae in which patches of obscuring material are conspicuous. Two such dark clouds are near the center of NGC 185. The only other notable features are two globular clusters, similar in structure and diameter to those of NGC 147. They are easily identified on Plate VI, where they have the co-ordinates 12.4 mm east, 3.5 mm south and 33.0 mm east, 37.3 mm north, referred to the center of NGC 185.

On the red exposure, NGC 185 is beautifully resolved into stars. It is best described as a slightly elongated, giant globular star cluster (see Pl. VI and the photographic insert[5]).

[3] See *Mt. W. Contr.*, No. 696; *Ap. J.*, **100**, 142, 1944.

[4] *Mt. W. Contr.*, No. 324; *Ap. J.*, **64**, 321, 1926. The fact that H. D. Curtis classified NGC 185 in *Lick Obs. Pub.*, **13**, as an irregular spiral shows that the real nature of these peculiar elliptical systems is not easily recognized as long as they remain unresolved.

[5] The photographic enlargement (2.7 X the original) will enable the reader to form his own judgment regarding the resolution of early-type nebulae on recent negatives. Two points may be mentioned in particular. (1) An examination of the halation rings around the brighter stars shows clearly that the grain pattern of the emulsion is very much smaller than that produced by the numerous faint stars in the nebula. (2) The resolution decreases markedly with the distance from the optical axis. Thus the south-preceding part of the nebula, which was closer to the optical axis, is better resolved than the north-following part, where the coma begins to cause blurring. As a result of the attempt to bring out the faintest stars on the photograph, the intensity gradient in the central region of the nebula has been badly exaggerated. The actual intensity distribution within NGC 185 is very well reproduced on the halftone (Pl. VI).

[The photographic reproduction on the opposite page is from a negative of NGC 185 by Dr. Baade. North is toward the binding; west is at top of page. The prints were made at the Yerkes Observatory by the Misses Maude Laidlaw and Doris Blakeley, under the supervision of Dr. W. W. Morgan from a duplicate negative prepared at Pasadena by Mr. E. R. Hoge.—EDITOR.]

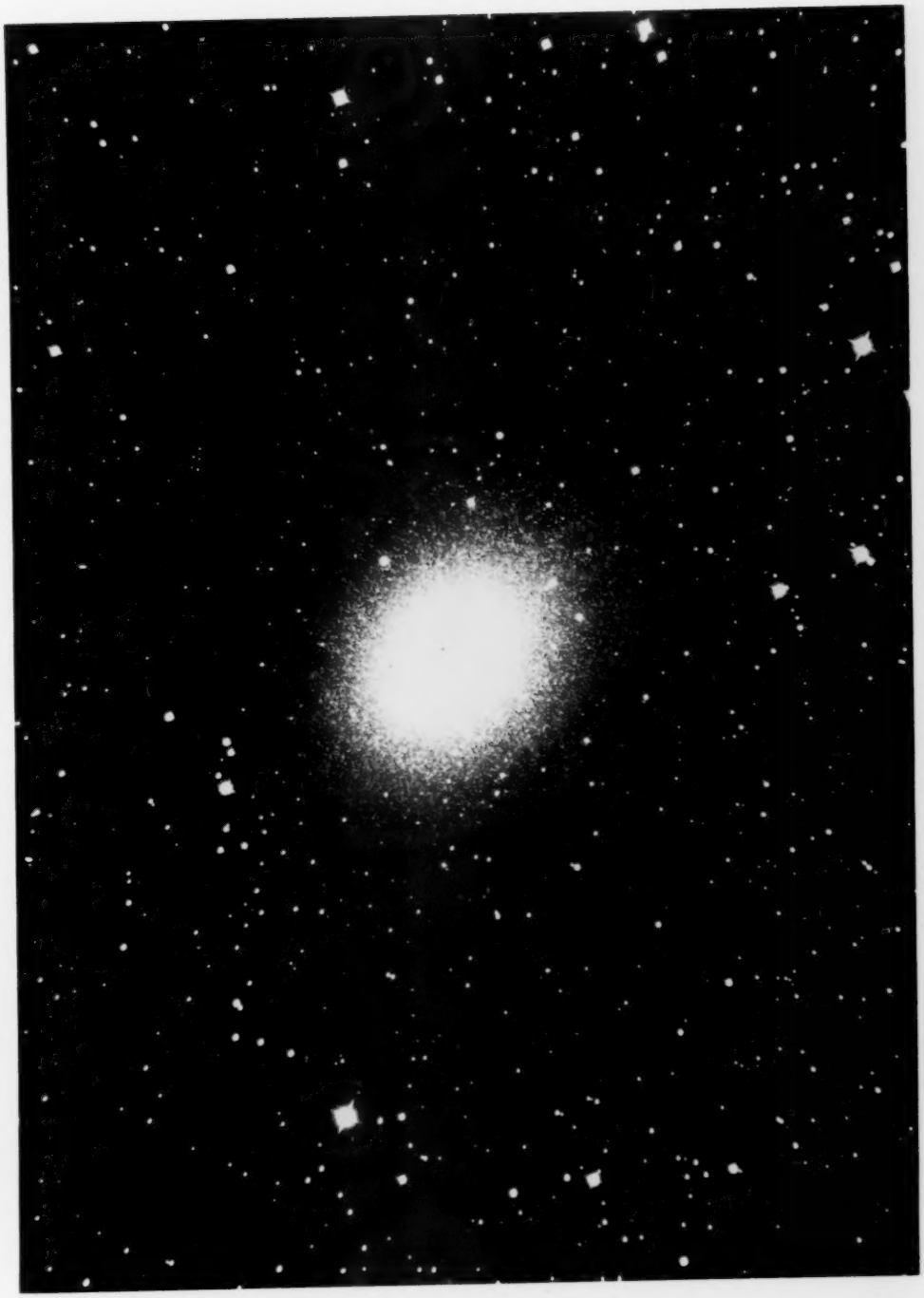

PLATE VI

N

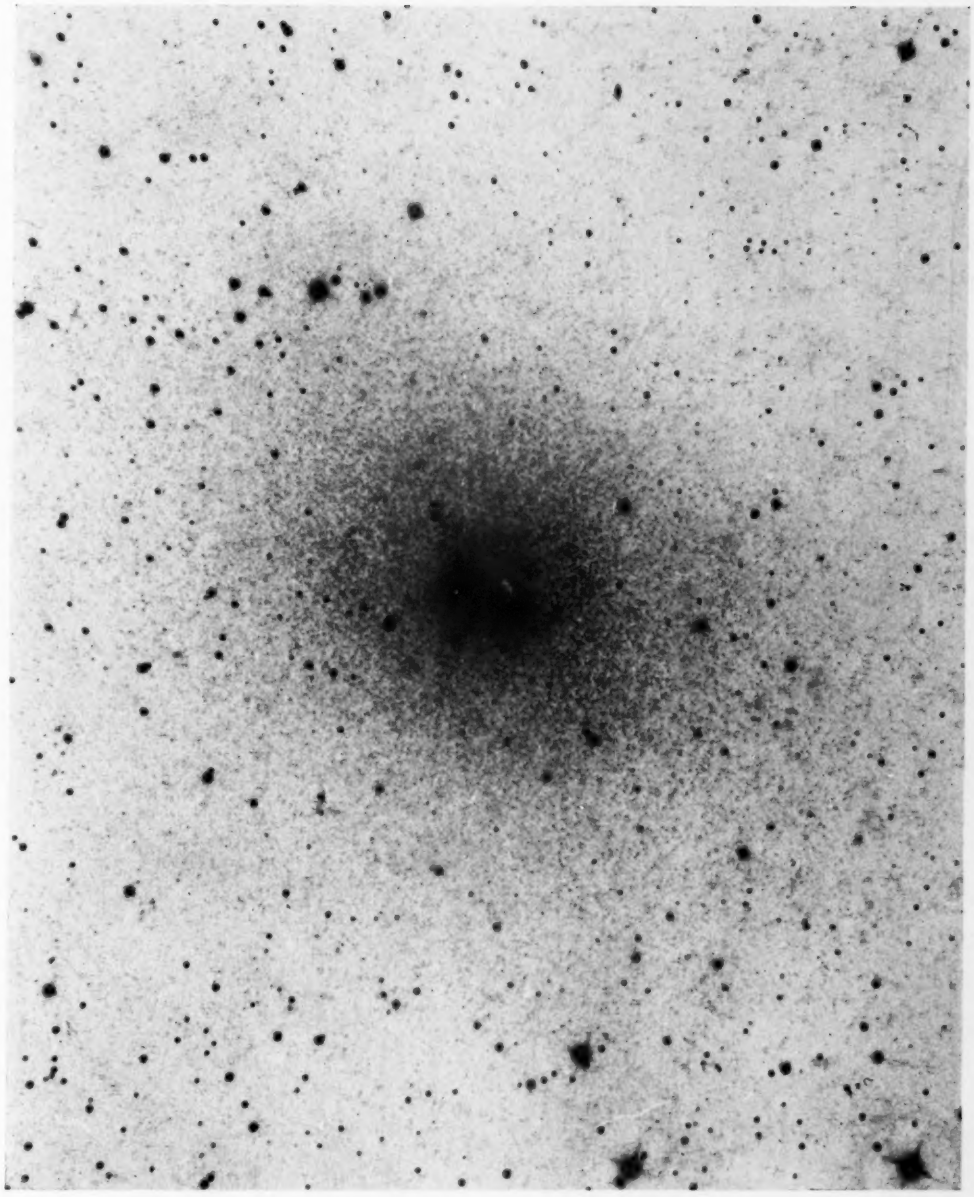

W

NGC 185

Four-hour exposure in red light (λλ 6000–6700) at 100-inch telescope, October 23, 1943. Scale, 1 mm = 4″.64.

A photographic reproduction of the same negative, scale 1 mm = 5″.89, faces page 148.

There is no nucleus, and the intensity distribution in the central region is very similar to that observed in rich globular clusters. The over-all dimensions of NGC 185, determined from its most distant members, are $14'.5 \times 12'.3$. As in NGC 147, the apparent magnitude of the brightest stars indicates a distance modulus closely comparable to that of the Andromeda group. The resulting absolute magnitude of NGC 185 is $M_{pg} = -10.6$.

The data presented in the preceding descriptions show that NGC 147 and NGC 185 are elliptical nebulae of very low luminosity. In structure they deviate considerably from what is considered the typical E-type nebula. In both objects the density gradient is abnormally low, and the central nucleus is either very faint, as in NGC 147, or absent, as in NGC 185. What makes the two nebulae especially interesting is the fact that they represent intermediate forms between systems like NGC 205, in which the first marked deviations from the intensity distribution of the typical E-type nebula are apparent, and the Sculptor and Fornax systems—globular systems of such a low concentration that observers have hesitated to assign them to the group of elliptical nebulae. The sequence of forms just mentioned leaves not the slightest doubt that the Sculptor and Fornax systems are extreme cases of this group—an interpretation supported by the fact that they are composed of populations of the pure type II.[1] Altogether, it seems that a marked change in the internal structure of the E-type nebulae takes place as we reach the systems of lowest luminosity. The strong concentration toward the center and the central nucleus disappear gradually until we encounter such limiting forms as the Sculptor and the Fornax systems. It is probably significant that a similar series of open structures makes its appearance among the globular clusters of lowest luminosity, with objects like NGC 5053 and NGC 6366 the perfect analogues of the Sculptor and Fornax systems. But not all globular clusters of low luminosity are of low concentration. The exceptional case of NGC 4147—a cluster comparable in stellar content to NGC 5053 but highly concentrated—shows that concentrated forms, although evidently very rare, occur simultaneously with the predominant loose structures. Whether this holds true for the E-type nebulae can be decided only by future discoveries.

As pointed out previously, the distance modulus of NGC 147 and NGC 185, judged by the magnitudes of their brightest stars, is closely the same as that of the Andromeda nebula, $m - M = 22.4$. Allowance for galactic obscuration (latitude effect) reduces this value to $m - M = 21.5$, corresponding to a distance of 205 kpc. The projected linear separation of the pair amounts to 3.5 kpc, its distance from the Andromeda nebula to 40 kpc. The latter value suggests that NGC 147 and NGC 185 are companions of the Andromeda nebula.

The addition of NGC 147 and NGC 185 increases the number of recognized members of the local group of galaxies to thirteen. All are listed in Table 1.

The list shows that the dwarfs now outnumber the giants almost in the ratio of two to one. Since it is certain that all the giant members of the group are known, future additions will only increase this ratio. Although caution is necessary in basing conclusions on a sample as small as the local group, there seems little doubt that the large percentage of dwarf systems is significant and that the symmetrical form of the luminosity function hitherto adopted has to be replaced by a skew distribution. In particular, it seems certain that the present value for the dispersion, $\sigma = 0.85$ mag., is too small because it does not allow for the high frequency of systems with luminosities below $M = -11.6$.

Another notable feature of the list is the percentage of the elliptical systems (E-types) which now make up nearly one-half of the total. All belong to the dwarf class and, with one exception, to the peculiar series which is characterized by low concentration. Since the search for group members of the elliptical type has hardly begun, a further increase of the E-types is to be expected.

Finally, our data throw some interesting light on the frequently discussed relation between elliptical nebulae and globular clusters. Because some of the richest globular clusters have luminosities almost comparable with those of the faintest elliptical galaxies, it

has been argued that globular clusters might be the continuation of the sequence of elliptical nebulae. The data now at hand do not support this view. According to Table 1 the linear diameters of the faintest elliptical galaxies range from 1.1 to 0.8 kpc if the most distant stars in each system are used to determine its extent. On the other hand, the linear diameters of the richest and largest globular clusters of our galaxy, determined in

TABLE 1

MEMBERS OF THE LOCAL GROUP OF GALAXIES

MEMBER	TYPE	MODULUS		DISTANCE (CORR. FOR LAT. EFFECT)	M_{pg}	DIAMETER	
		Obs.	Corr.			Apparent	Linear
Our galaxy	Sb	.....	.....	.....	.....	.....	24 kpc
M 31	Sb	22.4	21.8	231 kpc	−17.9	3.2°	12.9
LMC	I	17.1	16.7	22	−15.9	12°	4.6
M 33	Sc	22.3	21.9	239	−14.9	62′	4.3
SMC	I	17.3	17.0	25	−14.5	8°	3.6
M 32	E2	22.4	21.8	231	−12.9	.....	.....
Fornax system	E	21.0:	20.8:	142:	−11.9:	50′	2.1:
NGC 205	E5p	22.4	21.8	231	−11.5	15′.8	1.1
NGC 6822	I	21.6	21.0	161	−10.8	20′	0.94
IC 1613	I	22.0	21.8	225	−10.8	17′	1.1
Sculptor system	E	19.4	19.2	69	−10.6	45′	0.90
NGC 185	E	22.4±	21.5±	204±	−10.6	14′.5	0.86
NGC 147	E	22.4±	21.5±	204±	−10.3	14′.1	0.83

the same manner, are only of the order of 0.1 kpc. Even if highly concentrated forms should occur among the elliptical nebulae of lowest luminosity, it is highly improbable that they would bridge the gap in the linear dimensions of the two groups. What distinguishes a globular cluster from an elliptical galaxy is its mean mass density, which surpasses that of an elliptical galaxy by a factor of the order of 40–100. It has been pointed out in the preceding paper[1] that globular clusters should be regarded as condensations in stellar populations of type II. The high mean density in globular clusters compared with that in elliptical galaxies supports this view.

THE HELIUM ANOMALY IN ϕ PERSEI

J. A. HYNEK[1]
Perkins Observatory
Received June 14, 1944

ABSTRACT

All available velocity measures from the helium singlet (λ 3965) and triplet (λ 4026 and λ 4471) lines in the spectrum of ϕ Persei are gathered and discussed. The previously announced anomalous behavior of the triplet lines is corroborated by new observational material and by heretofore unpublished measures by Jordan. The triplet lines are shown to be composite and the velocity-curve from the major component to be complex, one part corresponding to the phase of great enhancement of the helium lines (45–70 days) and the other to the rest of the cycle of 126.696 days, during which time the lines are much fainter and of different character. Both parts differ from the velocity-curves of the Balmer lines and of *He* λ 3965. Probable errors of the triplet-line measures during the weak phase are small and indicate that the velocity-curve obtained from them is entitled to definite weight in the general problem of ϕ Persei.

The anomalous behavior of the helium triplet lines in the spectrum of ϕ Persei was first described several years ago[2] in the course of a detailed treatment of the spectrum features of this well-known Be star. The star ϕ Persei has a variable radial velocity with a period of 126.696 days. This variation, however, is common only to the sharp Balmer lines and to the singlet line of helium, λ 3965; *Ca* K and *Fe* II show small variation, while the helium triplet lines λ 4026 and λ 4471, when definitely measurable, show radically different velocities, which are, for the most part, 180° out of phase with the Balmer velocities. The triplet lines at certain phases are clearly composite, and, when both components are measurable, one component is in rough agreement with the Balmer lines, while the other is out of phase. When blended, intermediate values of the velocity are obtained.

The obvious interpretation of a binary with two spectra, however, cannot be made with impunity, since neither the Balmer curve, the *He* λ 3965 curve, nor that obtained from the helium triplet lines is capable of interpretation as the result of simple elliptical motion. The Balmer curve exhibits a pronounced "secondary variation," which shows a secular change, while the helium triplet lines at one phase (45–70 days) become greatly enhanced and the portion of the velocity-curve corresponding to this phase does not fit smoothly into the rest of the curve.

It was to examine these "secondary variations" further that additional spectrum plates in the photographic region were taken with the 69-inch Perkins reflector, using the two-prism spectrograph. The new observations have confirmed the velocity differences between the helium singlet and triplet lines; this has also received corroboration from unpublished measures by F. C. Jordan made available to the writer by Dr. K. Burns, of the Allegheny Observatory. These have been included in Table 1 and in Figures 1 and 2.

Although a complete solution of the ϕ Persei system is not yet at hand, it is of interest to present an account of the helium velocities from the new and old material, since any eventual solution of the ϕ Persei problem must take these into consideration. No attempt will be made now, during the press of wartime duties, to discuss the new material in relation to the other emission and absorption features of this highly interesting spectrum. It now appears, however, that a straightforward solution of the ϕ Persei problem should be possible and that very little new observational material should be required, except perhaps at critical phases.

[1] On leave from Perkins Observatory to the Applied Physics Laboratory of the Johns Hopkins University.

[2] *Perkins Obs. Contr.*, No. 14, 1940.

TABLE 1

OBSERVATIONS OF ϕ PERSEI

Phase	Plate	Mean H	λ 3965	λ 4026	λ 4471	Obs.	Remarks
		km/sec	km/sec	km/sec	km/sec		
0.....	459	+ 0.6	+ 13.0±1.0	− 20±9	0±4 −234	H	See Plate VII
1.0.....	130	+ 7.7	− 3.8±1.0	− 30±9	− 13±2	H, A	See Plate VII
3.2.....	A 4763	+ 6.8	.....	(− 54)	.....	J	Unpublished measure by Jordan
7.5.....	A 2789	+14.5	.....	.....	− 55.0	J	Unpublished measure by Jordan
7.9.....	469	+22.1	+ 27.0±2.0	− 80±3	+ 25±22	H	See Plate VII
8.8.....	474	+22.8	+ 44.0±1.0	− 82±2	− 25±15	H, A	See Plate VII
10.9.....	IRM 12317	+23.5	+ 18.0±3.0 −109.3±4.0	− 65±12	+ 52±9	H	Lines appear very wide; components completely blended
11.7.....	481	+19.0	+ 16.9±6.0	− 92.9±2	.....	H	103-0 Plate
12.5.....	IR 11439	+28.3	+ 51.0±3.0 (− 83.6)	− 90±6	− 20±22 + 51±9	H	
12.6.....	735	+28.4	+ 53.8±1.0	− 96±5 + 59±3	−109±2	H	See Plate VII. Note complex λ 4471 with broad line to red
14.1.....	IRM 12250	+38.1	+ 41.0±5.0 (− 85.3±6.0)	− 84±3 + 59±6	− 44±22	H	λ 4471 very weak
15.7.....	482	+32.1	.....	− 83±8	+ 47±16	H	*He* lines weak and indeterminate
17.8.....	500	+38.5	+ 49.8±2.0	− 39±18	+ 54±14	H	*He* lines weak and broad. (Components blended?)
19.6.....	750	+36.8	+ 48.6±4.0	−103±5	+ 66±7	H	See Plate VII. Broad component to violet in λ 4471
21.5.....	A 2837	+41.8	.....	.....	+ 85	J	Unpublished measure. No core visible on plate
21.6.....	754, 755	+44.8	+ 41.6±1.0	− 89±4	+ 16±18	H	λ 4471 unquestionably double, badly blended
21.9.....	IRM 12319	+42.6	+ 38.0±3.0	− 77±10	− 52±7 −181±5	H	4026 double red component indistinct
24.6.....	756	+43.4	+ 44.5±2.0	− 94±6	− 88±7	H	See Plate VII. Center of gravity of λ 4471 = −17 km/sec
26.7.....	521	+34.6	+ 34.0±2.0	− 94±3	− 30±9	H, A	See Plate VII
28.6.....	IR 11473	+32.8	+ 34.0±1.0	− 84±6 (+ 97±30)	− 99±7 + 62±9	H	Mean λ 4471 = −36±24 km/sec
31.2.....	A 4836	+29.4	.....	(− 91.1)	.....	J	Unpublished measure
32.9.....	75, 76, 77, 78	+25.8	+ 25.0±2.0	− 85±3	− 70±5 + 40±10	H	Mean λ 4471 = −23±20 km/sec
34.6.....	IR 11504	+17.4	+ 19.6±8.0	− 79±5	−113±31	H	
34.6.....	A 3344	+19.8	.....	.....	− 30.6	J	Unpublished measure
35.6.....	763	+ 8.2	− 3.6±7.0	− 90±5	− 29±7 −129±4	H	See Plate VII
37.2.....	A 4845	+11.5	.....	− 48.1	− 52.1	J	Unpublished measures
39.8.....	98, 99	+12.9	+ 10.8±2.0	− 30±8	− 5±7	H	
40.6.....	764	+ 7.3	+ 10.0±3.0	− 67±1	+ 12±2	H	See Plate VII
40.9.....	IRM 12327	− 1.9	.....	− 20±7	− 70±2 + 15±2	H	

TABLE 1—*Continued*

Phase	Plate	Mean *H*	λ 3965	λ 4026	λ 4471	Obs.	Remarks
		km/sec	km/sec	km/sec	km/sec		
41.2	A 4850	+ 5.0	.....	− 18	+ 27	J	Unpublished measures
42.6	765	+ 5.4	+ 1.7±2.0	− 63±2	+ 14±3	H	See Plate VII; λ 4471 has two faint components to violet
42.7	533	+ 6.3	+ 10.0±1.0	− 27±3	− 10±2	H, A	
43.5	IR 11544	− 2.4	+ 0.4±3.0	− 30±3	− 33±1	H	λ 4026 is 11 A wide. Measure of haze = +35 km/sec
44.7	538	+ 8.4	+ 25.0±1.0	− 41±2	− 23±1	H, A	See Plate VII
45.1	A 4864	− 7.3	.....	.....	− 10.1	J	Unpublished *He* measure
46.4	IR 11552	+ 5.9	+ 9.2±5.0	+ 2±3	− 1.1±2.0 −183.0±3.0	H	Plate poor
46.5	A 2983	− 8.2	.....	− 19.8	− 38.8	J	Unpublished *He* measures
46.6	766	+ 5.4	+ 17.9±1.0	− 9±1	+ 11±1 −238±2	H	See Plate VII
47.1	A 4868	− 3.1	.....	− 36.9	− 36.9	J	Unpublished *He* measures
47.5	A 2991	−10.9	.....	− 16.9	− 33.9	J	Unpublished *He* measures
50.1	IRM 12328	− 7.8	− 2.0±2.0 −113.6±3.0s	− 11±3 −182±3	− 11±1 −220±3	H	
52.1	A 4884	+ 3.8	.....	+ 11.1	+ 0.6	J	Unpublished *He* measures
52.8	118	+ 0.8	+ 11.0±1.0	+ 1±1	+ 5±1	H, A	See Plate VII
53.1	IR 12329	+17.7	+ 11.4±2.0	.....	− 1±3	H	
53.5	A 3013	− 1.5	.....	+ 0.2	− 14.8	J	Unpublished *He* measures
53.5	663	− 0.8	+ 11.8±4.0	[− 16.5]	[+ 58±1]	H, A	Hard to measure
53.7	IRM 12289	+11.3	+ 11.6±1.0	+ 6±4	+ 1±1	H	
53.8	IRM 12330	+17.7	+ 7.7±3.0	0±1	+ 6±1	H	
54.1	A 4889	− 2.1	.....	− 18.8	+ 14.7	J	Unpublished *He* measures
54.3	A 3897	+ 4.6	.....	− 2.1	− 15.1	J	Unpublished *He* measures
55.5	A 3023	− 7.0	.....	.....	+ 19.6	J	Unpublished *He* measure
56.5	A 3032	− 5.8	.....	− 29.8	− 22.8	J	Unpublished *He* measures
56.5	IR 11592	+ 8.3	+ 11.5±1.0	+ 12±1	+ 4±2	H	
56.5	667	− 0.8	+ 2.4±1.0	+ 15±4	+ 14±1	H, A	
56.6	A 3375	+ 7.8	.....	+ 12.4	+ 2.4	J	Unpublished *He* measures
57.1	A 4905	− 1.9	.....	+ 1.1	+ 3.1	J	Unpublished *He* measures
57.4	A 3927	+ 7.1	.....	0	+ 5.7	J	Unpublished *He* measures
57.5	673	+ 1.1	+ 11.3±1.0	−164±2 + 4±1	+ 1±1	H	See Plate VII
57.6	545	+ 5.9	+ 7.5±1.0	+ 21±2	+ 8±1	H	
57.6	A 2295	− 2.6	.....	.....	+ 14.1	J	Unpublished *He* measure
58.5	675	+ 4.9	+ 9.7±1.0	− 7±1	+ 2±1	H	
60.5	680	+ 4.1	+ 16.7±1.0	+ 9±2	+ 12±1	H	See Plate VII
61.3	A 3947	+ 4.4	+ 11.3	+ 34.3	+ 12.3	J	Unpublished *He* measures
61.4	A 3041	− 7.7	.....	− 2.3	+ 30.7	J	Unpublished *He* measures
62.6	553	+ 1.1	+ 7.0±1.0	+ 10±1	+ 6±1	H, A	See Plate VII
63.1	A 4920	− 0.4	0	0	− 6.3	J	Unpublished *He* measures

TABLE 1—*Continued*

Phase	Plate	Mean *H*	λ 3965	λ 4026	λ 4471	Obs.	Remarks
		km/sec	km/sec	km/sec	km/sec		
63.4.....	A 3049	− 2.6	− 1.4	+ 24.1	+ 9.1	J	Unpublished *He* measures
64.4.....	A 3060	− 2.1	+ 13.7	.....	+ 10.7	J	Unpublished *He* measures
65.1.....	A 4923	− 2.5	+ 13.8	+ 13.8	+ 13.3	J	Unpublished *He* measures
65.1.....	IR 11717	+ 2.5	+ 13.6±4.0	+ 7±3	+ 12±1	H	
65.3.....	A 3071	− 2.5	− 8.6	.....	− 0.6	J	Unpublished *He* measures
65.6.....	A 2325	− 0.3	− 1.6	+ 8.4	+ 4.4	J	Unpublished *He* measures
66.4.....	A 3082	− 8.4	.....	.....	− 19.0	J	Unpublished *He* measure
66.5.....	767	+ 2.6	+ 1.1±1.0	+ 16±1	+ 17±1	H	See Plate VII
67.3.....	A 3091	− 6.2	+ 7.7	.....	+ 2.7	J	Unpublished *He* measures
68.0.....	IRM 12331	− 2.0	(− 96.6) − 5.9±2.0	+ 30±3	+ 33±3	H	
68.2.....	A 4925	− 1.5	+ 22.4	+ 18.4	− 6.1	J	Unpublished *He* measures
68.4.....	A 3102	−10.2	.....	.....	+ 39.3	J	Unpublished *He* measure
69.4.....	A 3985	+ 4.9	.....	.....	+ 21.9	J	Unpublished *He* measure
70.1.....	A 4930	− 5.4	+ 1.6	+ 0.6	(+ 58.6)	J	Unpublished *He* measures
71.3.....	A 3113	−12.5	.....	.....	+ 34.7	J	Unpublished *He* measure
73.2.....	A 4937	− 5.0	+ 28.3	.....	+ 8.3	J	Unpublished *He* measures
74.3.....	A 3996	−10.5	− 28.0	.....	+ 16.0	J	Unpublished *He* measures
76.5.....	682	+ 5.3	− 4.6±1.0	.....	+ 74±1	H	See Plate VII
76.5.....	IR 11625	− 8.5	− 21.9±2.0	−177±3 + 26±2 +190±2	− 22±1	H	
80.5.....	686	+ 2.4	− 4.2±1.0	+106±2	− 13±20	H	See Plate VII
81.8.....	IRM 12300	− 4.1	− 16.8±1.0	+ 50±17	+ 80±4 − 23 −170	H	
84.9.....	IRM 12336	− 4.1	− 16.4±3.0	+ 7±15 + 99±1	.....	H	
86.1.....	A 4960	−24.6	.....	.....	+ 78.0?	J	Unpublished *He* measure
92.8.....	IRM 12303	−14.3	− 49.0±2.0	+205±5 + 40±10	− 95±4 + 65±3	H	
99.4.....	699	−18.2	.....	+101±2	+ 76±2 − 4±8	H	See Plate VII
100.7.....	P	−26.9	− 7.8±2.0 − 37.3±1.0	+ 75±2	+ 74±3	H	
101.6.....	389	−20.9	− 18.4±6.0	− 58±12 + 71±2	+ 33±2	H, A	
103.0.....	A 4663	−14.4	.....	.....	+ 27.3	J	Unpublished *He* measure
103.5.....	400	−18.3	.....	.....	+ 53±4	H	
107.6.....	IRM 12309	−19.5	− 41.7±6.0	+ 65±15	+ 32±3 −241±9	H	
109.3.....	A 3238	−20.6	.....	.....	− 3.3	J	Unpublished *He* measure
110.0.....	A 4695	−15.4	.....	.....	0.0	J	Unpublished *He* measure
111.4.....	712	− 9.2	+ 7.8±10.0	+ 40±3 +213±3	+ 32±2 −202±2	H	
111.8.....	IRM 12337	−16.1	− 28.0±1.0	− 1±1	+ 15±2 −230±6	H	

PLATE VII

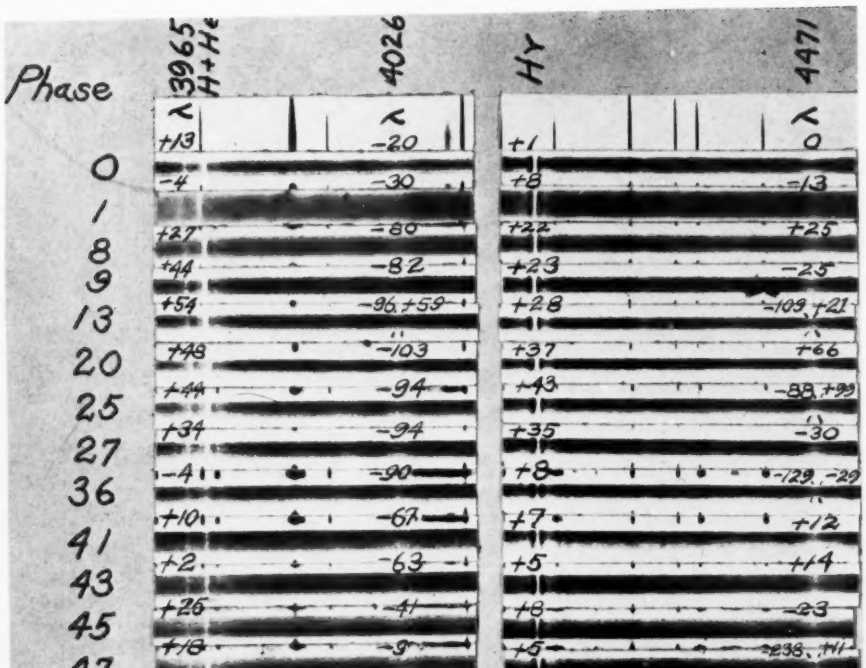

SPECTRUM OF ϕ PERSEI

TABLE 1—*Continued*

Phase	Plate	Mean *H*	λ 3965	λ 4026	λ 4471	Obs.	Remarks
		km/sec	km/sec	km/sec	km/sec		
113.6.....	125	−18.0	− 25.0±2.0	− 74±10	+ 11±2	H, [A]	See Plate VII
114.0.....	A 4710	−18.0	.....	.....	− 6.3	J	Unpublished *He* measure
114.3.....	A 3255	−11.3	.....	.....	+ 32.7	J	Unpublished *He* measure
116.4.....	720	−17.4	− 3.9±2.0	− 21±15	+ 15±3	H	See Plate VII
117.6.....	IRM 12311	−13.4	− 5.0±2.0	+190±1 − 27±2	+ 8±2 −182±2	H	
117.8.....	IRM 12312	−20.9	− 24.0	+150±1 − 12±1	+ 6±2 −200±5	H	
118.1.....	A 4999	−13.3	.....	− 13.8	.....	J	Unpublished *He* measure
118.7.....	127	−11.0	− 10.0±1.0	+ 5±1	− 8±2	H	See Plate VII
119.3.....	A 3276	−15.5	.....	.....	− 36.3	J	Unpublished *He* measure
119.7.....	128	−10.0	− 14.1±1.0	− 10±2	− 2±1	H	See Plate VII
121.2.....	A 3289	−16.0	.....	.....	− 10.0	J	Unpublished *He* measure
121.5.....	449	−13.1	− 9.1±1.0	0±2	− 5±2	H	
122.5.....	457	− 3.8	− 3.3±1.0	− 30±3	− 8±2	H	See Plate VII
125.3.....	723	− 2.0	− 2.4±1.0	+ 6±1	− 7±1	H	
125.4.....	724	− 2.0	+ 3.6±2.0	+ 2±2	+ 21±6	H	See Plate VII
126.0.....	A 4739	+ 3.8	.....	.....	− 7.8	J	Unpublished *He* measure

Table 1 brings together the old and new velocity measures from the hydrogen and helium lines. In successive columns are given the phase, plate designation (numbers alone refer to Perkins plates, "IR" and "IRM" denote Yerkes plates, and "A" indicates Allegheny plates), the mean velocity from the sharp hydrogen lines, the velocity of the helium line at λ 3965 which arises from a metastable level ($2^1S - 3^1P$), the velocities of λ 4026 and λ 4471 ($2^3P - n^3D$), the measurer (H = Hynek, A = Aller, J = Jordan), and remarks.

Plate VII shows portions of the spectrum at representative phases. Process emulsion spectrograms were enlarged on Kodalith film, which, in turn, was developed in D-72 for two minutes and then printed on high-contrast paper. This procedure was necessary in order to bring out the character of the helium lines, much of which is at the threshold level and is entirely glossed over in ordinary enlargements.

Figures 1 and 2 represent graphically the λ 4026 and λ 4471 material of Table 1. Closed circles represent recent measures (individual) of good weight, and crosses indicate the early mean measures of Jordan. Since the lines are obviously composite, a large range in weight occurs; on poorer plates the detail is frequently obliterated. Measures of low weight are represented by open circles.

The velocity-curves of λ 4026 and λ 4471 are somewhat different. Both lines arise from the same level and should, accordingly, have the same character. It must be remembered, however, that we deal with weak composite lines and that differences in prismatic dispersion and in plate density at λ 4026 and λ 4471 may cause supposedly equal threshold features to appear quite differently. To ascribe this apparent difference to blends, as has been suggested, is unwarranted, since this calls for blends at precisely λ 4026 and λ 4471 (in a spectrum which has few measurable features) and which have the property of so blending as to produce a smooth velocity-curve of large range.

The anomalous behavior is best illustrated by Plate VII and particularly at maximum phase of the Balmer lines (20–30 days), when the hydrogen and *He* λ 3965 velocities are

markedly positive. The line λ 4026 appears as a fairly sharp line, easily measurable, and shows a markedly negative velocity. The line λ 4471 clearly shows its composite character at this phase; and, when the components are separately measurable, reasonably good agreement, at least in sign, is obtained with both the Balmer lines and with λ 4026. The composite character of λ 4026 is not shown so clearly at this phase, but the spectrogram at phase 13 days shows it best. The velocities shown in Plate VII are the values actually observed and are not smoothed.

Plate VII also demonstrates clearly that at most phases the helium triplet lines show "cores" or have sufficient "condensation" to be measurable; this was not apparent from earlier reproductions and hence represented a debatable point. Table 1 shows that a majority of the triplet-line measures have small probable errors in terms of the total velocity variation. Probable errors were derived from the range of measures of a given line and are expressed in units of kilometers per second. Measures on these lines must, there-

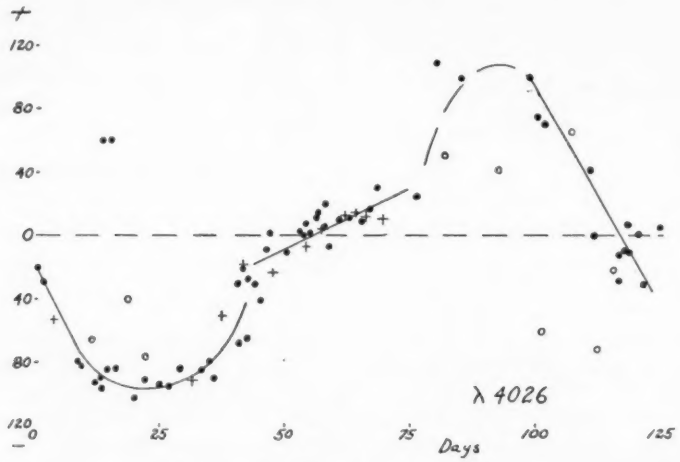

FIG. 1.—Velocity-curve of ϕ Persei

fore, be considered real and must be entitled to some weight in the general problem of ϕ Persei.

For some reason, λ 4026 yields a more consistent velocity-curve (Fig. 1) than λ 4471 (Fig. 2). The latter line, possibly because of difference in dispersion and plate quality in that region of the spectrum, appears more conspicuously composite, or blended, and more frequently so, than λ 4026; this undoubtedly contributes to the variance of λ 4026 and λ 4471 measures.

Figure 1 deserves especial attention. It appears that the velocity-curve does not represent simple orbital motion. At phases 45–70 days the curve is well defined and is essentially a straight line, rising from −25 to +25 km/sec. This phase interval corresponds exactly to that in which the helium lines are greatly enhanced in strength and sharpness. Without question, a mass of gas capable of absorbing λ 4026 must be moving in front of a light-source in an opposite sense to that indicated by the principal velocity-curve. It is difficult to see how this might arise from a simple jet of gas coming from the principal star, as has been suggested,[3] for in this case the velocities should dip to more negative values as the ejection jet came into the line of sight.

The "transiting" gas mass also produces hydrogen lines and the singlet helium line at λ 3965, as is evidenced by the sharpening of these lines in the spectrum at this phase and

[3] Struve, *Pop. Astr.*, **49**, 129, 1941.

the temporary interruption of their velocity-curves. This manifests itself as the well-known "secondary variation" in the velocity-curve of ϕ Persei.

The line λ 4471 (Fig. 2) shows the same general velocity-curve as λ 4026; but, because its composite character is more frequently clear (Pl. VII) from 0 to 45 days, two curves are indicated. Often, however, the two lines do not appear resolved, and an intermediate velocity value results. From 100 to 125 days only one component is visible; and its velocity-curve is well defined and, again, opposite in sense to that of the primary Balmer lines.

It can be concluded, then, that from 45 to 70 days, corresponding to the appearance of strong and sharp helium triplet lines, the velocity-curve is well defined, unique, and of opposite sense to that of the Balmer lines. At other phases the triplet lines, when well defined and uniquely measurable, show a curve which is not a simple continuation of the 45–70 day curve but which is also out of phase with the primary Balmer curve.

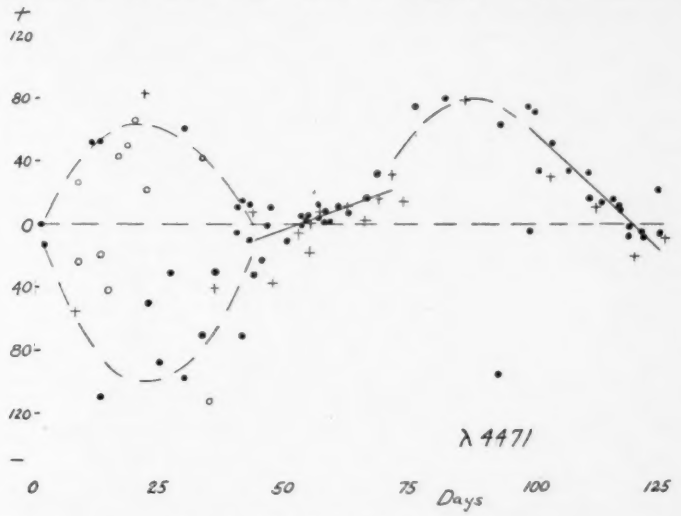

FIG. 2.—Velocity-curve of ϕ Persei

It appears necessary to postulate a gas mass, capable of absorbing helium and hydrogen lines, crossing the line of sight at phases 45–70 days in a sense opposite to that of the primary spectrum source. It also appears that this particular gas mass is not responsible for the composite helium triplet lines, though the source of these weak helium lines at other phases obviously cannot be the atmosphere of the primary star.

If a fainter companion of similar spectral class exists, then it is necessary to ask, as pointed out by Struve,[3] why features other than the helium triplets are not found to be composite and, second, why the Balmer lines, which show exceedingly sharp cores at phases 115–25 days, are not "filled in" by the superposition of the continuous spectrum of the secondary.

The first objection is not insuperable; indeed, the only other measurable features (absorption) of the spectrum (*Ca* K and *Fe* I. other than the shell-produced Balmer cores, show little velocity variation and might be ascribed to the blending of two sources. The deep central absorption of the sharp Balmer lines at 115–25 days, however, denies a second source unless one adopts highly arbitrary hypotheses such as, for instance, that the extended envelope producing the sharp Balmer lines intercepts the light of both components at these phases.

When wartime duties have been concluded, the writer hopes to examine this and other suggestions with the aid of a spectrophotometric study.

PARTIALLY DEGENERATE STELLAR MODELS[1]

GORDON W. WARES
San Antonio, Texas, and Yerkes Observatory
Received April 17, 1944

ABSTRACT

Partially degenerate stellar models based on the Fermi-Dirac equation of state of an electron gas are used to study stars that are too degenerate at the center for the perfect gas law to apply but not dense enough for the white-dwarf models to be valid. The relation of the Fermi-Dirac equation of state to the other equations of state of an electron gas, together with the percentage of error committed in using them, is presented in Figure 1. The log ρ, log T diagram of Figure 1 illustrates and summarizes chapter x on the quantum statistics in Chandrasekhar's monograph on stellar structure, which is basic to the present investigation.

In Part I the theory of the standard-model case is developed. Table 1 and Figure 2 present the three numerical integrations, and Table 2 gives the boundary values. Section 11, Table 3, and Figures 3 and 4 present the accurate solution of Milne's problem (for small masses), namely, the determination of the course of the ($\mathfrak{R}$, $1 - \beta$) curves of constant mass in the domain of degeneracy. This constitutes our most important result.

In Part II a parallel development of the isothermal case is given. The results of seven numerical integrations are summarized in Figure 5 and Table 4. All configurations are found to extend to infinity mathematically, but finite boundaries can be defined for not too low central degeneracy.

In Part III it is shown that the present theory is required for the more extreme subdwarfs and perhaps for the old novae, but probably not for any main-sequence stars.

1. *Partially degenerate stellar models.*—It is the purpose of the present paper to use partially degenerate stellar models based on the Fermi-Dirac equation of state of an electron gas to study stars that are too degenerate at the center for the perfect gas law

$$P = \frac{k}{\mu_e H}\,\rho T \tag{1}$$

to apply but not dense enough for the white-dwarf models, based on the equation of state[2]

$$\rho = Bx^3\,, \qquad p = A\,f(x)\,, \tag{2}$$

of a completely degenerate electron gas to be valid; in particular it is our purpose to solve Milne's problem (cf. § 11).

In Figure 1 and its caption are summarized and illustrated (*a*) the various relatively simple forms to which the general equation of state of an electron gas reduces in each of the "domains" of the log ρ, log T diagram, (*b*) the "criteria" defining the boundaries between domains, and (*c*) the series expansions required to "approach" and the integral formulae required to actually "cross" the degeneracy-criterion locus. Figure 1 is useful not only in telling at a glance the correct equation of state for any point (log ρ, log T) but also in giving, by inspection, the percentage of error committed in using either the perfect gas law or the completely degenerate gas law.

It is anticipated that for the above-mentioned stars of intermediate density the central density and temperature will correspond to a point (log ρ_c, log T_c) dangerously close to, if not actually below, the degeneracy-criterion locus of Figure 1. It is also anticipated

[1] The present paper is a condensation of the writer's doctoral dissertation, "Partially Degenerate Stellar Models" (University of Chicago, 1940). It was completed while the author was in military service.

[2] In general, the notation in this paper is that of S. Chandrasekhar, *An Introduction to the Study of Stellar Structure* (Chicago: University of Chicago Press, 1939) (hereafter "*Stellar Structure*").

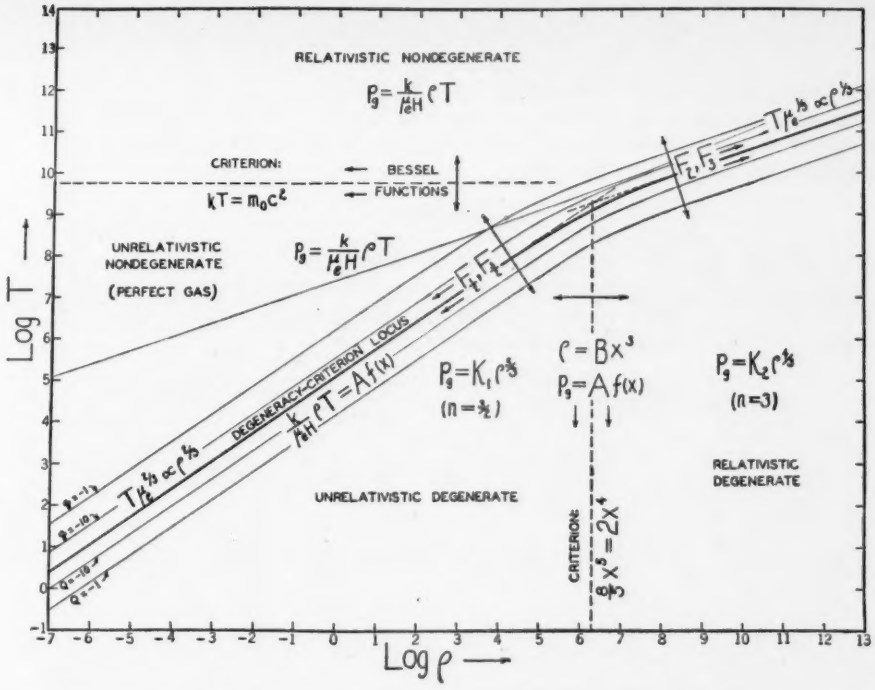

FIG. 1.—The log ρ, log T diagram of the equations of state of an electron gas. The diagram is based upon and illustrates chapter x of *Stellar Structure*, to which the equation numbers below refer. The stellar degeneracy-criterion locus, p_g (perfect gas) $= k/(\mu_e H)\rho T = Af(x) = p_g$ (degenerate), divides the diagram into two domains: nondegenerate (above) and degenerate (below). These two domains correspond to two limiting cases in which it is possible to integrate in series the general equation of state (170) and (172), which is valid over the entire diagram. Over the entire nondegenerate domain the Bessel function infinite series form (252) and (253) is valid; and over the entire degenerate domain the algebraic infinite series form, $\rho = Bx^3\ [1 + \ldots.]$, $p_g = Af(x)\ [1 + \ldots.]$, (204) and (198), is valid. The equation of state is known in integrated form, therefore, for every point on the diagram, but each series breaks down if one attempts to "cross" the degeneracy-criterion locus. To effect this crossing, i.e., to take exact account of partial degeneracy, a numerical quadrature of (170) and (172) is always required. In the two limiting cases of low density and temperature and of high density and temperature this quadrature involves but a single parameter and is expressed in terms of the Fermi-Dirac functions $F_{1/2}$, $F_{3/2}$, and F_2, F_3, respectively, which have been tabulated in the former case. The partially degenerate stellar models of the present paper are based upon the $F_{1/2}$ and $F_{3/2}$ functions. Sufficiently far ($\psi \gg 1$) below the degeneracy-criterion locus the algebraic infinite series reduce approximately to their first terms, namely, the relativistic completely degenerate gas law (white-dwarf equation of state), $\rho = Bx^3$, $p_g = Af(x)$, which always gives the pressure too low, the error being $Q\% = -1\%$ and $Q\% = -10\%$ along the loci labeled $Q = -1$ and $Q = -10$ on the diagram. The two criterion-loci, $(8/5)x^5 = 2x^4$ at log $\rho = 6.2828$ ($\rho \approx 2 \times 10^6$) and $kT = m_0c^2$ at log $T = 9.773$ ($T \approx 6 \times 10^9$), indicate the setting-in of the relativity correction to mass on account of high velocity caused by high density (Pauli exclusion principle) and high temperature, respectively. To the left ($\rho \ll 2 \times 10^6$) and to the right ($\rho \gg 2 \times 10^6$) of the criterion-locus $(8/5)x^5 = 2x^4$ the equation of state $\rho = Bx^3$, $p_g = Af(x)$ reduces to $p_g = K_1\rho^{5/3}$ (unrelativistic degenerate or polytrope $n = 3/2$) and to $p_g = K_2\rho^{4/3}$ (relativistic degenerate or polytrope $n = 3$), respectively. Sufficiently far ($\psi \ll -1$) above the degeneracy-criterion locus the Bessel function infinite series reduce approximately to their first terms, namely, the perfect gas law, $p_g = k/(\mu_e H)\rho T$, which always gives the pressure too low, the error being $q\% = -1\%$ and $q\% = -10\%$ along the loci labeled $q = -1$ and $q = -10$ on the diagram. In general, the physical properties of an electron gas have to be expressed in terms of Bessel functions in the presence of relativity effects due to high temperature, i.e., above and in the vicinity of the criterion-locus $kT = m_0c^2$. The perfect gas equation of state, however, is unaltered by such relativity effects. Hence the $kT = m_0c^2$ locus would be of little importance for stellar structure, even if temperatures of 10^9 were of interest. The locus of $s\% = -1\%$ error caused by relativity effects due to high density in the pressure calculated from the Fermi-Dirac $F_{3/2}$ function passes through the points (5.74, 8) and (5.27, 6) but is not indicated on the diagram. The error is -10 per cent at the point (5.84, 6). The light line passing through the perfect gas domain with slope $\frac{1}{3}$ is the locus of minimum radius for given ψ_0 (for $\mu_e = 1$) for the partially degenerate standard model (cf. § 9). The $q = -1$, $q = -10$, $k/(\mu_e H)\rho T = Af(x)$, $Q = -10$, and $Q = -1$ loci correspond, respectively, to the following constant values of the parameter ψ in the region $\rho \ll 2 \times 10^6$: -2.852, -0.371, $+2.099$, $+6.28$, and $+20.25$.

that this point will be safely to the left of the criterion locus $\frac{8}{5}x^5 = 2x^4$ (i.e., $\rho_c \ll 2 \times 10^6$, which is found to mean $\rho_c \leqq 2 \times 10^5$), so that relativity effects can properly be neglected. The problem is then to take account of the gradual change in the equation of state from the unrelativistic degenerate equation,

$$p = K_1 \rho^{5/3}, \tag{3}$$

to the perfect gas equation (1) (i.e., to cross the degeneracy-criterion locus from right to left) in integrating outward from the center of the stellar model to the boundary. As indicated in Figure 1, the required form of the equation of state is that of the Fermi-Dirac statistics, which we here write in the parametric form[3]

$$\left.\begin{aligned} \rho \equiv n_e \mu_e H &= \left[\frac{2\,(2\pi mkT)^{3/2}}{h^3}\,\mu_e H\,\frac{2}{\sqrt{\pi}}\right] F_{1/2}(\psi) \equiv B_1 F_{1/2}(\psi), \\ p = p_g = p_e &= \left[\frac{2\,(2\pi mkT)^{3/2}}{h^3}\,kT\,\frac{2}{\sqrt{\pi}}\right] \tfrac{2}{3} F_{3/2}(\psi) \equiv A_1 F_{3/2}(\psi), \end{aligned}\right\} \tag{4}$$

where[4]

$$B_1 = \frac{4\pi \mu_e H\,(2mkT)^{3/2}}{h^3} \equiv |B_1|\,\mu_e T^{3/2} = 9.11 \times 10^{-9} \mu_e T^{3/2}\ \mathrm{gm/cm^3} \tag{5}$$

and

$$A_1 = B_1 \frac{kT}{\mu_e H} \equiv |A_1|\,T^{5/2} = 0.752 T^{5/2}\ \mathrm{dynes/cm^2} = 7.42 \times 10^{-7} T^{5/2}\ \mathrm{atm} \tag{6}$$

and where $F_{1/2}(\psi)$ and $\mathfrak{F}_{3/2}(\psi) \equiv \frac{2}{3}F_{3/2}(\psi)$ are the Fermi-Dirac functions defined by

$$F_v(\psi) = \int_0^\infty \frac{u^v du}{e^{-\psi+u}+1}. \tag{7}[5]$$

In order to calculate the structure of configurations obeying the parametric equation of state (4) (the equation for pressure being modified by the addition of the radiation pressure $(a/3)T^4$), we must make an assumption as to the temperature gradient and the distribution of energy sources; to each such assumption there will correspond a particular "partially degenerate stellar model." In this paper we shall study two such models: (I) the standard model and (II) the isothermal gas sphere. The former leads to the most important specific result of the present paper: the solution of Milne's problem (cf. § 11).

I. THE PARTIALLY DEGENERATE STANDARD MODEL

2. *The fundamental differential equation.*—The definitive condition of the standard model may be taken as

$$p_g = \beta P, \qquad \beta = \text{constant}, \tag{8}$$

where $P = p_g + p_r$ is the total pressure. The equation of state of the model, corresponding to the equation of state (4) of the electron gas, is

$$\rho = |B_1|\,\mu_e T^{3/2} F_{1/2}(\psi), \qquad P = |A_1|\,\beta^{-1} T^{5/2}\,\mathfrak{F}_{3/2}(\psi). \tag{9}$$

[3] These equations are equivalent to eqs. (151) and (152), p. 447, of *Stellar Structure*.

[4] In the present paper, symbols like A_1, B_1, C_1, α_1, A_2, B_2, C_2, and α_2 represent quantities that for a particular model (subscripts 1 for isothermal gas sphere and 2 for standard model) are constants involving parameters. The corresponding symbols $|A_1|$, $|B_1|$, etc., represent the numerical values of these constants apart from parameters but including physical constants. The physical constants (in cgs units) adopted in this paper are the same as those used in Appen. I of *Stellar Structure*.

[5] The functions $\frac{2}{3}F_{3/2}(\psi)$, abbreviated in this paper to $\mathfrak{F}_{3/2}(\psi)$, or $\mathfrak{F}_{3/2}$, or $\mathfrak{F}$; and $F_{1/2}(\psi)$, abbreviated to $F_{1/2}$, or F, are tabulated by J. McDougall and E. C. Stoner in *Phil. Trans.*, A, **257**, 67, 1938.

Using for the gas pressure p_g from equation (4) and for the radiation pressure

$$p_r = \frac{a}{3} T^4 , \tag{10}$$

we find

$$T = \left(\frac{3}{a} |A_1|\right)^{2/3} \mathfrak{F}_{3/2}^{2/3}(\psi) \left(\frac{1-\beta}{\beta}\right)^{2/3} = 4.47 \times 10^9 \mathfrak{F}_{3/2}^{2/3}(\psi) \left(\frac{1-\beta}{\beta}\right)^{2/3}, \tag{11}$$

by means of which we can eliminate the temperature from (9). We thus obtain for the equation of state of the partially degenerate standard model:

$$\left.\begin{aligned} \rho &= B_2 \mathfrak{F}_{3/2}(\psi) F_{1/2}(\psi) \equiv |B_2| \mu_e \frac{1-\beta}{\beta} \mathfrak{F}_{3/2}(\psi) F_{1/2}(\psi) , \\ P &= A_2 \mathfrak{F}_{3/2}^{8/3}(\psi) \equiv |A_2| \left(\frac{1-\beta}{\beta^{8/5}}\right)^{5/3} \mathfrak{F}_{3/2}^{8/3}(\psi) , \end{aligned}\right\} \tag{12}$$

where

$$|B_2| = \frac{3}{a} |B_1| \, |A_1| = 2.72 \times 10^6 \text{ gm/cm}^3 \tag{13}$$

and

$$|A_2| = \left(\frac{3}{a}\right)^{5/3} |A_1|^{8/3} = 1.003 \times 10^{24} \text{ dynes/cm}^2 = 9.89 \times 10^{17} \text{ atm} . \tag{14}$$

Using equation (12) and the recurrence relations[6]

$$F_v'(\psi) = v F_{v-1}(\psi) , \qquad \mathfrak{F}_{3/2}'(\psi) = F_{1/2}(\psi) \qquad \text{or} \qquad \mathfrak{F}' = F , \tag{15}$$

and proceeding in the usual manner, introducing the dimensionless variable ξ through the relation

$$r = a_2 \xi , \tag{16}$$

where

$$a_2 = \left[\frac{2A_2}{3\pi G B_2^2}\right]^{1/2} = \frac{|a_2|}{\mu_e [\beta^2(1-\beta)]^{1/6}} = \frac{0.00944 R_\odot}{\mu_e [\beta^2(1-\beta)]^{1/6}} , \tag{17}$$

we obtain for the two equivalent forms of the fundamental differential equation of the partially degenerate standard model:

$$\left.\begin{aligned} \frac{1}{\xi^2} \frac{d}{d\xi} \left(\xi^2 \mathfrak{F}_{3/2}^{2/3}(\psi) \frac{d\psi}{d\xi}\right) &= - \mathfrak{F}_{3/2}(\psi) F_{1/2}(\psi) ; \\ \frac{d^2\psi}{d\xi^2} + \frac{2}{3} \frac{F_{1/2}(\psi)}{\mathfrak{F}_{3/2}(\psi)} \left(\frac{d\psi}{d\xi}\right)^2 + \frac{2}{\xi} \frac{d\psi}{d\xi} &= - \mathfrak{F}_{3/2}^{1/3}(\psi) F_{1/2}(\psi) . \end{aligned}\right\} \tag{18}$$

The required solution[7] is the function $\psi(\xi)$ with the usual boundary conditions:

$$\left.\begin{aligned} &\text{at the center} \quad (\xi = 0): \qquad \psi(0) = \psi_0 , \qquad \left(\frac{d\psi}{d\xi}\right)_0 = 0 ; \\ &\text{at the boundary} \quad (\xi = \xi_1): \qquad \psi(\xi_1) = -\infty . \end{aligned}\right\} \tag{19}$$

There is no homology relation.

[6] McDougall and Stoner, *ibid.*, eq. (6.3).

[7] We shall concern ourselves only with solutions analogous to the *E*-solutions of polytropic theory; cf. *Stellar Structure*, pp. 103 and 159.

For given values of the relative radiation pressure $(1-\beta)/\beta$ and molecular weight μ_e it is clear from equations (11) and (12) that the central values ρ_c, P_c, and T_c depend upon the choice of the integration parameter ψ_0, which is a measure of the degree of degeneracy at the center. Conversely, we can think of a given ψ_0 as follows:

$$\psi_0 \text{ specifies } \frac{\rho_c}{\mu_e \dfrac{1-\beta}{\beta}} \text{ and } \frac{P_c}{\left(\dfrac{1-\beta}{\beta^{8/5}}\right)^{5/3}} \text{ and } \frac{T_c}{\left(\dfrac{1-\beta}{\beta}\right)^{2/3}}, \text{ or } \frac{\rho_c}{\mu_e T_c^{3/2}}, \quad (20)$$

the second and third quantities being independent of μ_e and the last independent of $(1-\beta)$.

3. *The density at any point in terms of the central density.*—By equation (19), the first of equations (12), and the fact that β and μ_e are assumed constant throughout the configuration, we find that

$$\frac{\rho}{\rho_c} = \frac{\mathfrak{F}_{3/2}(\psi) F_{1/2}(\psi)}{\mathfrak{F}_{3/2}(\psi_0) F_{1/2}(\psi_0)}. \quad (21)$$

4. *The mass relation or "generalized quartic equation" for* $(1-\beta)$.—By equation (16) the mass inclosed in a sphere of radius ξ is given by

$$M(\xi) = 4\pi a_2^3 \int_0^\xi \rho \xi^2 d\xi, \quad (22)$$

or, according to equations (12) and (18), by

$$M(\xi) = -C_2 \mathfrak{F}_{3/2}^{2/3}(\psi) \xi^2 \frac{d\psi}{d\xi} \equiv -|C_2| \mu_e^{-2} \left(\frac{1-\beta}{\beta^4}\right)^{1/2} \mathfrak{F}_{3/2}^{2/3}(\psi) \xi^2 \frac{d\psi}{d\xi}, \quad (23)$$

where

$$|C_2| = 4\pi |a_2|^3 |B_2| = 9.67 \times 10^{33} \text{ gm} = 4.87 \odot. \quad (24)$$

The mass of the entire configuration is given by

$$M = -|C_2| \mu_e^{-2} \left(\frac{1-\beta}{\beta^4}\right)^{1/2} [\mathfrak{F}_{3/2}^{2/3}(\psi_1) \xi_1^2 \psi'(\xi_1)], \quad (25)$$

which is a quartic equation in β determining the relative radiation pressure $(1-\beta)$ uniquely in terms of the mass $M\mu_e^2$, or vice versa, for a given solution ψ_0. Equation (25) may be considered as a generalization of Eddington's quartic equation for the classical standard model. It is, however, important to note that M is not independent of the radius and central density, as is the case with the classical standard model.

5. *The relation between the mean and the central density.*—From elementary considerations involving equations (12), (16), and (25) we find

$$\frac{\rho_c}{\rho} = -\mathfrak{F}_{3/2}(\psi_0) F_{1/2}(\psi_0) \left[\frac{\xi_1}{3\psi'(\xi_1) \mathfrak{F}_{3/2}^{2/3}}\right]. \quad (26)$$

6. *The limiting cases of very low and of very high central degeneracy.*—It is not difficult to verify that the partially degenerate standard model reduces as it should to the classical standard model or Lane-Emden polytrope $n = 3$ as $\psi \to -\infty$ and in the opposite limiting case of $\psi \to +\infty$ and for negligible radiation pressure $(\beta \to 1)$ to a Lane-Emden polytrope $n = \frac{3}{2}$ or white-dwarf configuration in the limiting case of low central density.

Thus, our partially degenerate standard-model configurations based on the Fermi-Dirac equation of state (12) and described by $\psi(\xi)$ of equation (18) are appropriate for

taking into exact account the effects of incomplete degeneracy. The white-dwarf configurations based on equation (2) take complete account of relativity effects but break down at "low density" (strictly low degeneracy) with approach from the right (Fig. 1) to the degeneracy-criterion locus. In a somewhat complementary manner our partially degenerate configurations based on equation (4) take exact account of incompleteness of degeneracy but break down at high density with the approach from the left to the $\frac{8}{5}x^5 = 2x^4$ criterion locus on account of the setting-in of relativity effects. In the region of intermediate density, where the two conditions $\psi \gg 1$ and $\rho \ll 2 \times 10^6$ are both satisfied, the white-dwarf and the partially degenerate configurations are equally valid.

7. *The numerical integrations.*—The following starting series for the standard-model differential equation (18) was derived and used:

$$\psi(\xi) = \psi_0 + a\xi^2 + b\xi^4 + c\xi^6 + g\xi^8 + \dots, \tag{27}$$

where (using $\mathfrak{F}' = F$)

$$\left.\begin{aligned} a &= -\frac{1}{3!}\mathfrak{F}^{1/3}F, \qquad b = +\frac{1}{6!}\tfrac{2}{3}\mathfrak{F}^{-1/3}[9\mathfrak{F}FF' - F^3], \\ c &= -\frac{1}{9!}\frac{8}{9}\left[103\frac{F^5}{\mathfrak{F}} - 111F^3F' + 135\mathfrak{F}F^2F'' + 81\mathfrak{F}F(F')^2\right], \\ g &= -\left\{\frac{a^4}{54\mathfrak{F}^3}[2F^3 - 3\mathfrak{F}FF' + \mathfrak{F}^2F''] + \frac{a^3}{11{,}664\mathfrak{F}^{2/3}}\left[\frac{10F^4}{\mathfrak{F}^2} - \frac{36F^2F'}{\mathfrak{F}}\right.\right. \\ &\quad + 27(F')^2 + 36FF'' + 27\mathfrak{F}F'''\Big] + \frac{5a^2b}{27\mathfrak{F}}\left[F' - \frac{F^2}{\mathfrak{F}}\right] + \frac{ab}{648\mathfrak{F}^{2/3}}\left[9FF'\right. \\ &\quad \left.\left. - 2\frac{F^3}{\mathfrak{F}} + 9\mathfrak{F}F''\right] + \frac{2acF}{9\mathfrak{F}} + \frac{4b^2F}{27\mathfrak{F}} + \frac{c}{216\mathfrak{F}^{2/3}}[\mathfrak{F}^2 + 3\mathfrak{F}F']\right\}. \end{aligned}\right\} \tag{28}$$

For any ψ_0, all the required values[8] of $F = F_{1/2}(\psi_0)$ and its derivatives and of $\mathfrak{F} \equiv \mathfrak{F}_{3/2}(\psi_0)$ can be obtained by interpolation in the tables of McDougall and Stoner.

The numerical integrations have been carried out for the three values 0, 2, and 5 of the parameter ψ_0. In Table 1 the following measures of physical quantities: ψ, $\mathfrak{F}_{3/2}(\psi)F_{1/2}(\psi)$ (density) and $-\mathfrak{F}_{3/2}^{2/3}(\psi)\xi^2(d\psi/d\xi)$ (mass inside radius ξ) are tabulated as functions of ξ (radius) at intervals sufficiently close to permit interpolation if differences of high-enough order are used. The relative density-distribution-curves are shown in Figure 2. Table 2 gives the following boundary-value constants: ξ_1; $-\mathfrak{F}_{3/2}^{2/3}(\psi_1)\xi_1^2\psi'(\xi_1)$; the constant ratio M/M_E, of the mass to the Eddington mass; $\rho_c/\bar{\rho}$ (calculated from eq. [26]); and the proportionality constants $J_M(\psi_0)$ between $\mathfrak{M} \equiv M\mu_e^2/\odot$ and $(1-\beta)^{1/2}$ and $J_R(\psi_0)$ between $\mathfrak{R} \equiv R\mu_e/R\odot$ and $(1-\beta)^{-1/6}$, respectively (calculated from eq. [34] below).

8. *The mass-radius relation.*—From equation (25) and from equations (16) and (17) we have the following pair of simultaneous equations determining the mass-radius relation:

$$\frac{M\mu_e^2}{|C_2|} = -[\mathfrak{F}_{3/2}^{2/3}(\psi_1)\,\xi_1^2\psi'(\xi_1)]\left(\frac{1-\beta}{\beta^4}\right)^{1/2}; \qquad \frac{R\mu_e}{|a_2|} = \frac{\xi_1}{[\beta^2(1-\beta)]^{1/6}}. \tag{29}$$

The limiting cases $\psi_0 \gg 1$ and $\psi_0 \ll -1$ may be noted. In the former case,

$$\frac{M\mu_e^2/|C_2|}{(R\mu_e/|a_2|)^{-3}} = -\frac{243}{2048}[\eta_1^5\theta'_{3/2}(\eta_1)]\beta^{-3} = 5.2359\beta^{-3} \quad (\psi_0 \gg 1), \tag{30}$$

[8] In eq. (28) we have used the abbreviation F for $F_{1/2}(\psi_0)$ and $\mathfrak{F}$ for $\mathfrak{F}_{3/2}(\psi_0)$. Elsewhere in this paper F and $\mathfrak{F}_{3/2}$ refer to the variable ψ.

TABLE 1

THE PARTIALLY DEGENERATE STANDARD-MODEL FUNCTION

ξ	ψ	$\mathfrak{F}_{3/2}F_{1/2}$	$-\mathfrak{F}^{2/3}\xi^2\psi'$	ξ	ψ	$\mathfrak{F}_{3/2}F_{1/2}$	$-\mathfrak{F}^{2/3}\xi^2\psi'$
			$\psi_0=0$				
0.0.....	−0.000000	0.521140	0.0000	5.5.....	−2.11297	0.010790	4.0083
0.2.....	0.004137	.517544	0.0014	6.0.....	2.41950	.0059380	4.1420
0.4.....	0.016507	.506932	0.0109	6.5.....	2.74737	.0031210	4.2273
0.6.....	0.036982	.489806	0.0362	7.0.....	3.10524	.00154078	4.2782
0.8.....	0.065359	.466956	0.0834	7.2.....	3.25972	.00113501	4.2916
1.0.....	0.101362	.439390	0.1569	7.4.....	3.42247	.00082211	4.3019
1.2.....	0.144655	.408248	0.2596	7.6.....	3.59516	.00058361	4.3098
1.4.....	0.194849	.374719	0.3919	7.8.....	3.77986	.00040432	4.3156
1.6.....	0.251520	.339960	0.5529	8.0.....	3.97942	.00027185	4.3197
1.8.....	0.314219	.305031	0.7388	8.2.....	4.19766	.00017604	4.3226
2.0.....	0.382484	.270845	0.9464	8.4.....	4.43999	.00010861	4.3246
2.5.....	0.574494	.193021	1.5258	8.6.....	4.71439	.00006283	4.3258
3.0.....	0.791662	.130637	2.1270	8.8.....	5.03342	.00003324	4.3265
3.5.....	1.02833	.084707	2.6836	9.0.....	5.41855	.00001540	4.3269
4.0.....	1.28038	.052991	3.1561	9.2.....	5.91119	.00000576	4.3270
4.5.....	1.54536	.032127	3.5303	9.4.....	6.60944	.00000143	4.3271
5.0.....	−1.82256	0.018909	3.8100	9.6.....	−7.86857	0.00000011	4.3271
			$\psi_0=2$				
0.0.....	+2.000000	9.23783	0.00000	1.4.....	+0.904018	2.15574	3.7699
0.1.....	1.993560	9.16688	0.00307	1.5.....	+0.763085	1.74991	4.1786
0.2.....	1.974304	8.95746	0.02419	1.6.....	+0.616582	1.40156	4.5553
0.3.....	1.942429	8.61965	0.07977	1.7.....	+0.464697	1.10739	4.8950
0.4.....	1.898251	8.16925	0.18314	1.8.....	+0.307484	0.86281	5.1948
0.5.....	1.842198	7.62650	0.34346	1.9.....	+0.144827	0.66253	5.4541
0.6.....	1.774789	7.01448	0.56510	2.0.....	−0.023569	0.50096	5.6737
0.7.....	1.696621	6.35743	0.84754	2.2.....	−0.37990	0.272069	6.003
0.8.....	1.608344	5.67912	1.18577	2.4.....	−0.76918	0.136069	6.211
0.9.....	1.510641	5.00143	1.57103	2.6.....	−1.20613	0.060889	6.328
1.0.....	1.404202	4.34332	1.99184	2.8.....	−1.71907	0.023063	6.385
1.1.....	1.289707	3.72016	2.4352	3.0.....	−2.36892	0.0065549	6.407
1.2.....	1.167798	3.14337	2.8877	3.2.....	−3.32592	0.0009955	6.413
1.3.....	+1.039063	2.62055	3.3364	3.4.....	−5.62393	0.0000102	6.414
			$\psi_0=5$				
0.0.....	+5.00000	145.2766	0.00000	0.95....	+2.33338	13.5951	12.776
0.1.....	4.96551	141.7900	0.04773	1.00....	+2.07041	10.0441	13.334
0.2.....	4.86303	131.8135	0.36557	1.05....	+1.7915	7.1624	13.782
0.3.....	4.69537	116.6844	1.1484	1.10....	+1.4929	4.88616	14.126
0.4.....	4.46685	98.2924	2.4656	1.15....	+1.1687	3.14716	14.377
0.5.....	4.18271	78.6910	4.2506	1.20....	+0.8094	1.87500	14.547
0.6.....	3.84843	59.7307	6.3290	1.25....	+0.3991	0.99851	14.652
0.7.....	3.46885	42.8066	8.4720	1.30....	−0.0918	0.44653	14.709
0.80.....	3.04704	28.7528	10.455	1.35....	−0.7272	0.14681	14.733
0.85.....	2.82044	22.9143	11.331	1.40....	−1.6904	0.02436	14.740
0.90.....	+2.58286	17.8707	12.107	1.45....	−4.2456	0.00016	14.742

which shows that the mass is inversely proportional to the cube of the radius. The condition $\psi_0 \gg 1$, or its equivalent form: $\rho_c/\mu_e\,(1-\beta/\beta) \gg |B_2| \approx 3\times 10^6$ implies that $1-\beta$ must be very small in order that $\rho_c\mu_e^{-1}$ and T_c be much smaller than their criterion values. For $\rho_c\mu_e^{-1}$ equals one-tenth of its criterion value of 2×10^6, $1-\beta =$

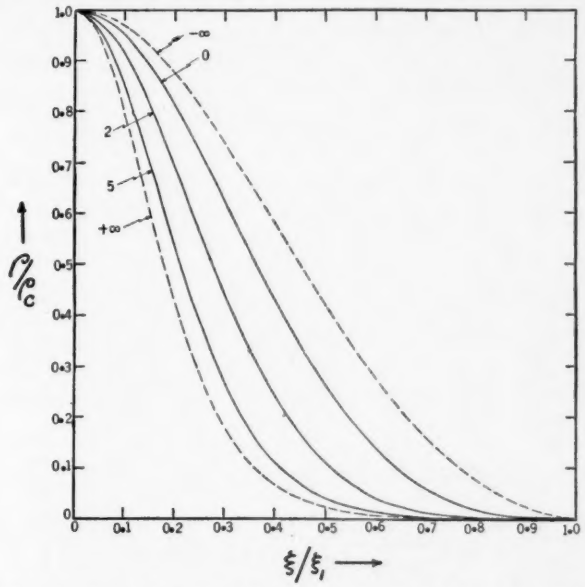

FIG. 2.—Relative density distributions for the partially degenerate standard model for the indicated values of ψ_0.

TABLE 2

THE BOUNDARY-VALUE CONSTANTS OF THE PARTIALLY DEGENERATE STANDARD MODEL

ψ_0	ξ_1	$-\mathfrak{d}_{3/2}^{2/3}(\psi_1)\xi_1^2\psi'(\xi_1)$	$\frac{M}{M_E}$	$\frac{\rho_c}{\bar{\rho}}$	$J_M(\psi_0)$	$J_E(\psi_0)$
$-\infty$ $(n=3)$	∞	3.707736	1	54.18248	17.98	.....
0	9.75789	4.3271	1.1670	37.300	21.08	0.0921
2	3.45971	6.414_3	1.7300	19.880	31.2	.0327
5	1.4617	14.74_2	3.976	10.26	71.8	0.01380
$+\infty$ $(n=\frac{3}{2})$	0	∞	∞	5.99071	.....	.....

0.1, 0.008, and 0.0005 for $\psi_0 = 0$, 2, and 5, respectively; for T_c equals one-tenth of its criterion value of 6×10^9, $1-\beta = 0.07$, 0.02, and 0.003 for $\psi_0 = 0$, 2, and 5, respectively. In any case, for negligible radiation pressure, we readily verify that equation (30) reduces precisely to the well-known mass-radius relation[9] of a Lane-Emden polytrope with index $n = \frac{3}{2}$ and $K = K_1$, which we have seen is appropriate in the present case. In the opposite limiting case, $\psi_0 \ll -1$, we find

$$\frac{M\mu_e^2/|C_2|}{(R\mu_e/|a_2|)^{-3}} = \frac{\frac{27}{2\pi}[-\eta_1^5\theta_3'(\eta_1)]}{\beta^3 e^{2\psi_0}} = 2845.17\beta^{-3}e^{-2\psi_0} \quad (\psi_0 \ll -1), \quad (31)$$

[9] *Stellar Structure*, eq. (72), p. 98.

which breaks down in the limit $\psi \to -\infty$, corresponding to the well-known fact that there is no mass-radius relation for the classical standard model.

9. *The* $\log \rho_c$, $\log T_c$ *locus of minimum radius for given central degeneracy* (ψ_0).—According to equation (29), the value $(1-\beta) = \frac{1}{3}$ makes the radius a minimum for a given value of ξ_1 and hence of ψ_0. Hence, we set $(1-\beta) = \frac{1}{3}$ in equation (11) and the first of equations (12) and obtain as the locus on the $\log \rho$, $\log T$ diagram (Fig. 1) of pairs of values of ρ_c and T_c that make the radius of the star a minimum for a given degree of central degeneracy (ψ_0) the straight line

$$\log T_c = \tfrac{1}{3} \log (\rho_c \mu_e^{-1}) - 7.66 \qquad (\rho_c \ll 2 \times 10^6). \quad (32)$$

This line necessarily cuts across the lines of constant ψ_0, all of which have slope $\frac{2}{3}$ (parallel to the $T\mu_e^{2/3} \propto \rho^{2/3}$ portion of the degeneracy-criterion locus), with a slope just one-half as great when $\mu_e = 1$. The linear portion (eq. [32]), as well as the upward-curving extrapolated portion, of the locus is shown in Figure 1.

10. *The approximate mass-radius relation for* $(1-\beta) \ll 1$.—For $(1-\beta) = 0.006$, corresponding at the upper limit to masses of $1.41\odot$ for $\psi_0 = -\infty$ (Eddington mass) and to $5.63\odot$ for $\psi_0 = 5$, we can set $\beta = 1$ in equations (29) and study the variations of mass and radius with $(1-\beta)$ and with each other with a maximum error of 1.2 per cent at $(1-\beta) = 0.006$. We can write equations (29) for the mass $\mathfrak{M}$ and radius $\mathfrak{R}$, both measured in solar units, in the form

$$\left.\begin{aligned} \mathfrak{M} &\equiv \frac{M\mu_e^2}{\odot} = J_M(\psi_0)\,(1-\beta)^{1/2}; \\ \mathfrak{R} &\equiv \frac{R\mu_e}{R_\odot} = J_R(\psi_0)\,(1-\beta)^{-1/6} \end{aligned}\right\} \qquad (1-\beta \ll 1), \quad (33)$$

where

$$J_M(\psi_0) = \frac{|C_2|}{\odot}\left[\mathfrak{F}_{3/2}^{2/3}(\psi_1)\,\xi_1^2\psi'(\xi_1)\right]; \qquad J_R(\psi_0) = \frac{|a_2|}{R_\odot}\,\xi_1 \quad (\psi_0 = \psi_0). \quad (34)$$

Using Table 2, we can write equation (29) in numerical form convenient for the determination of the $(\mathfrak{R}, 1-\beta)$ curves for given mass. For the values of ψ_0 for which boundary values are known we have

$$\left.\begin{aligned}
\psi_0 = \infty: &\quad \left\{\begin{aligned} 1-\beta &= 0 \\ \mathfrak{R} &= 0.04009\,\mathfrak{M}^{-1/3} \equiv \mathfrak{R}_1 \end{aligned}\right\} (a) \\
\psi_0 = 5: &\quad \left\{\begin{aligned} 1-\beta &= 1.939 \times 10^{-4}\mathfrak{M}^2 \\ \mathfrak{R} &= 0.01380\,(1-\beta)^{-1/6} \end{aligned}\right\} (b) \\
\psi_0 = 2: &\quad \left\{\begin{aligned} 1-\beta &= 1.025 \times 10^{-3}\mathfrak{M}^2 \\ \mathfrak{R} &= 0.03267\,(1-\beta)^{-1/6} \end{aligned}\right\} (c) \\
\psi_0 = 0: &\quad \left\{\begin{aligned} 1-\beta &= 2.251 \times 10^{-3}\mathfrak{M}^2 \\ \mathfrak{R} &= 0.0921\,(1-\beta)^{-1/6} \end{aligned}\right\} (d) \\
\psi_0 = -\infty: &\quad \left\{\begin{aligned} 1-\beta &= 3.093 \times 10^{-3}\mathfrak{M}^2 \\ \mathfrak{R} &= \text{Undetermined} \\ (\mathfrak{R}_0 &= 2.7362\,\mathfrak{R}_1) \end{aligned}\right\} (e)
\end{aligned}\right\} (1-\beta \ll 1). \quad (35)$$

11. *The accurate solution of Milne's problem.*—Milne considered the problem of determining the locus on the $(\mathfrak{R}, 1-\beta)$ diagram of the representative point of a perfect-gas

standard-model configuration of given mass contracting from $\mathfrak{R} = \infty$ to $\mathfrak{R} = \mathfrak{R}_{\min} \geqq 0$, corresponding to "the maximum density of which matter is capable." He concluded that the locus would be the straight line (the Eddington line) $1 - \beta = 1 - \beta\mathfrak{M}$, where $(1 - \beta\mathfrak{M})$ is the value of the relative radiation pressure corresponding to $\mathfrak{M}$ through Eddington's

TABLE 3

POINTS DETERMINING THE $(\mathfrak{R}, 1-\beta)$ CURVES FOR CONSTANT MASS

$\mathfrak{M} = \frac{M\mu_e^2}{\odot}$		$\psi_0 = \infty$ $(n = \frac{3}{2})$ $(\mathfrak{R} = \mathfrak{R}_1)$	$\psi_0 = 5$	$\psi_0 = 2$	$\psi_0 = 0$	$\psi_0 = -\infty$ (Eddington or $n = 3$) $(\mathfrak{R}_0)$
0.0	$1-\beta$	0	0	0	0	0
	$\mathfrak{R}$	∞	∞	∞	∞	∞
0.1	$1-\beta$	0	0.000001939	0.00001025	0.00002251	0.00003093
	$\mathfrak{R}$	0.0864	0.1236	0.2217	0.548	(0.2363)
0.2	$1-\beta$	0	0.00000776	0.00004109	0.0000900	0.0001237
	$\mathfrak{R}$	0.0686	0.0981	0.1760	0.4352	(0.1876)
0.3	$1-\beta$	0	0.00001745	0.0000922	0.0002026	0.0002783
	$\mathfrak{R}$	0.0599	0.0857	0.1537	0.3801	(0.1639)
0.4	$1-\beta$	0	0.00003103	0.0001640	0.0003602	0.0004948
	$\mathfrak{R}$	0.0544	0.0779	0.1396	0.3454	(0.1489)
0.5	$1-\beta$	0	0.0000485	0.0002562	0.000563	0.000773
	$\mathfrak{R}$	0.0505	0.0723	0.1296	0.3206	(0.1382)
0.6	$1-\beta$	0	0.0000698	0.0003689	0.000810	0.001113
	$\mathfrak{R}$	0.0475	0.0680	0.1220	0.3017	(0.1301)
0.7	$1-\beta$	0	0.0000950	0.000502	0.001103	0.001515
	$\mathfrak{R}$	0.0452	0.0646	0.1159	0.2866	(0.1235)
0.8	$1-\beta$	0	0.0001241	0.000656	0.001441	0.001979
	$\mathfrak{R}$	0.0432	0.0618	0.1108	0.2741	(0.1182)
0.9	$1-\beta$	0	0.0001571	0.000830	0.001823	0.002505
	$\mathfrak{R}$	0.0415	0.0594	0.1066	0.2636	(0.1136)
1.0	$1-\beta$	0	0.0001939	0.001025	0.002251	0.003093
	$\mathfrak{R}$	0.0401	0.0574	0.1029	0.2545	(0.1097)
1.1	$1-\beta$	0	0.0002346	0.001240	0.002724	0.003742
	$\mathfrak{R}$	0.0388	0.0556	0.0997	0.2465	(0.1063)
1.2	$1-\beta$	0	0.0002792	0.001476	0.003241	0.004453
	$\mathfrak{R}$	0.0377	0.0540	0.0968	0.2395	(0.1032)
1.3	$1-\beta$	0	0.0003277	0.001732	0.003804	0.00523
	$\mathfrak{R}$	0.0367	0.0526	0.0943	0.2332	(0.1005)
1.4	$1-\beta$	0	0.0003801	0.002008	0.004412	0.00606
	$\mathfrak{R}$	0.0358	0.0513	0.0920	0.2275	(0.0981)
1.5	$1-\beta$	0	0.0004363	0.002306	0.00506	0.00696
	$\mathfrak{R}$	0.0350	0.0501	0.0899	0.2223	(0.0958)
1.6	$1-\beta$	0	0.0004964	0.002623	0.00576	0.00792
	$\mathfrak{R}$	0.0343	0.04905	0.0880	0.2176	(0.09380)

quartic equation. The line extends parallel to the $\mathfrak{R}$-axis from infinity to that value of $\mathfrak{R}$ at which complete degeneracy is just beginning to develop at the center; the end-point on the $\mathfrak{R}$-axis would be that value of $\mathfrak{R}$ which corresponds to $\mathfrak{M}$ through the mass-radius relation for a polytrope of index $n = \frac{3}{2}$ (the second of eqs. [35a]) appropriate to the ultimate "completely collapsed" (completely degenerate) configuration. Milne proposed to determine the course of the $(\mathfrak{R}, 1 - \beta)$ curves within the domain of degeneracy between the above-mentioned end-points by considering composite configurations consisting of unrelativistic completely degenerate $n = \frac{3}{2}$ cores surrounded by (standard model) $n = 3$

perfect-gas envelopes. The curves were to be carried from the intersection of the Eddington line with the degeneracy-criterion locus (open circles on Figs. 3 and 4, *b*) to the endpoints on the $\mathfrak{R}$-axis by allowing the fractional radius $\mathfrak{R}_{\text{core}}/\mathfrak{R}$ of the $n = \frac{3}{2}$ core to vary parametrically from 0 to 1. This proposal was carried through by Fairclough.

Now that tables of the Fermi-Dirac functions $F_{1/2}$ and $F_{3/2}$ have been made available, it is possible to solve Milne's problem accurately, as is done in the present paper, by taking exact account of the gradual setting-in of partial degeneracy in going toward the center of the star. Our Table 3 and Figures 3 and 4 give the accurate solution of Milne's

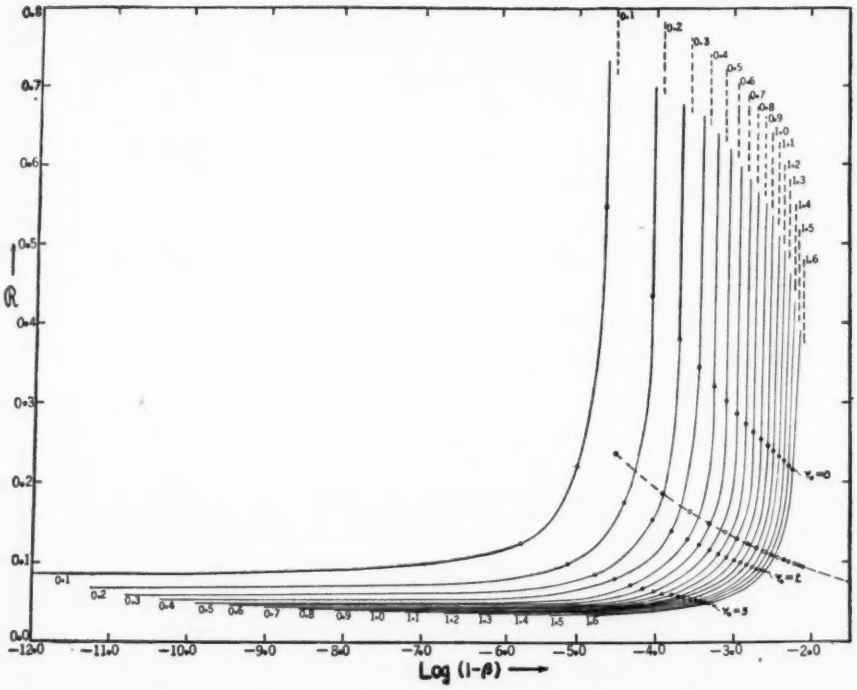

FIG. 3.—The Milne diagram. The accurate ($\mathfrak{R}$, log $1 - \beta$) curves of constant mass in the domain of degeneracy. For each curve the value of the mass $\mathfrak{M} = M\mu_e^2/\odot$ is indicated beside the vertical asymptote (the Eddington line) and also below the horizontal asymptote (the line $\mathfrak{R} = R\mu_e/R\odot = \mathfrak{R}_1$). The foot of each Eddington line at the point (log $1 - \beta$, $\mathfrak{R}_0$) is indicated by an open circle.

problem, restricted, however, to masses that are small enough that relativity effects may be neglected. For definiteness we may state that the error of the present theory for our values of $\psi_0 \geqq 0$ does not exceed about 10 per cent for $\mathfrak{M} \equiv M\mu_e^2/\odot \leqq 1.6$, or about 1 per cent for $\mathfrak{M} \leqq \frac{1}{2}$. This estimate includes the error due to the neglect of $1 - \beta^2$, which decreases rapidly for $\mathfrak{M} < 1.6$ and/or $\psi_0 > 0$.

In Figure 3 the ($\mathfrak{R}$, $1 - \beta$) curves for the masses $\mathfrak{M} = 0.1, 0.2, \ldots, 1.6$, for which the error should be less than 10 per cent, are plotted (from Table 3), using a logarithmic scale in $(1 - \beta)$ to avoid the crowding-together of the curves of small mass. The curves all have both vertical and horizontal asymptotes, the former being the Eddington line for mass $\mathfrak{M}$ and the latter the line $\mathfrak{R} = \mathfrak{R}_1$. The curved portion of each curve is determined by the three points corresponding to the numerical integrations for $\psi_0 = 0$, 2, and 5. Since there is some arbitrariness in the drawing of the curves, these three points, as well

as the asymptotes, are clearly indicated. The point $(\log_{10}[1-\beta], \mathfrak{R}_0)$ at the "foot" of each Eddington line is indicated as an open circle. The segment of a curve drawn through the latter points is very nearly ($\leqq$ 10 per cent for the present relatively small masses) a portion of the $(\mathfrak{R}_0, 1-\beta)$ curve[10] defining the domain of degeneracy on the Milne diagram in the theory of composite configurations having degenerate cores. In Figure 4, *a*, the curves of Figure 3 are transformed by the use of a natural, instead of a logarithmic, scale for $(1-\beta)$; the figure is, therefore, directly comparable to Chandrasekhar's figure. In Figure 4, *b*, the scale of abscissas of Figure 4, *a*, is magnified to show some of the

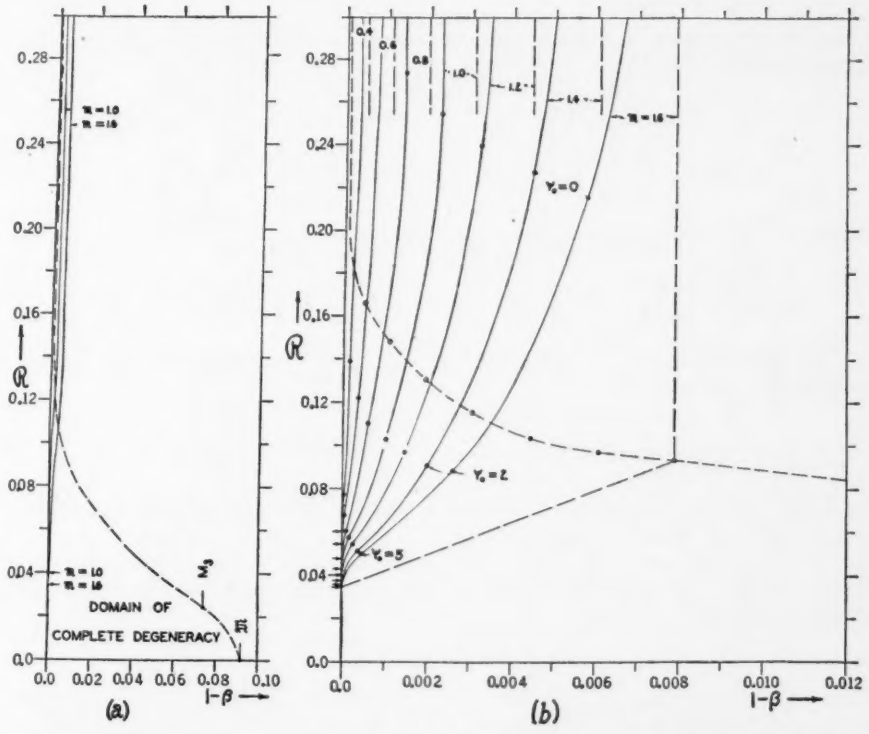

FIG. 4.—The Milne diagram (natural scale). The dashed curve is Chandrasekhar's $(\mathfrak{R}_0, 1-\beta)$ curve defining the domain of degeneracy. The arrows on the $\mathfrak{R}$-axis indicate, from top to bottom, the end-points $(0, \mathfrak{R}_1)$ for $\mathfrak{M} = 0.4, 0.6, 0.8, \ldots, 1.6$, respectively in (*b*).

$(\mathfrak{R}, 1-\beta)$ curves more clearly. On the natural scale for $(1-\beta)$ these curves approach the end-points $(0, \mathfrak{R}_1)$ on the $\mathfrak{R}$-axis vertically instead of horizontally as on the logarithmic scale.

On Milne's theory the $(\mathfrak{R}, 1-\beta)$ curve of constant mass on Figure 4, *b*, for $\mathfrak{M} = 1.6$, for example, would be the Eddington line labeled "$\mathfrak{M} = 1.6$" down to the open circle corresponding to $\mathfrak{R}_0$, then some curve ending at $\mathfrak{R}_1$ on the $\mathfrak{R}$-axis, the latter curve being represented as a dashed straight line in the figure. The error in $\mathfrak{R}$, as read from the latter straight line instead of from the accurate curve, is of the order of from -100 per cent to -200 per cent; and the Milne curves would be expected to lie below, rather than above, the straight line, at least near the junction with the Eddington line.

[10] S. Chandrasekhar, *M.N.*, **95**, 226, 1935, Fig. 3, or *Stellar Structure*, Fig. 34.

II. THE PARTIALLY DEGENERATE ISOTHERMAL GAS SPHERE

12. *The fundamental differential equation.*—By definition of the isothermal gas sphere, T = constant. Hence the equation of state of the model is simply the Fermi-Dirac equation of state (4), with the radiation pressure $p_r = (a/3)T^4$ added to the gas pressure p_g to give the total pressure:

$$\left.\begin{aligned} \rho &= B_1 F_{1/2}(\psi) \equiv |B_1|\,\mu_e T^{3/2} F_{1/2}(\psi)\,, \\ P &= A_1 \mathfrak{F}_{3/2}(\psi) + \frac{a}{3}T^4 \equiv |A_1|\,T^{5/2}\mathfrak{F}_{3/2}(\psi) + \frac{a}{3}T^4\,, \end{aligned}\right\} \tag{36}$$

where A_1, B_1, $|A_1|$, and $|B_1|$ are constants defined by equations (5) and (6). Using the transformations

$$r = a_1 \xi\,, \tag{37}$$

where

$$a_1 = \left[\frac{A_1}{4\pi G B_1^2}\right]^{1/2} \equiv \frac{|a_1|}{\mu_e T^{1/4}} = \frac{1.495}{\mu_e T^{1/4}} R_\odot\,, \tag{38}$$

we obtain, as our fundamental differential equation,

$$\frac{1}{\xi^2}\frac{d}{d\xi}\left(\xi^2 \frac{d\psi}{d\xi}\right) = -F_{1/2}(\psi)\,, \qquad \text{or} \qquad \frac{d^2\psi}{d\xi^2} + \frac{2}{\xi}\frac{d\psi}{d\xi} = -F_{1/2}(\psi)\,, \tag{39}$$

subject to the usual boundary conditions (cf. eqs. [19]). In the present case, according to the first of equations (36),

$$\frac{\rho_c}{\mu_e T^{3/2}} = |B_1|\,F_{1/2}(\psi_0)\,, \qquad \text{or} \qquad \psi_0 \text{ specifies } \frac{\rho_c}{\mu_e T^{3/2}}\,, \tag{40}$$

which is analogous to the last of specifications (20) for the standard model. As in the latter case, there is no homology relation.

13. *The density at any point in terms of the central density.*—By equation (19), the first of equations (36), and the assumption that the parameters T and μ_e are constant throughout the configuration we find

$$\frac{\rho}{\rho_c} = \frac{F_{1/2}(\psi)}{F_{1/2}(\psi_0)}\,. \tag{41}$$

14. *The mass relation.*—Proceeding as in § 4, we find

$$M(\xi) = -C_1 \xi^2 \frac{d\psi}{d\xi} \equiv -|C_1|\,\mu_e^{-2} T^{3/4} \xi^2 \frac{d\psi}{d\xi}\,, \tag{42}$$

where

$$|C_1| = 4\pi |a_1|^3 |B_1| = 6.47 \times 10^{-8} \odot\,. \tag{43}$$

15. *The relation between the mean and the central density.*—Proceeding as in § 5, we find from equations (36), (37), and (42) the expression

$$\frac{\rho_c}{\bar{\rho}} = -F_{1/2}(\psi_0)\frac{\xi_1}{3\psi'(\xi_1)}\,. \tag{44}$$

16. *The limiting cases of very low and of very high central degeneracy.*—In the limit of very low central degeneracy our present partially degenerate isothermal configurations reduce to the classical isothermal gas sphere (polytrope with $n = \infty$), and in the limit of very high central degeneracy they reduce to precisely the same limit as do the partially

degenerate standard-model configurations, namely, to the low-density limit (polytrope with $n = \frac{3}{2}$) of the white-dwarf configurations.

17. *The numerical integrations.*—Seven integrations of the partially degenerate isothermal equation (39) for the values $\psi_0 = 0$, 2, 3, 5, 10, 20, and 100 have been carried through with from seven to nine significant figures in the integration variable $\varphi \equiv \psi\xi$, each integration being carried at least as far as the point where $\rho/\rho_c < 10^{-4}$. Tables of measures of the same three physical quantities as in Table 1 for the standard model are given elsewhere.[11] These tables are summarized by Table 4 and Figure 5. In Figure 5 the density-distribution-curves for partially degenerate isothermal configurations having

TABLE 4

THE PARTIALLY DEGENERATE ISOTHERMAL GAS SPHERE WITH CENTRAL DENSITY $\rho_c = 10^3$ GM/CM^3

ψ_0	$T\mu_e^{2/3} \times 10^6$ (° K)	$\rho/\rho_c = 10^{-1}$	$\rho/\rho_c = 10^{-2}$		$\rho/\rho_c = 10^{-3}$		$\rho/\rho_c = 10^{-4}$	
		$r^*\mu_e^{5/6}$ $M(r^*)\mu_e^{5/2}$	Multiple of "*" Value	$r\mu_e^{5/6}$ $M(r)\mu_e^{5/2}$	Multiple of "*" Value	$r\mu_e^{5/6}$ $M(r)\mu_e^{5/2}$	Multiple of "*" Value	$r\mu_e^{5/6}$ $M(r)\mu_e^{5/2}$
$-\infty (n = +\infty)$	∞	∞	(2.5400)	∞	(7.2929)	∞	(24.910)	∞
		∞	(2.6179)	∞	(6.1469)	∞	(19.780)	∞
0	29.7	0.14131	(2.4159)	0.34139	(6.8969)	0.9746	(24.339)	3.4393
		0.46934	(2.3397)	1.0980	(5.1680)	2.4255	(17.188)	8.0670
2	12.4	0.09791	(2.1426)	0.20979	(5.7986)	0.5678	(22.554)	2.2084
		0.17087	(1.8729)	0.32002	(3.3952)	0.5801	(11.781)	2.0129
3	9.13	0.08825	(1.9818)	0.17489	(4.9846)	0.4399	(20.767)	1.8328
		0.13136	(1.6658)	0.21882	(2.5957)	0.3410	(8.5606)	1.1245
5	5.81	0.07867	(1.7243)	0.13565	(3.5131)	0.2764	(14.2032)	1.1174
		0.10035	(1.4122)	0.14171	(1.7282)	0.1734	(3.3590)	0.3371
10	2.98	0.07200	(1.4332)	0.10319	(2.0627)	0.14852	(3.5171)	0.2532
		0.08347	(1.2107)	0.10105	(1.2672)	0.10576	(1.2963)	0.1082
20	1.50	0.07002	(1.2916)	0.09044	(1.5412)	0.10792	(1.8733)	0.13117
		0.07926	(1.1397)	0.09033	(1.1562)	0.09163	(1.1592)	0.09188
100	0.300	0.06949	(1.2265)	0.08522	(1.3003)	0.09035	(1.3462)	0.09354
		0.07815	(1.1142)	0.08707	(1.1190)	0.08745	(1.1193)	0.08747
$+\infty (n = \frac{3}{2})$	0	0.06947	(1.2242)	0.08504	(1.2835)	0.08916	(1.2970)	0.09010
		0.07811	(1.1134)	0.08696	(1.1175)	0.08728	(1.1176)	0.08729

$\rho_c = 10^3$ gm/cm^3 are plotted against radial distance $r\mu_e^{5/6}$ in both centimeter and solar units. The curve for the limiting case, $\psi_0 \to -\infty$, is the sensibly straight line $\rho/\rho_c = 1$ on the scale of Figure 5. For the other limiting case, $\psi_0 \to +\infty$, the curve cuts the $r\mu_e^{5/6}$ axis abruptly at 6.28×10^9 cm $= 0.0904\ R\odot$ with the slope $\theta'_{3/2}(\eta_1) = -0.2033013$. For finite positive values of ψ_0 the solutions have no mathematically finite boundaries, but they approach the finite boundary of, as well as the curve of, the latter limiting case asymptotically as $\psi_0 \to +\infty$, so that it is possible to define a physical boundary for only moderately large values of ψ_0. Note that the curve for $\psi_0 = 100$ is indistinguishable in Figure 5 from that for $\psi_0 = +\infty$.

After a certain low density has been reached, the solutions can be continued analytically by means of the formula

$$\psi(\xi) = a + b\,\xi^{-1} - c^2 \log \xi \qquad (45)$$

[11] See n. 1, above.

where a, b, and c^2 are arbitrary constants of integration, the latter being inherently positive.

In Table 4 are given the values of the radius $r\mu_e^{5/6}$, of the mass $M(r)\mu_e^{5/2}$, and of the isothermal temperature $T\mu_e^{2/3}$ for the various solutions ψ_0, all calculated for central density $\rho_c = 10^3$ gm/cm.^{3} The radii and masses are each given both in solar units and (in parentheses) in terms of their respective values at $r = r^*$, defined as where $\rho/\rho_c = 10^{-1}$. Pairs of values of $r\mu_e^{5/6}$ and $M(r)\mu_e^{5/2}$ are given for each of the four values: $\rho/\rho_c = 10^{-1}$, 10^{-2}, 10^{-3}, and 10^{-4}, the value of $r\mu_e^{5/6}$ being given above, and that of $M(r)\mu_e^{5/2}$ below, for each solution ψ_0. Between successive columns of pairs of radius and mass values are given, in parentheses, the multiple that each quantity $r\mu_e^{5/6}$ and $M(r)\mu_e^{5/2}$ is of its value at $r^*\mu_e^{5/6}$.

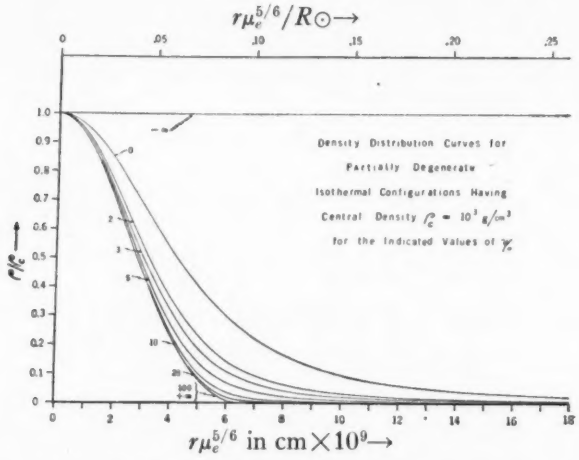

FIG. 5.—Relative density distributions for partially degenerate isothermal configurations

Table 4 may be converted immediately for use for any other value of ρ_c or of T by noting equations (37), (38), (40), and (42). Specifically, Table 4 may be transformed by the following relations which hold for a given solution ψ_0:

$$r\mu_e^{5/6} \propto \rho_c^{-1/6}\,; \qquad M(r)\,\mu_e^{5/2} \propto \rho_c^{1/2}\,; \qquad T\mu_e^{2/3} \propto \rho_c^{2/3}\,. \tag{46}$$

III. APPLICATIONS

18. *The relevant range of* M, R, *and* μ_e *values.*—For applications of the theory of the partially degenerate standard model we see from Figure 3 that we should look for stars having

$$\tfrac{1}{30}R\odot \leqq R \leqq 0.4R\odot\,, \qquad M \leqq 1.6\odot \qquad (\mu_e = 1)\,. \tag{47}$$

The theory is perfectly applicable, of course, to stars having $R > 1/30R\odot$ and $M < 1.6\odot$ but whose representative points are far removed from the curved portion of Figure 3; but, since either the classical standard model $n = 3$ or the $n = \frac{3}{2}$ model is applicable to such stars with sufficient accuracy, we do not consider them here. We note that the effect of $\mu_e > 1$ is to multiply $\mathfrak{R}$ by μ_e and $\mathfrak{M}$ by μ_e^2, so that the representative point on Figure 3 moves upward and to the right in the direction of nondegeneracy. For $\mu_e = 2$ the specification (47) becomes

$$\tfrac{1}{60}R\odot \leqq R \leqq 0.2R\odot\,, \qquad M \leqq 0.4\odot \qquad (\mu_e = 2)\,. \tag{48}$$

19. *The subdwarf stars.*—Among the subdwarf stars, Kuiper[12] has recently discovered[13] two extreme cases, Wolf 134 and Wolf 1037, of spectral type K3 and K5, respectively. The absolute magnitudes are roughly +12.6 and +12.5, which means that they are about 5.7 and 4.5 magnitudes, respectively, below the main sequence. If they are of the same color as main-sequence K stars, their radii should be about one-tenth as great, or about 0.08 $R\odot$; if their color is not the same, it would be expected to be slightly bluer, corresponding to slightly smaller radii. There is no direct way of determining the masses, but theoretical considerations lead to the expectation of low hydrogen content ($\mu_e \approx 2$) and masses of the order of 0.1 $\odot$. We shall consider the following three sets of numerical values:

$$\left.\begin{array}{llll} (a) & R = 0.05R\odot\,, & M = 0.05\odot\,; \\ & \mathfrak{R} = 0.10\quad, & \mathfrak{M} = 0.2\quad; \\ (b) & R = 0.08R\odot\,, & M = 0.1\odot\,; \\ & \mathfrak{R} = 0.16\quad, & \mathfrak{M} = 0.4\quad; \\ (c) & R = 0.16R\odot\,, & M = 0.3\odot\,; \\ & \mathfrak{R} = 0.32\quad, & \mathfrak{M} = 1.2\quad, \end{array}\right\} \tag{49}$$

corresponding to (*a*) improbably high central degeneracy, (*b*) the most probable values, and (*c*) improbably low central degeneracy,[14] all for $\mu_e = 2$. The values of $\log(1-\beta)$ and the approximate values of ψ_0 are read from Figure 3 and used to calculate $\log \rho_c$ and $\log T_c$ on the basis of the classical Eddington standard model[15] and on the basis of the present partially degenerate standard model as follows:

$$\left.\begin{array}{ll} (a) & \psi_0 = +5.0 \\ & \log(1-\beta) = -5.20 \\ (b) & \psi_0 = +1.7 \\ & \log(1-\beta) = -3.70 \\ (c) & \psi_0 = -0.5 \\ & \log(1-\beta) = -2.46 \end{array}\right\} \tag{50}$$

Classical (Eddington) Standard Model

$$\left.\begin{array}{llll} (a) & \log \rho_c = 4.49 & (b) \quad \log \rho_c = 4.17 & (c) \quad \log \rho_c = 3.75 \\ & \log T_c = 7.60 & \log T_c = 7.69 & \log T_c = 7.87 \end{array}\right\} \tag{51}$$

Partially Degenerate Standard Model

$$\left.\begin{array}{llll} (a) & \log \rho_c = 3.7 & (b) \quad \log \rho_c = 3.8 & (c) \quad \log \rho_c = 3.6 \\ & \log T_c = 7.0 & \log T_c = 7.5 & \log T_c = 7.8 \end{array}\right\} \tag{52}$$[16]

[12] I am indebted to Dr. Kuiper for kindly communicating to me his unpublished estimates of the best values (as of April, 1941) of the spectra, masses, and radii of the subdwarfs and also of the old novae discussed in § 20. I am also indebted to him for helpful discussions and suggestions regarding subdwarf and white-dwarf stars and for access to his unpublished paper on this subject presented before the 1939 Paris meeting of the I.A.U.

[13] G. P. Kuiper, *Ap. J.*, **91**, 269, 1940.

[14] High central degeneracy is not directly correlated with high mean density, for two reasons: (1) the degeneracy-criterion locus is not vertical, and (2) $\rho_c/\bar{\rho}$ decreases with increasing degeneracy, according to Table 2. Thus, $\mathfrak{R} = 0.10$, $\mathfrak{M} = 1.2$ is more dense than (*a*), but $\psi_0 = +2.0$, as compared with +5.0; also $\mathfrak{R} = 0.32$, $\mathfrak{M} = 0.20$ is less dense than (*c*), but $\psi_0 = +0.5$, as compared with −0.5.

[15] Using the formulae: $\rho_c = 54.18\,\bar{\rho}$ and $T_c = 19.72 \times 10^6\,\beta\mathfrak{M}/\mathfrak{R}$.

[16] The values of $\log \rho_c$ are uncertain by about ± 0.1 in (*a*) and (*b*) and by a somewhat larger amount in (*c*), on account of the uncertainty in the interpolation of ψ_0. The uncertainty in $\log T_c$ is about one-third that in $\log \rho_c$.

We note that all three cases, with the possible exception of case (*c*), fall in the curved region of Figure 3, which is just the region in which the present theory is required. Comparing equations (51) and (52) with Figure 1, we see that the representative point for the center of these subdwarfs falls near the $Q = -10$ locus, the degeneracy-criterion locus, and the $q = -10$ locus, respectively, in cases (*a*), (*b*), and (*c*). The classical theory predicts the central density too high by about 0.8, 0.3, and 0.1 in log ρ_c in cases (*a*), (*b*), and (*c*), respectively. The error in log T_c is about two-thirds as great and is in the same sense.

There are several other subdwarf stars in Kuiper's lists[17] that are less extreme than the two discussed above but which probably fall in the realm of the present theory.

20. *The old novae.*—Humason's investigation[18] of sixteen old novae gives the spectrum as type O and the mean absolute visual magnitude, $\bar{M}_v$, as about +3. 0. From theoretical considerations Kuiper[12] expects these stars to have low hydrogen content ($\mu_e \sim 2$). Accordingly, he considers $M = 0.3 - 0.5\odot$ as more probable for $\bar{M}_v = +3$ than the value $M = \odot$ adopted by Humason. He finds log $R = -0.43$, -0.71, or -0.91, corresponding, respectively, to temperature 25,000°, 50,000°, or 100,000°, the first and last values being limits and the second the most probable. Only if the radii and masses should both be near their lower limits would the representative points fall in the curved portion of Figure 3, if $\mu_e = 2$. In no case would the representative point, log ρ_c, log T_c, on Figure 1 fall below the degeneracy-criterion locus. In the most extreme case we have for the partially degenerate and for the Eddington models:

$$\left.\begin{aligned} R &= 0.12R_\odot, \quad M = 0.3\odot; \\ \mathfrak{R} &= 0.24 \quad , \quad \mathfrak{M} = 1.2 \quad ; \\ \log(1-\beta) &= -2.48; \\ \psi_0 &= 0.00 \quad ; \\ &\quad \text{(P.D.)} \quad \text{(ED.)} \\ \log \rho_c &= 3.97, \quad 4.12; \\ \log T_c &= 7.92, \quad 7.99 \qquad (\mu_e = 2), \end{aligned}\right\} \tag{53}$$

corresponding to a point about 0.2 units above the degeneracy-criterion locus. In the most probable case we have:

$$\left.\begin{aligned} R &= 0.20R_\odot, \quad M = 0.4\odot; \\ \mathfrak{R} &= 0.40 \quad , \quad \mathfrak{M} = 1.6 \quad ; \\ \log(1-\beta) &= -2.12; \\ \psi_0 &\approx -1 \quad ; \\ &\quad \text{(P.D.)} \quad \text{(ED.)} \\ \log \rho_c &= 3.6, \quad 3.58; \\ \log T_c &= 7.9, \quad 7.90 \qquad (\mu_e = 2), \end{aligned}\right\} \tag{54}$$

corresponding to a point very nearly on the $q = -10$ locus of Figure 1. Thus, the Eddington theory should be adequate in the most probable case. We conclude that the partially degenerate standard model would be required for the old novae only under the following improbable circumstances: (*a*) both radii and masses fall at the lower limits; (*b*) the radii and masses lie anywhere between the above limits, and $\mu_e = 1$; or (*c*) the radii and masses have their most probable values, and $\mu_e < 1.6$.

21. *The validity of the classical standard model for a star of given mass and radius.*—We note the convenient coincidence that for $\mu_e = 2$ the Eddington model can be used to test

[17] G. P. Kuiper, *Ap. J.*, **91**, 269, 1940; **92**, 128, 1940, Table 1.

[18] M. L. Humason, *Ap. J.*, **88**, 228, 1938.

accurately its own validity. In cases in which we suspect that the perfect-gas theory may fail, we expect $\mu_e \sim 2$, in which case the representative point (log ρ_c, log T_c) calculated on the classical model, is found empirically to bear very nearly the same relation to the degeneracy-criterion locus as when calculated on the partially degenerate standard model, even though the actual values of log ρ_c and log T_c may be greatly overestimated by the classical theory.

If $\mu_e = 1$ instead of $\mu_e = 2$, then the representative point is actually shifted horizontally to the left by 0.3 units on Figure 1 in the direction of nondegeneracy, but the Eddington theory predicts that it is moved by the same amount vertically downward in the direction of degeneracy. Thus, regardless of the value of μ_e (which must lie in the range 1.00 to 2.03 for a Russell mixture), we can say that, if the Eddington values of log ρ_c and log T_c indicate a point safely above the degeneracy-criterion locus, the Eddington model may be used with confidence (at least for $\mathfrak{M} \leqq 1.6$). This will be the case if

$$\left.\begin{array}{lll} \log T_c > \frac{2}{3} \log \rho_c + 5.560\,, & \text{or} & \log T_c \gg \frac{2}{3} \log \rho_c + 5.080\,. \\ \text{(above the } q = -10 \text{ locus)} & & \text{(far above degeneracy-criterion locus)} \end{array}\right\} \quad (55)$$

Otherwise the representative point should be calculated as in equations (49), (50), and (52); if log ρ_c and log T_c are not required, the central degeneracy (ψ_0) can be estimated by mere inspection of Figure 3 more exactly than by the use of the Eddington theory.

The classical standard model is probably adequate for main-sequence M-dwarf stars such as Krüger 60A and Krüger 60B. The mass of the latter is about the same as that of the subdwarfs, for which we found the partially degenerate standard model to be required; but the radius is so much larger (of the order of $0.4R_\odot$ instead of $0.1R_\odot$) that even for $\mu_e = 1$ the representative point on Figure 3 falls somewhat above the sharply curved portions of the ($\mathfrak{R}$, $1 - \beta$) curves at $\psi_0 \sim 0$. If $\mu_e > 1$, as seems likely, then the central degeneracy is much less and should be negligible.

It is a pleasure to acknowledge my deep indebtedness to Dr. S. Chandrasekhar for his suggestion of the present problem and for his indispensable guidance throughout its solution. I am also very grateful to Dr. Otto Struve for his kind encouragement and for access to the facilities of the Yerkes Observatory. My thanks are also due the University of Chicago for financial assistance in the form of a University fellowship for two years.

SOME REMARKS ON THE NEGATIVE HYDROGEN ION AND ITS ABSORPTION COEFFICIENT

S. CHANDRASEKHAR
Yerkes Observatory
Received June 28, 1944

ABSTRACT

Some remarks on the quantum theory of the negative hydrogen ion are made, and attention is drawn to certain facts which make the evaluation of its continuous absorption coefficient a problem of extreme difficulty.

This paper will consist of a few disconnected remarks on the quantum theory of the negative hydrogen ion.

1. *The wave function for the ground state of* H^-.—Since the discovery of the stability of the negative ion of hydrogen by Bethe[1] and Hylleraas[2] and the recognition of its astrophysical importance by Wildt,[3] attempts[4] have been made to determine the electron affinity of hydrogen with as high a precision as possible. In these latter attempts the energy of the ground state is determined by applications of the Ritz principle, using forms for the wave functions suggested by Hylleraas' successful treatment of the ground state of the helium atom. Thus Williamson's six-parameter wave function is of exactly the same form as the "best" wave function of Hylleraas for helium. Similarly, Henrich's eleven-parameter wave function includes terms beyond those used by Williamson. While there can hardly be any doubt that Henrich's value for the electron affinity of 0.747 electron volts can be in error by more than a fraction of 1 per cent, the relatively weak convergence of the entire process (cf., e.g., Table 7 in Henrich's paper) leaves one with a suspicion that the formal analogy between the atomic configurations of H^- and He has perhaps been taken too literally. From one point of view it would seem that the structures of these two atoms must be very different indeed; for, while helium is a stable closed structure, the negative hydrogen ion is an open structure which exists principally on account of incomplete screening and polarization (see below). This suggests that it might be possible to obtain better representations of the true wave function by seeking forms which will explicitly take into account this difference. That such attempts may not prove unsuccessful is suggested by the following preliminary considerations.

As is well known, the success of Hylleraas' investigations on helium is due principally to the circumstance that a wave function of the form

$$\psi = e^{-\alpha(r_1+r_2)}\,, \tag{1}$$

which ascribes a hydrogen-like wave function to each of the electrons in a suitably screened Coulomb field, already provides a good first approximation. More particularly the wave function of the form (1), which gives the lowest energy, is

$$\psi = e^{-(Z-[5/16])(r_1+r_2)}\,. \tag{2}$$

(In the foregoing equation r_1 and r_2 are measured in units of the Bohr radius. Similarly, in the rest of the paper we shall systematically use Hartree's atomic units.)

[1] *Zs. f. Phys.*, **57**, 815, 1929.

[2] *Zs. f. Phys.*, **60**, 624, 1930.

[3] *Ap. J.*, **89**, 295, 1939.

[4] R. E. Williamson, *Ap. J.*, **96**, 438, 1942; and L. R. Henrich, *Ap. J.*, **99**, 59, 1943.

When $Z = 1$, the wave function (2) predicts an energy $E = -0.473$, which actually makes H^- an unstable structure and is in error by fully 12 per cent. In other words, the first approximation, which is so satisfactory for *He*, fails completely for H^-. That this should happen is not surprising in view of our earlier remarks concerning the difference between the two atoms. On the other hand, it would appear that in contrast to *He* a natural first approximation for H^- is to ignore the screening of one of the electrons and adjust the screening constant for the second electron only. In other words, the starting-point for H^- should rather be a wave function of the form

$$\psi = e^{-r_1-br_2} + e^{-r_2-br_1}, \tag{3}$$

where b is the screening constant for the second electron. More generally, we may write

$$\psi = e^{-ar_1-br_2} + e^{-ar_2-br_1}, \tag{4}$$

where a and b are constants to be appropriately chosen. The Ritz principle applied to a wave function of the form (4) showed that the lowest value of energy is attained when

$$a = 1.03925 \quad \text{and} \quad b = 0.28309. \tag{5}$$

The corresponding value for the energy is

$$E_1 = -0.51330, \tag{6}$$

which predicts the stability of H^-. Moreover, in confirmation of our expectations it is seen that, while the inner electron is practically unscreened, the outer one is screened considerably and to the extent of 72 per cent. In view of this, it appears that a good second approximation may be provided by considering a wave function of the form

$$\psi = (e^{-ar_1-br_2} + e^{-ar_2-br_1})(1 + c r_{12}), \tag{7}$$

where a, b, and c are constants to be so chosen as to lead to a minimum value for the energy. It is found that with

$$a = 1.07478, \quad b = 0.47758, \quad \text{and} \quad c = 0.31214 \tag{8}$$

we minimize the energy integral and obtain for it the value

$$E_2 = -0.52592. \tag{9}$$

This value for the energy, while inferior to those predicted by Williamson (0.5265) and Henrich (0.5276), is substantially better than the value 0.5253 given by the three-parameter wave function of Bethe and Hylleraas.

An interesting feature of the wave function (7) with the constants as given by equation (8) is that the inclusion of the term r_{12} reduces the screening of the outer electron from 0.72 to 0.52. This relatively large reduction in the screening is due to the strong polarizability of the hydrogen atom. Indeed, according to equations (6) and (9) we may say that the electron affinity of hydrogen is due about equally to the incomplete screening of the nucleus and to the polarization of the hydrogenic core.

The foregoing discussion suggests that it might be profitable to improve the wave function (7) by including further terms. This would be particularly useful for estimating the inherent uncertainty in the absorption cross-sections derived from different wave functions, all of which predict (within limits) the same value for energy. The practical importance for carrying out such a discussion will be apparent from our remarks in the following section.

2. *The absorption cross-sections for* H^-.—The calculations of the absorption cross-sections which have been carried out so far (Massey and Bates; Williamson; Henrich)

are based on two approximations. The first consists in the use of the wave function for describing the bound state the ones derived from the minimal calculations and the second, in the use of a plane wave representation of the ejected outgoing electron. The validity or otherwise of these approximations will depend upon whether the principal contributions to the matrix element,

$$\mu = \int \Psi_d (r_1 + r_2) \Psi_c d\tau \,, \tag{10}$$

come from those regions of the configuration space in which the two approximations may be expected to be satisfactory. In equation (10) Ψ_d denotes the normalized wave function for the ground state of H^-, and Ψ_c the wave function of the continuous state normalized to correspond to an outgoing electron of unit density.

It appears that the use of the plane-wave representation for the free electron will not introduce any very serious error, since, as has been pointed out on an earlier occasion,[5] parts of the configuration space which are only relatively far from the hydrogenic core are relevant for the absorption process. But if this be admitted, the question immediately arises as to whether the wave function for the ground state derived from the Ritz principle can be trusted to these distances. It appears that the matter can be decided in the following manner.

First, we may observe that it might prove to be an adequate approximation to use for the continuous wave function that of an electron moving in the Hartree field of a hydrogen atom. In other words, it might be sufficient to use for Ψ_c the expression

$$\Psi_c = \frac{1}{\sqrt{2\pi}} \{ e^{-r_2} \phi(r_1) + e^{-r_1} \phi(r_2) \} \,, \tag{11}$$

where $\phi(r)$ satisfies the wave equation

$$\nabla^2 \phi + \left[k^2 + 2 \left(1 + \frac{1}{r} \right) e^{-2r} \right] \phi = 0 \tag{12}$$

and tends asymptotically at infinity to a plane wave of unit amplitude along some chosen direction. If this direction in which the ejected electron moves at infinity be chosen as the polar axis of a spherical system of co-ordinates, it is readily shown that the appropriate solution for ϕ can be expressed in the form

$$\phi = \sum_{l=0}^{\infty} \frac{1}{kr} (2l+1) P_l(\cos\vartheta) \chi_l(r) \,, \tag{13}$$

where the radial function χ_l is a solution of the equation

$$\frac{d^2\chi_l}{dr^2} + \left\{ k^2 - \frac{l(l+1)}{r^2} + 2 \left(1 + \frac{1}{r} \right) e^{-2r} \right\} \chi_l = 0 \,, \tag{14}$$

which tends to a pure sinusoidal wave of unit amplitude at infinity. Thus, on our present approximation Ψ_c can be written in the form

$$\left.\begin{aligned} \Psi_c = \frac{1}{\sqrt{2\pi}} \Bigg\{ & e^{-r_2} \sum_{l=0}^{\infty} \frac{1}{k r_1} (2l+1) P_l(\cos\vartheta_1) \chi_l(r_1; k) \\ & + e^{-r_1} \sum_{l=0}^{\infty} \frac{1}{k r_2} (2l+1) P_l(\cos\vartheta_2) \chi_l(r_2; k) \Bigg\} . \end{aligned}\right\} \tag{15}$$

[5] S. Chandrasekhar and M. K. Krogdahl, *Ap. J.*, **98**, 205, 1943.

Using the foregoing form for Ψ_c, the standard formula for the absorption cross-section for a process in which a photoelectron with k atomic units of momentum is ejected can be reduced to the form

$$\kappa = 9.266 \times 10^{-19} \frac{k^2 + 0.05512}{k} \left| \int_0^\infty W(r)\, \chi_1(r)\, dr \right|^2 \text{cm}^2, \qquad (16)$$

where $W(r)$ is a certain weight function which can be derived from and depends only on the wave function for the bound state. It is seen that, according to equation (16), the absorption cross-section depends only on the single radial function χ_1. This is to be expected, since the ground state, being an s-state, transitions can take place only to a p-state. It may be noted here that on the plane-wave representation of the free electron the appropriate form for χ_1 is

$$\chi_1(\text{plane wave}) = \frac{\sin kr}{kr} - \cos kr\,. \qquad (17)$$

The function $W(r)$ corresponding to Henrich's eleven-parameter wave function has been computed and is tabulated in Table 1. The run of the function is further illustrated in Figure 1.

TABLE 1

THE WEIGHT FUNCTION $W(r)$

r	$W(r)$	r	$W(r)$	r	$W(r)$	r	$W(r)$
0	0	4.0	1.597	11.0	0.833	19.0	0.131
0.5	0.210	4.5	1.623	12.0	.703	20.0	.096
1.0	0.553	5.0	1.620	13.0	.585	21.0	.069
1.5	0.861	6.0	1.548	14.0	.478	22.0	.049
2.0	1.108	7.0	1.422	15.0	.383	23.0	.034
2.5	1.298	8.0	1.273	16.0	.301	24.0	.024
3.0	1.439	9.0	1.120	17.0	.233	25.0	0.016
3.5	1.538	10.0	0.972	18.0	0.177	∞	0

An examination of the values given in Table 1 discloses the somewhat disquieting fact that substantial contributions to the integral

$$\int_0^\infty W(r)\, \chi_1(r)\, dr \qquad (18)$$

arise from values of r up to 25, while as much as 30–40 per cent of the entire value comes from $r \geqslant 10$. This result has two consequences. The first is that the use of the p-spherical wave (17) instead of the solution derived from (cf. eq. [14])

$$\frac{d^2\chi_1}{dr^2} + \left\{ k^2 - \frac{2}{r^2} + 2\left(1 + \frac{1}{r}\right) e^{-2r} \right\} \chi_1 = 0\,, \qquad (19)$$

will not lead to any serious error; for the solution of equation (19), which tends to a sine wave of unit amplitude at infinity, has the behavior

$$\chi_1 \rightarrow \frac{\sin(kr + \delta)}{kr} - \cos(kr + \delta) \qquad (r \rightarrow \infty), \quad (20)$$

and the "phase shift" δ may be taken as a measure of the distortion of the p-spherical wave by the hydrogen atom at the origin. Integrations of equation (19) for various values of k^2 have been carried out numerically, and the resulting phase shifts for some of them are given in Table 2. It is seen that the phase shifts are indeed quite small for values of k^2, which are of astrophysical interest.

The second consequence of the run of the function $W(r)$ is not so satisfactory; for an examination of the energy integral minimized in the Ritz principle reveals that over 95 per cent of the contribution to the integral arises from regions of the configuration space which correspond to $r < 10$. Accordingly, it would appear that the choice of the wave

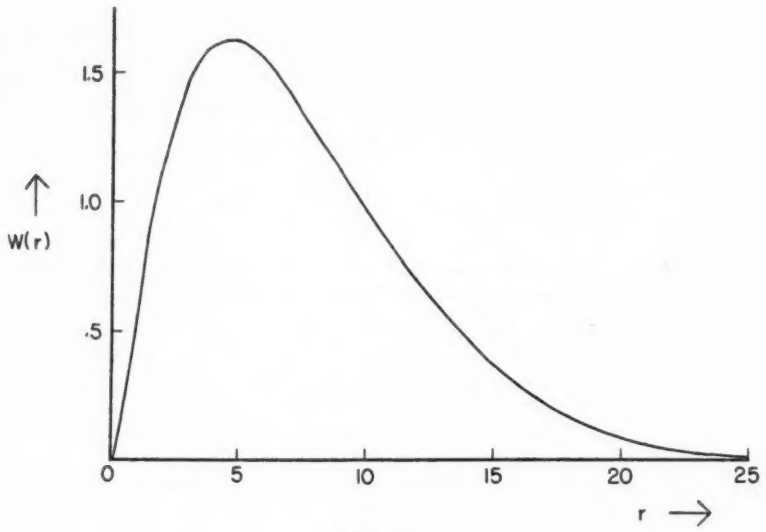

FIG. 1

TABLE 2

PHASE SHIFTS δ FOR THE p-SPHERICAL WAVES IN THE HARTREE FIELD OF A HYDROGEN ATOM

k^2	δ	k^2	δ	k^2	δ	k^2	δ
1.50.....	0.1486	0.80.....	0.09244	0.25.....	0.02605	0.100.....	0.007689
1.00.....	0.1115	0.50.....	0.05838	0.125.....	0.01046	0.035.....	0.001709

function in accordance only with the Ritz principle cannot be expected to lead to values of $W(r)$ which are necessarily trustworthy for $r > 10$. Under these circumstances the best hope for improving the current wave functions would consist in first determining the true asymptotic forms of the wave function for large distances and later choosing functions which would lead not only to the best value for the energy but also to the correct asymptotic forms. However, such calculations are likely to be extremely laborious.

I am greatly indebted to Miss Frances Herman for valuable assistance in the numerical parts of the present investigation.

THE SPECTROSCOPIC ORBIT OF BD VIRGINIS*

OTTO STRUVE, CARLOS U. CESCO, and JORGE SAHADE
McDonald and Yerkes Observatories
Received June 15, 1944

ABSTRACT

The spectrographic elements of the eclipsing variable BD Virginis are: $P = 2.5485$ days, $\gamma = +8.6$ km/sec; $K = +42.0$ km/sec; $e = 0.17$, $\omega = 123°$, $T =$ JD 2431111.06, $a \sin i = 1{,}400{,}000$ km, $f(m) = 0.02\odot$. The lines of only one component are visible. The type is A5, but the neutral lines of the metals are relatively strong, and the ionized lines of the metals are weak. The mass of the A-type component must be very small. For any reasonable value of the mass ratio it must be of the order of between 0.4 and 0.1 times the mass of the sun.

The star HD 116857 = BD −15°3666 was found to be an eclipsing binary in 1936, by Soloviev,[1] who described it as "a typical Algol variable with amplitude between magnitudes 9.5–11.5"; it was provisionally designated as SVS 775 Virginis.

In order to determine its spectroscopic orbit, 34 spectrograms were taken on Eastman 103a0 emulsion, using the Cassegrain quartz spectrograph of the 82-inch reflecting telescope of the McDonald Observatory, which gives a dispersion of 40 A/mm at λ 3933.

The spectrograms were obtained (some of them by Dr. Helen Steel) in January, February, and March, 1944, covering twenty-three consecutive cycles of the variable. Under good weather conditions the exposure time was 120 minutes, with a slit width of 0.075 mm; but during the period of observation the weather was rather unfavorable, so that on many nights the exposures were longer.

The lines that we have used for the determination of the radial velocities are listed in Table 1. Sometimes the quality of the spectrogram did not allow us to measure all the lines, but the total number of lines measured on one plate was never less than nine.

Table 2 shows the radial velocities; very poor plates are indicated by a dagger and were given a weight of ½ in the computation of the normal places.

In plotting the measurements, we have adopted 2.5485 days as the period—a value that was determined by Soloviev[2] from his estimations of magnitudes, which gave for the time of minimum JD 2428343.239 + 2.5485 E days.

A graphical solution of the orbit showed that it is nearly circular; hence it was decided to use Sterne's method[3] for the least-squares solution. We grouped the observations in ten normal places for which the phases are the averages of those for the individual plates and for which the δV are the average differences O − C between the observed velocities and those given by the preliminary orbit. Each normal place was given a weight equal to the square root of the number of observations.

Sterne's method gave the following elements:

$$K = +40.8 \qquad T_0 = +1.83$$
$$\omega = 129.07° \qquad \gamma = +8.59$$
$$e = +0.15$$

* *Contributions from the McDonald Observatory, University of Texas*, No. 95.

[1] *N.N.V.S.*, **52**, 114, 1936; *Tadjik Circ.*, No. 17, 1936; *B.Z.*, **18**, 84, 1936; *A.N.*, No. 6251, 1936. HD: $\alpha = 13^h21^m3$, $\delta = -15°35'$ (mag. ptm. 9.3; Sp. A5).

[2] *Tadjik Circ.*, No. 38, 1936.

[3] *Proc. Natl. Acad.*, **27**, 175, 1941.

TABLE 1

STELLAR WAVE LENGTHS

Ca II.....	3933.67	*Ni* II.....	4067.05	*Sr* II.....	4215.52	*Hγ*.....	4340.47
Fe I.....	3997.40	*Fe* I.....	4071.75	*Ca* I.....	4226.73	*Fe* II.....	4351.77
Fe I.....	4005.25	*Sr* II.....	4077.71	*Fe* II.....	4233.16	*Fe* I.....	4383.55
Fe I.....	4045.82	*Hδ*.....	4101.74	*Fe* I.....	4260.49	*Ti* II.....	4443.80
Fe I.....	4057.36	*Fe* I.....	4143.87	*Ti* II.....	4289.84	*Mg* II.....	4481.23
Fe I.....	4063.60	*Fe* II.....	4173.45	*Sc* II.....	4314.09		

TABLE 2

RADIAL VELOCITIES OF BD VIRGINIS

Plate	Date 1944	U.T.	Phase in Days	No. of Measures	*V*	O−C	
CQ 2766.....	Jan. 21	11:34	0.072	3	−13.1	− 5.0	*
2995.....	Mar. 7	10:03	0.136	1	−18.2	− 1.4	
2968.....	2	9:10	0.196	1	−17.9	+ 6.1	
2806.....	Jan. 29	10:28	0.381	1	−29.9	+ 6.8	
2807.....	29	12:04	0.448	2	−46.6	− 8.6	
2780†.....	24	10:51	0.494	1	−28.3	+ 8.6	
2781†.....	24	12:29	0.562	1	−34.7	+ 0.1	
3009.....	Mar. 10	11:00	0.627	1	−33.5	− 1.9	
2983.....	5	9:09	0.647	1	−32.7	− 2.2	
2951.....	Feb. 29	10:35	0.804	2	−14.4	+ 5.0	
2794.....	Jan. 27	11:06	0.955	1	+ 3.0	+10.2	
3037.....	Mar. 13	9:54	1.033	1	− 9.1	− 8.2	
2773.....	Jan. 22	11:01	1.049	1	− 0.5	− 0.9	
2774.....	22	12:24	1.107	3	− 8.3	−13.3	
2842.....	Feb. 9	12:31	1.273	2	+25.8	+ 8.2	
2833.....	4	10:17	1.276	1	+24.9	+ 7.1	
2834.....	4	12:07	1.353	3	+18.5	− 4.6	
2812†.....	Jan. 30	11:25	1.421	1	+20.1	− 7.4	
2787†.....	25	10:38	1.485	1	+11.2	−20.1	
3016.....	Mar. 11	7:55	1.499	3	+34.7	+ 2.6	
2788.....	Jan. 25	12:22	1.557	1	+34.9	− 0.3	
2760.....	20	10:36	1.581	3	+32.1	− 4.3	
2761.....	20	12:18	1.651	1	+50.0	+10.4	
2988.....	Mar. 6	9:39	1.667	3	+54.6	+14.3	
2872.....	Feb. 12	12:11	1.710	1	+49.7	+ 7.8	
2937.....	25	11:11	1.751	1	+44.1	+ 0.8	
2959.....	Mar. 1	8:06	1.751	3	+43.4	+ 0.1	
2820.....	Feb. 2	12:10	1.903	3	+36.9	− 9.5	
2799†.....	Jan. 28	10:30	1.931	1	+41.0	− 5.6	
3046.....	Mar. 14	9:34	2.019	1	+48.7	+ 2.5	
2924.....	Feb. 20	11:40	2.043	1	+40.6	− 5.2	
2819†.....	Jan. 31	11:16	2.414	1	+12.1	− 8.2	
3060.....	Mar. 17	8:58	2.446	2	+27.6	+11.3	
3025.....	12	9:04	2.547	1	− 2.2	− 4.6	

* The groups indicated by the braces correspond to the normal places. † Poor plates.

Since e is equal to 0.15, we performed a second least-squares solution applying the method of Schlesinger with the modification by Sterne,[3] which consists in considering T_0 (the time at which the mean longitude $\omega + M$ is zero) as unknown instead of the usual T.

The final values and the probable errors are shown in Table 3. From these elements the time of periastron passage is T = Phase 0.15 ($\pm$0.11) days = JD 2431111.06.

The eccentricity of the spectrographic orbit is fairly large for a period of $2\frac{1}{2}$ days. The velocity-curve shows that this eccentricity depends largely upon the normal point near phase 2.4 days, which is based upon only two plates—one of very poor quality. It is not improbable that the true eccentricity is smaller than the one found from the least-squares solution. The velocity-curve is shown in Figure 1.

The time of principal mid-eclipse is given by the condition $v + \omega = 90°$. This corresponds to phase -0.02 day—in excellent agreement with Soloviev's light-elements. Visual estimates of the magnitude of BD Virginis at the finder of the 82-inch telescope agree with this conclusion.

TABLE 3

P = 2.5485 days (assumed)	γ = +8.6 $\pm$ 2.4 km/sec
K = +42.0 $\pm$ 1.7 km/sec	$a \sin i$ = 1,400,000 km
ω = 123° $\pm$ 15°	$\dfrac{m_2^3 \sin^3 i}{(m_1 + m_2)^2} = 0.02\odot$
e = 0.17 $\pm$ 0.04	
T_0 = Phase 1.82 $\pm$ 0.016 day	

The spectrum undergoes no noticeable change during the eclipse. The spectrum remains that of the brighter component, despite the fact that at the most critical phases—2.547 and 0.072 days—the light of the system was reduced by more than 1 mag.

The spectrum shows only one set of absorption lines. Even at the elongations there is no indication of the lines of the secondary component. We conclude that the A-type component, which is eclipsed at primary minimum, is much brighter than the secondary.

The light-curve derived by Soloviev is shown in Figure 2. Disregarding the relatively small effect of ellipticity, we derive from the curve $\Delta m_1 = 1.38$ mag.; $\Delta m_2 = 0.12$ mag. Hence, the surface brightnesses are

$$\frac{J_2}{J_1} = \frac{1 - \lambda_1}{1 - \lambda_2} = 0.14 .$$

The eclipsing star at primary minimum has a surface brightness which should correspond to a spectral type of early G. The light-curve is not suitable for the determination of accurate photometric elements. There is no constant phase at minimum, and the eclipse may be partial. Hence it is impossible to derive a reliable value of $k = r_2/r_1$. If the eclipse were total (or nearly so), we could use the expression $k^2 = 1 - \lambda_2/\lambda_1$. This gives

$$k_1 = 0.60 \qquad \text{and} \qquad k_2 = 0.89 ,$$

where the former value corresponds to the case in which the primary eclipse is total, while the latter corresponds to an annular eclipse. It is, however, not possible to decide whether the A star or the secondary star is the larger. In the former case the ratio L_A/L_G is about 10; in the latter it is about 2.5. In neither case should we expect to observe the lines of the G star at full light. At mid-eclipse the G-type spectrum should become visible in the red part of the spectrum, if the G star is larger than the A star. But our failure to observe the G-type spectrum in the photographic region is not a sufficient criterion for preferring the hypothesis of a small G star.

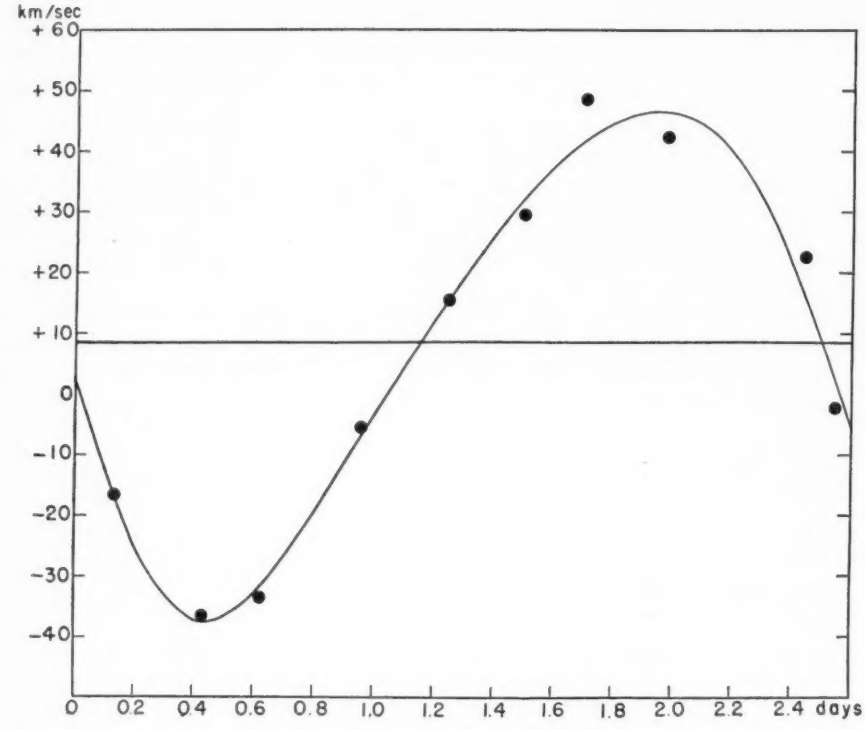

FIG. 1.—Velocity-curve of BD Virginis

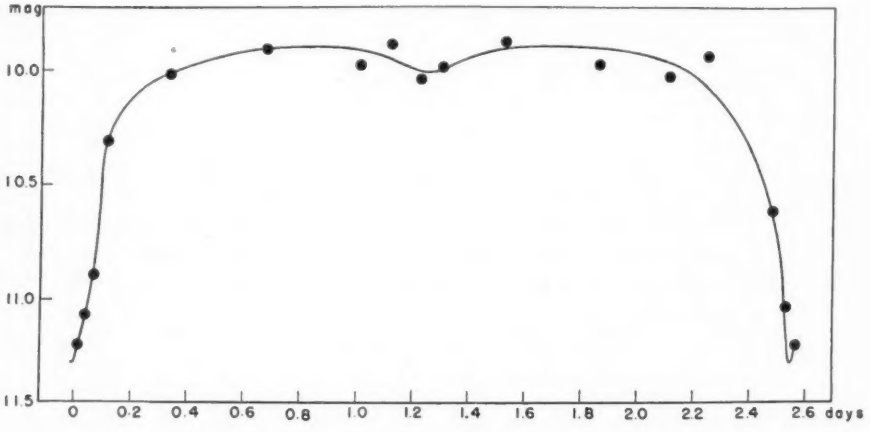

FIG. 2.—Light-curve of BD Virginis according to Soloviev

PLATE VIII

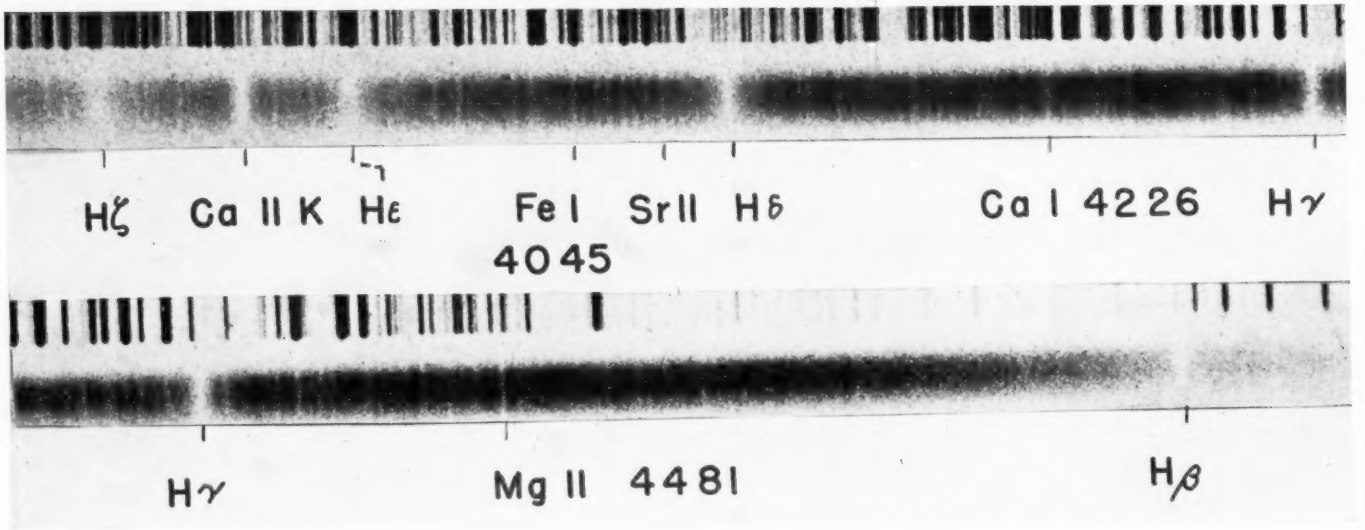

Spectrum of BD Virginis Taken January 22, 1944

Since the principal eclipse is quite deep, we may provisionally assume $i = 90°$. In that case the masses of the stars are somewhat smaller than the average for type A. The mass ratio is not known; hence we give several hypothetical values, as shown in the accompanying table. Since in reality the inclination is not 90°, these values are somewhat smaller than the real masses. But even for $i = 80°$, the factor $\sin^3 i = 0.955$. Hence we conclude that for all reasonable values of m_A/m_G we are concerned with stars of relatively small mass.

m_A/m_G	m_G	m_A	m_A/m_G	m_G	m_A
0.5	0.05⊙	0.02⊙	1.5	0.12⊙	0.18⊙
1.0	0.08	0.08	2.0	0.18	0.36

This is especially interesting in the case of the A-type component because its spectrum is somewhat abnormal (Pl. VIII). The lines of *Fe* I and *Ca* I are relatively strong, while those of *Fe* II and of other ionized metals are exceptionally weak for an A-type star. The lines of *H* are strong and broad, corresponding approximately to type A5. From the metallic lines alone a considerably later type would be indicated. The lines of *Ca* II are strong, and the star resembles such "metallic-line" A stars as the fainter components of α Geminorum and ζ Ursae Majoris, or such A2 stars as μ Orionis and ϵ Serpentis. The spectral lines of BD Virginis are sharp, and there is no indication of a rotational velocity at the equator in excess of 50 km/sec. Since the period is short, this suggests that these stars are relatively small.

THE ECLIPSING STAR BD VIRGINIS

CECILIA PAYNE GAPOSCHKIN
Harvard College Observatory
Received July 15, 1944

ABSTRACT

The eclipsing star BD Virginis is studied on the basis of 773 Harvard plates. It is apparently a normal Algol star. The range is from 10^m25 to 11^m45. A grazing eclipse is adopted, the inclination of the orbit being 77°. If the earlier star is of spectral class A2, the other is an F or G star, a typical subgiant. In period, light-curve, dimensions, and masses the system resembles that of Algol.

A visual light-curve has been published by A. Soloviev,[1] the discoverer of BD Virginis, together with the revised elements:

$$\text{Min. hel.} = 2428343.239 + 2^d5485E\,.$$

In the systematic study of the brighter variable stars on plates in the Harvard photographic collection, financed by a grant from the Milton Fund of Harvard University, 773 estimates of BD Virginis were made by Mrs. Helen Thomas. The present note summarizes the results.

All available subnormal points, between JD 15000 and JD 30000, were used to test the published elements. The period was slightly revised and found to be constant. The revised elements are

$$\text{Minimum} = 2428343.212 + 2^d5483643E\,.$$

The comparison stars and their photographic magnitudes are given in Table 1; the star is very close to Selected Area 129, with which the comparisons were made.

The photographic estimates were combined to form the mean light-curve of Table 2 and Figure 1. The curve has the form of a normal Algol type, and the depth of the secondary minimum is inappreciable.

The elements, derived from the photographic light-curve, are summarized in Table 3.

A mass function of 0.02 has been derived by Struve, Cesco, and Sahade.[2] If the ratio of masses is 1/4, this leads to masses of $2.2\odot$ and $0.5\odot$ for the two components, values not incompatible with those given in Table 4, which were obtained by an application of a method given by S. Gaposchkin.[3]

Photometrically, the system is quite normal and in many respects resembles the system of Algol, which also has a small mass function, $0.025.\odot$

[1] *Tadjik Obs. Circ.*, No. 38, 1938.

[2] *Ap. J.*, **100**, 181, 1944.

[3] *Harvard Reprint*, No. 201, 1940.

TABLE 1

COMPARISON STARS FOR BD VIRGINIS

Designation		BD	IPG	Remarks
This Paper	Soloviev			
x		−15°3664	9^m58	
a′		−15 3663	10.40	
a	A	−15 3660	10.46	
b	a	−15 3665	10.45	Discarded; variable?
c	c	−15 3671	11.39	
d			11.61	
f			12.20	

TABLE 2

MEAN LIGHT-CURVE OF BD VIRGINIS

Phase (P)	IPg (m)	No. of Obs.	Phase (P)	IPg (m)	No. of Obs.	Phase (P)	IPg (m)	No. of Obs.
0.024	10.30	20	0.160	10.58	10	0.517	10.28	50
.046	10.36	10	.175	10.43	10	.586	10.25	50
.058	10.47	10	.188	10.39	10	.651	10.27	50
.075	10.74	10	.223	10.26	50	.728	10.24	50
.094	10.87	10	.278	10.27	50	.791	10.25	50
.115	11.40	10	.333	10.28	50	.849	10.26	50
.132	11.29	10	.403	10.30	50	.912	10.26	50
0.144	10.95	10	0.457	10.28	50	0.977	10.25	53
Total								773

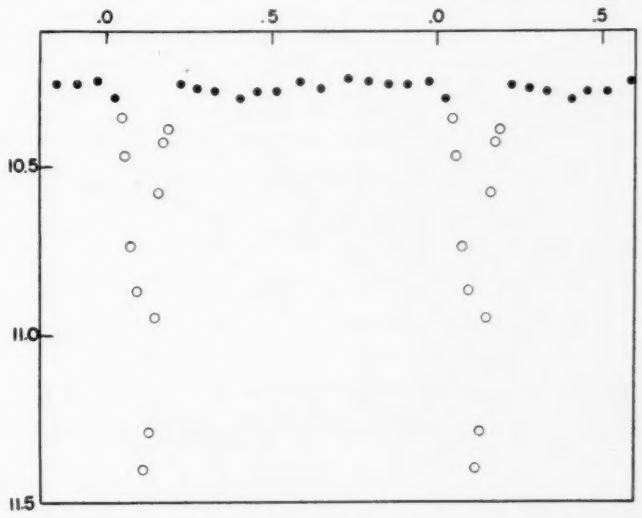

FIG. 1.—Photographic light-curve of BD Virginis. Ordinate and abscissa are photographic magnitude and phase. Dots denote means of fifty points; circles, means of twenty-five.

TABLE 3

RELATIVE ELEMENTS OF BD VIRGINIS

Maximum$_1$ = 10^{m}25	Maximum$_2$ = 10^{m}25
Minimum$_1$ = 11^{m}45	Minimum$_2$ = ...
Amplitude$_1$ = 1^{m}20	Amplitude$_2$ = 0^{m}03 (adopted)

Duration of eclipse: 0^{P}224; grazing eclipse adopted
Inclination of orbit = 77°
Relative radii = A2, 0.24; ?, 0.44
Ratio of surface brightness (A2/?):24.7 = 3^{m}5, sp ? = G–K
Ratio of luminosity (A2/?):6.2 = 2^{m}0
Luminosity: A2, 0.86; ?, 0.14

TABLE 4

APPROXIMATE DIMENSIONS FOR BD VIRGINIS

	A2 Star	Unknown Star		A2 Star	Unknown Star
Mass.....	3⊙	2⊙	M_{vis}.....	1^{m}1	2^{m}4
Radius.....	2.7⊙	5.4⊙			

RADIAL VELOCITIES OF TWENTY STARS OF EARLY TYPE IN AND NEAR THE GALACTIC CLUSTER NGC 6231*

O. STRUVE
Yerkes and McDonald Observatories
Received June 30, 1944

ABSTRACT

The radial velocities of 16 normal stars of types cO9–cB2 have been derived, together with those of 2 Wolf-Rayet stars and 2 P Cygni type stars. All 20 stars belong to one physical group. The emission lines of the WN7 star show appreciable red shifts of different amounts. The phenomenon is correlated with the intensities of the violet absorption lines. The violet absorptions of certain lines change in intensity, and there may also be structural changes in the emission lines. The radial velocity was constant. The WC6 star shows central absorptions in some of the emission lines which are shifted toward the violet. These central absorptions and the centers of the emission bands show large, but uncorrelated, shifts over intervals of several days. The 2 P Cygni type stars show pronounced red shifts for those emission lines which are accompanied by violet absorption borders.

I. INTRODUCTION

Several years ago Shapley and Sawyer[1] remarked that "the open cluster NGC 6231 is one of the bright groups in the Milky Way that appears to be closely connected with a widely scattered cloud of bright stars in the neighborhood." Photographs of the region surrounding ζ Scorpii show unmistakably that a large, connected group of fairly bright stars (magnitudes 6–8) surrounds the dense galactic cluster which is designated as NGC 6231. Many of these bright stars belong to early spectral types, and, as Shapley and Sawyer point out, "the comparability of spectral classes and apparent photographic magnitudes in the cluster and in the adjacent field seems to show conclusively that the cluster is but the concentrated part of a larger system."[2] The physical connection of the early-type stars in and around the cluster is confirmed by the fact that all these stars possess supergiant characteristics. This was pointed out by C. A. Rieke,[3] but I believe it is not generally recognized that the spectra of all the brighter, normal, early-type stars are so remarkably similar in character that their connection cannot be doubted.

The region of NGC 6231 is particularly interesting because among the brighter stars there are 4 whose spectra are peculiar.[4] These stars are HD 152270, of spectral class WC6+; HD 151932, of spectral type WN7; HD 151804, of spectral type O7f; and HD 152408, also of spectral type O7f. The first is a member of the compact cluster. The others are all within a fraction of a degree from the cluster and undoubtedly belong to the same physical group.[5] It is, of course, not possible to prove this connection. But the two Of stars resemble in spectral characteristics the rest of the early B stars in the group, while the two WR stars are so close to the cluster that a chance association is very improbable.

* *Contributions from the McDonald Observatory, University of Texas*, No. 96.

[1] *Harvard Bull.*, No. 846, p. 1, 1927.

[2] The tendency of galactic clusters to be surrounded by extended groups of supergiant stars is probably one of their most important structural characteristics. Shapley and Sawyer mention as other clusters of this kind h and χ Persei (see also Bidelman, *Ap. J.*, **98**, 61, 1943), the Orion nebula cluster, and probably Messier 11.

[3] *Harvard Circ.*, No. 397, 1935.

[4] I am greatly indebted to Mrs. C. Payne Gaposchkin for having called my attention to this group.

[5] MacRae, *Harvard Bull.*, No. 914, 1940.

The purpose of this paper is to investigate the radial velocities of the normal stars in the group and to compare them with the radial velocities obtained from different features in the spectra of the peculiar stars. This comparison should be of great interest in the case of the two WR stars. If we may assume that they are members of the group, it should give a reliable determination of the mysterious red shift discovered by O. C. Wilson in the WR spectroscopic binary, HD 193576,[6] and also observed by Hiltner in the WR binary, HD 214419.[7] Wilson[8] has collected some wave-length measurements in other WR stars and has shown that the red shift of the emission lines is probably a fairly widespread phenomenon among these stars. But it almost certainly is also encountered in various Be and Of stars. For example, it is present in 29 Canis Majoris[9] and in other O-type stars in which *He* II 4686 is bright. It is suspected in the case of the Be star, HD 163181,[10] and is definitely present in the P Cygni star, MWC 374.[11]

The observations were made with the Cassegrain quartz spectrograph of the McDonald Observatory, giving a dispersion of 40 A/mm at λ 3930. The slit was kept wide (0.10 mm) in order to reduce the exposure times. It was oriented east-west, despite the large effect of atmospheric dispersion at declination −42°. An effort was made to guide on the violet images in all cases.

All the stars have strong interstellar *Ca* II lines. The radial velocities are also approximately the same, except for star HD 152270, which is a member of the cluster. There is no explanation for its divergent *Ca* II velocity, but the intensities of these lines are such as to exclude the possibility that the star is in front of the cluster.

II. THE NORMAL STARS

The radial velocities of 16 normal stars (Nos. 1–16 in Fig. 1) are shown in Tables 1 and 2. The photographic magnitudes and spectral types in Table 2 are from the *Henry Draper Catalogue* or from the paper by Shapley and Sawyer.[1] Star 11 (HD 152249) had been announced as a spectroscopic binary by Neubauer.[12] Stars 10 (HD 152248) and 5 (HD 152218) are new binaries of large range, showing double lines. In both stars the lines are diffuse because of rapid rotation. The approximate orbital elements of HD 152248 are as follows:

$P = 3.10$ days	$T =$ ph. 1.75 (maximum relative velocity)
$K_1 = 215$ km/sec	
$K_2 = 215$ km/sec	$a_1 \sin i = a_2 \sin i = 9 \times 10^6$ km
$\gamma = -35.0$ km/sec	$m_1 \sin^3 i = m_2 \sin^3 i = 12.2\odot$
$e = 0.00$	

Phase zero was assumed at JD 2431210.906 = 1944 Apr. 30.406 U.T. The velocity-curve is shown in Figure 2. It is of interest that on all plates showing double lines the violet component is the stronger. This may be an effect of variation in line-intensity similar to that found in several other double-lined B-types stars.[13] But it should be remembered that, because of the low altitude of the cluster as observed at the McDonald Observatory, it is almost impossible to exclude the related period $P = 1.475$ days.

The orbital elements of the other binary, HD 152218, have not been determined; but, since the lines are double and of comparable intensities, a provisional value of the γ-velocity has been obtained by averaging the double lines on each plate. Star 7 (HD 152234) is almost certainly a spectroscopic binary of fairly long period. Moore's catalogue[14] gives -13 ± 4 km/sec from six plates. Star 13 (CD−41°11042) is a binary of large range.

[6] *Ap. J.*, **91**, 379, 1940.

[7] *Ap. J.*, **99**, 273, 1944.

[8] *Op. cit.*, p. 396.

[9] *Ap. J.*, **82**, 250, 1935; **93**, 84, 1941.

[10] *Ap. J.*, **99**, 215, 1944.

[11] C. S. Beals, *J.R.A.S. Canada*, **37**, 241, 1943.

[12] *Pub. A.S.P.*, **42**, 235, 1930.

[13] *Ap. J.*, **85**, 41, 1937.

[14] *Lick Obs. Pub.*, Vol. **18**, 1932.

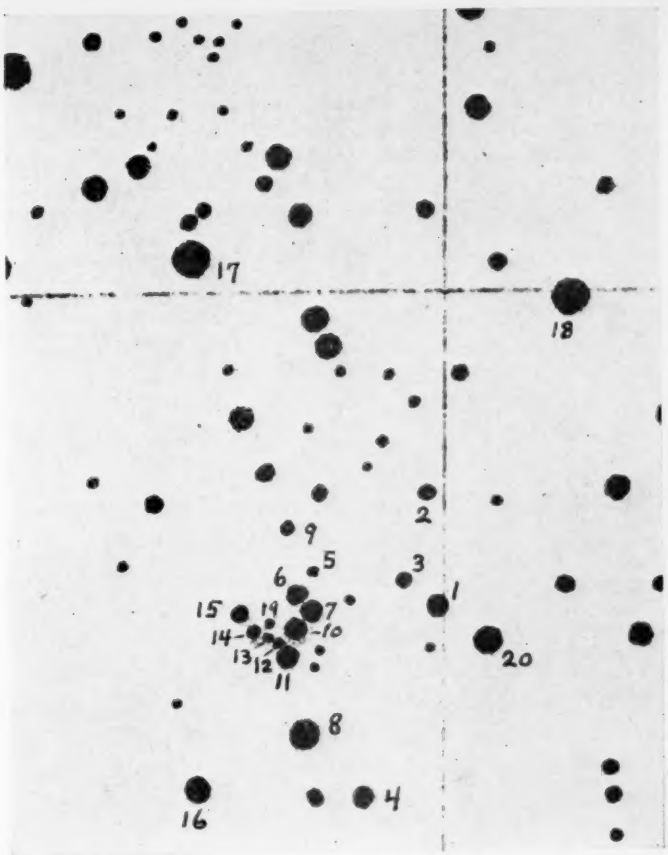

FIG. 1.—Map of NGC 6231 from CD, showing stars whose radial velocities have been measured

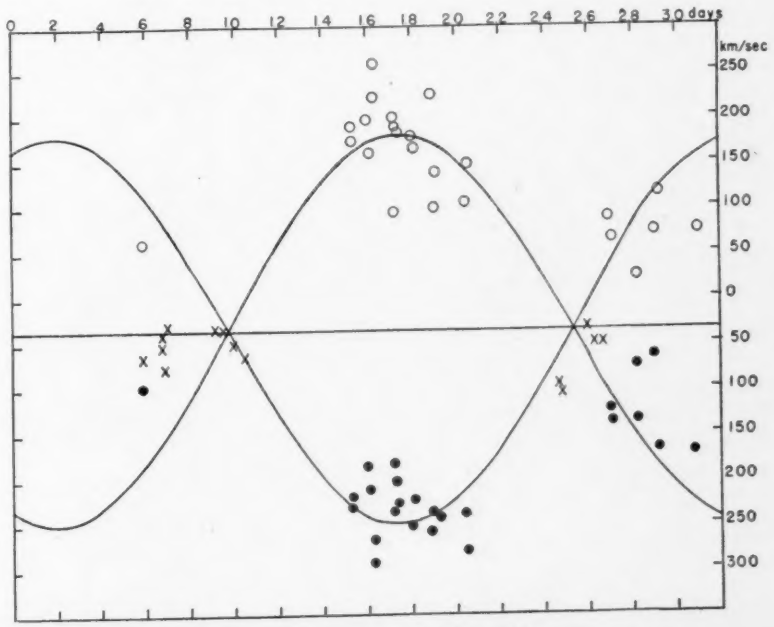

FIG. 2.—Velocity-curve of HD 152248

Star 12 (CD−41°11037) is probably a binary, considering the discrepancy in its radial velocity from the mean of the other stars. The last 2 stars have precisely the same character of spectrum as the other stars and undoubtedly belong to the cluster. Omitting three doubtful velocities, we find for the radial velocity of the cluster -29.1 ± 2.4(m.e.) km/sec from 13 stars and for the associated interstellar calcium lines -8.5 ± 1.8(m.e.) km/sec from 16 stars. The spectral types in Table 1 are those estimated from the McDonald spectrograms (Pl. IX). The similarity in type is even more conspicuous than is shown by the Harvard types. There is no noticeable correlation between apparent magnitude and spectral type.

TABLE 1

SUMMARY OF RADIAL VELOCITIES OF NORMAL STARS

No.	Name	Sp.	Mag.	Star	*Ca* II	Remarks
1.....	HD 152003	cB0	6.9	−27.6	− 5.1	
2.....	HD 152042	cB2	7.9	−29.6	− 2.3	
3.....	HD 152076	cB0	8.7	−30.3	− 3.4	
4.....	HD 152147	cB0	7.4	−28.0	+ 2.0	
5.....	HD 152218	cO9	7.1	−44.1	− 3.8	Sp. binary, double lines
6.....	HD 152233	cO8	6.4	−15.6	− 5.2	
7.....	HD 152234	cO9	5.9	.....	−13.0	Sp. binary
8.....	HD 152235	cB0*	6.5	−36.2	−20.4	
9.....	HD 152247	cB0	7.0	−16.6	−10.2	
10.....	HD 152248	cO9	6.2	−35.0	−11.8	Sp. binary, double lines
11.....	HD 152249	cB0	6.8	−25.2	− 6.4	Sp. binary (Neubauer)
12.....	−41°11037	cO9	8.5	.....	−22.2	Sp. binary
13.....	−41°11042	cB0	8.5	.....	−17.4	Sp. binary, large range
14.....	−41°11044	cB2	7.2	−38.4	− 8.1	
15.....	HD 152314	cB0	7.5	−34.2	− 8.4	
16.....	HD 152424	cB0	6.4	−17.7	+ 0.2	Sp. binary?
Mean..	.....	.....	.....	−29.1(13)	− 8.5(16)	

* Strong *O* II.

III. THE PECULIAR STARS

Table 3 gives the radial velocities for the 4 peculiar stars. They are based upon the best available wave lengths. All 4 show conspicuous departures from the mean velocity of the cluster. In order to appreciate this result we shall discuss each star separately. The spectral features of these 4 stars have been discussed by Swings[15] and by Mrs. Gaposchkin.[16] I have made extensive use of Swings's identifications.

Star 20 (HD 151932).—The mean radial velocity from thirteen emission features is +23.4 km/sec. There is, thus, an average red shift of +52.5 km/sec. This is unquestionably the same phenomenon as that observed by O. C. Wilson in HD 193576. The star HD 151932 is not a spectroscopic binary, and the effect is therefore not confined to binaries. The amount differs greatly from line to line. In some cases these individual differences are probably caused by blends, but in several cases they are with great probability attributed to the effect of self-absorption in an expanding shell. Table 4 gives the results for all lines.

In discussing these results it should be noted that the mean shift of +52.5 km/sec with respect to the cluster has not been included in Table 4. If it were added, the shift of *He* II 4686 would be +80.3 km/sec, or very nearly the value +90 km/sec found by O. C. Wilson in HD 193576.

[15] *Ap. J.*, **95**, 112, 1942.

[16] *Harvard Bull.*, Nos. 842, 843, and 844, 1927.

PLATE IX

NORMAL SPECTRA IN AND NEAR NGC 6231

PLATE X

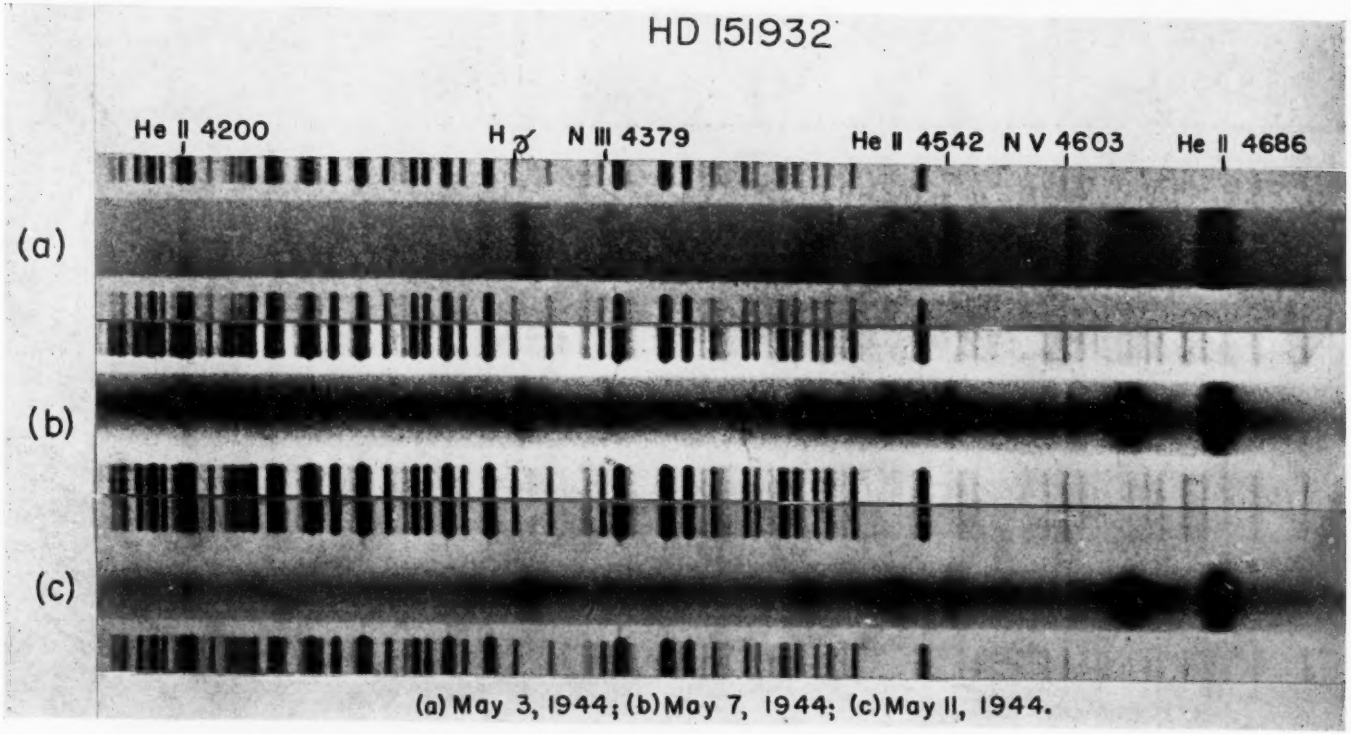

SPECTRUM OF HD 151932

TABLE 2

NORMAL STARS

DATE	U.T.	VELOCITY IN KM/SEC		
		Star		*Ca* II
	1. HD 152003		B0	6.9
May 7	7:41	− 19.1(7)	.....	− 9.4(1)
May 8	8:52	− 36.1(7)	.....	− 0.8(1)
Mean	.....	− 27.6(2)	.....	− 5.1(2)
	2. HD 152042		B2	7.9
May 9	8:17	− 36.3(7)	.....	− 4.2(1)
May 14	9:15	− 23.0(7)	.....	− 0.4(1)
Mean	.....	− 29.6(2)	.....	− 2.3(2)
	3. HD 152076		B2	8.7
May 8	9:20	− 35.7(9)	.....	.....
May 14	8:49	− 24.9(9)	.....	− 3.4(1)
Mean	.....	− 30.3(2)	.....	− 3.4(1)
	4. HD 152147		B0	7.4
Apr. 30	9:01	− 23.8(6)	.....	− 9.9(1)
May 1	9:06	− 28.3(5)	.....	− 1.1(1)
May 1	10:21	− 20.1(5)	.....	.....
May 2	8:49	− 18.1(7)	.....	+16.9(1)
May 6	9:44	− 49.6(5)	.....	.....
Mean	.....	− 28.0(5)	.....	+ 2.0(3)
	5. HD 152218		B5	7.1
May 9	8:50	−166.0(2)	+ 64.3(2)	.....
May 12	8:55	+143.4(2)	−192.3(2)	− 5.6(1)
May 13	10:03	− 3.7(3)	.....	+ 3.0(1)
May 14	8:26	−151.5(4)	+ 87.6(4)	− 1.4(2)
May 15	8:23	−109.5(4)	.....	−10.9(2)
Mean	.....	[− 44.1(5)]	.....	− 3.8(4)

TABLE 2—*Continued*

Date	U.T.	Velocity in Km/Sec		
		Star		*Ca* II
	6. HD 152233		B	6.4
Apr. 30	9:38	− 21.3(6)	.....	−12.9(1)
May 1	10:44	− 4.9(5)	.....	− 1.3(1)
May 2	9:27	− 16.3(6)	.....	− 1.5(1)
May 6	9:09	− 29.9(3)	.....	.....
Mean	.....	− 15.6(4)	.....	− 5.2(3)
	7. HD 152234		B0	5.9
Apr. 30	9:32	− 2.9(8)	.....	−12.9(1)
May 1	9:26	− 5.3(7)	.....	− 7.2(1)
May 2	9:35	+ 1.4(8)	.....	− 4.6(1)
May 6	9:03	− 2.0(10)	.....	−27.4(1)
Mean	.....	− 2.2(4)	.....	−13.0(4)
	8. HD 152235		B0	6.5
Apr. 30	9:21	− 27.3(9)	.....	+ 2.3(1)
May 1	9:20	− 35.4(9)	.....	−31.6(1)
May 2	9:04	− 29.1(10)	.....	−32.0(1)
May 6	9:59	− 52.8(10)	.....	.....
Mean	.....	− 36.2(4)	.....	−20.4(3)
	9. HD 152247		B2	7.0
Apr. 30	10:04	− 14.2(6)	.....	+ 5.3(1)
May 1	8:10	− 14.5(6)	.....	−10.2(1)
May 2	7:41	− 4.6(5)	.....	−25.7(1)
May 6	9:25	− 33.2(7)	.....	.....
Mean	.....	− 16.6(4)	.....	−10.2(3)
	10. HD 152248		B	6.2
Apr. 30	9:44	−193.6(3)	+ 76.4(3)	−19.0(1)
May 1	7:55	− 32.7(3)	.....	−13.1(1)
May 1	8:01	− 33.4(3)	.....	−13.1(1)
May 1	9:43	− 50.6(4)	.....	−19.3(1)
May 1	10:56	− 64.0(4)	.....	−13.5(1)
May 2	7:26	−231.6(2)	101.0(2)	−24.1(2)
May 2	7:31	−235.7(3)	139.3(2)	−22.6(2)
May 2	10:48	−238.0(2)	+106.1(2)	.....

TABLE 2—*Continued*

Date	U.T.	Velocity in Km/Sec		
		Star		*Ca* II
	10. HD 152248—*Continued*	B		6.2
May 2	10:56	−278.7(1)	+147.8(1)	−38.2(1)
May 3*	7:25	64.5(1)	72.7(1)	.....
May 3	7:42	166.9(3)	116.4(2)	− 7.4(2)
May 5	9:28	257.2(3)	225.1(3)	− 6.7(2)
May 6	7:46	75.3(3)	.....	−14.6(2)
May 6	7:53	135.7(3)	24.3(1)	−18.2(1)
May 7	7:12	75.6(4)	.....	− 6.4(1)
May 7	7:17	29.3(3)	.....	− 9.4(1)
May 8	7:55	182.0(2)	96.3(2)	− 1.8(2)
May 8	8:22	225.5(3)	183.5(3)	−16.0(1)
May 8	9:45	252.0(3)	178.8(3)	− 0.9(1)
May 8	9:59	222.0(4)	165.8(4)	− 7.0(1)
May 9	7:26	124.4(2)	89.2(2)	−17.7(2)
May 9	7:32	136.8(3)	66.0(1)	−16.3(1)
May 10	9:10	40.2(3)	.....	+ 7.5(1)
May 10	9:16	50.0(3)	.....	+ 1.4(1)
May 11	8:00	292.2(3)	222.3(3)	−14.3(1)
May 11	8:09	265.9(3)	258.6(3)	−14.3(1)
May 11	10:06	235.9(2)	199.0(2)	.....
May 11	10:22	202.2(2)	189.3(2)	.....
May 12	8:13	50.0(2)	.....	−14.8(1)
May 12	8:20	48.6(4)	.....	−14.8(1)
May 13	9:31	97.5(4)	61.5(1)	− 4.1(1)
May 13	9:36	63.5(3)	.....	− 9.2(1)
May 14	8:03	230.8(4)	189.6(4)	−10.5(2)
May 14	8:08	218.1(4)	173.7(4)	−24.6(2)
May 14	9:45	184.7(2)	197.5(2)	− 3.5(1)
May 14	9:52	211.1(4)	+160.8(4)	− 4.6(2)
May 15	6:39	94.9(4)	.....	− 0.6(1)
May 15	6:46	101.1(4)	.....	− 9.8(1)
May 15*	9:41	− 35.2(2)	.....	.....
Mean	.....	− 35.0	.....	−11.8(34)
	11. HD 152249	B0		6.8
Apr. 30	10:25	− 28.9(7)	.....	−34.4(1)
May 1	8:20	− 12.5(7)	.....	+ 2.0(1)
May 2	7:52	− 25.4(6)	.....	− 7.4(1)
May 3	8:22	− 32.5(6)	.....	−20.2(1)
May 5	9:36	− 15.9(6)	.....	− 7.7(1)
May 6	8:00	− 38.1(6)	.....	− 6.0(1)
May 7	7:24	− 18.5(6)	.....	+21.1(1)
May 8	8:42	− 38.2(6)	.....	−16.0(1)
May 9	7:54	− 23.9(6)	.....	− 1.2(1)
May 10	9:25	− 12.8(6)	.....	+13.5(1)
May 11	8:32	− 34.1(6)	.....	−29.5(1)
May 12	8:27	− 19.8(6)	.....	− 5.6(1)
May 13	9:42	+ 2.2(6)	.....	0.0(1)
May 14	8:13	− 40.8(6)	.....	− 6.4(1)
May 15	9:27	− 38.8(6)	.....	+ 2.1(1)
Mean	.....	− 25.2(15)	.....	− 6.4(15)

* Poor.

TABLE 2—*Continued*

Date	U.T.	Velocity in Km/Sec		
		Star		Ca II
	12. −41°11037	....		8.5
May 15.....	8:59	+ 22.6(7)	.....	−22.2(1)
Mean....	.....	[+ 22.6(1)]	.....	−22.2(1)
	13. −41°11042	....		8.5
May 15†.....	7:34	[− 51.5(5)]	.....	−25.0(1)
May 15.....	7:54	−150.0(5)	.....	− 9.9(1)
Mean....	.....	[−100.8(2)]	.....	−17.4(2)
	14. −41°11044	....		7.2
May 2.....	9:57	− 20.4(4)	.....	−13.2(1)
May 6.....	8:14	− 56.3(4)	.....	− 3.0(1)
Mean....	.....	− 38.4(2)	.....	− 8.1(2)
	15. HD 152314	B		7.5
May 2.....	10:29	− 35.2	.....	− 4.7(1)
May 6.....	8:37	− 33.2	.....	−12.2(1)
Mean....	.....	− 34.2(2)	.....	− 8.4(2)
	16. HD 152424	B0		6.4
Apr. 30.....	11:01	− 40.8(3)	.....	.....
May 1.....	8:41	− 3.7(7)	.....	− 4.4(1)
May 2.....	8:15	− 8.5(7)	.....	+ 4.7(1)
Mean....	.....	− 17.7(3)	.....	+ 0.2(2)

† Poor.

TABLE 3

RADIAL VELOCITIES OF PECULIAR STARS

Date	U.T.	Abs.	Em.	*Ca* II
	17. HD 152408		Oep	5.6
Apr. 30	8:20	−128.7(9)	− 9.3(9)	−18.9(1)
Apr. 30	11:13	−138.7(8)	+ 14.4(8)	.....
May 1	9:50	−139.4(12)	+ 0.8(11)	− 4.9(1)
May 2	9:12	−127.7(10)	+ 31.9(9)	−14.5(1)
May 6	10:11	−148.4(9)	+ 23.5(9)	− 3.1(1)
Mean	.....	−136.6(5)	+ 12.3(5)	−10.4(4)
	18. HD 151804		Oe	4.6
Apr. 30	8:31	− 55.0(16)	+101.2(2)	−25.9(1)
Apr. 30	11:18	− 62.7(8)	+ 73.2(4)	+ 8.3(1)
May 1	9:56	− 54.7(15)	− 32.9(2)	−14.2(1)
May 2	9:18	− 60.4(15)	+111.7(1)	− 5.3(1)
May 6	10:20	− 82.7(8)	+ 6.6(3)	−21.4(1)
Mean	.....	− 63.1(5)	+ 52.0(5)	−11.7(5)
	19. HD 152270		Oa	7.1
Apr. 30	10:43	− 80.4(2)	.....	+11.4(1)
May 1	8:30	− 94.0(2)	.....	+14.1(1)
May 2	8:04	− 88.4(2)	.....	+ 4.8(1)
May 5	9:44	− 31.9(2)	.....	− 2.7(1)
May 6	8:55	+ 30.7(2)	.....	.....
Mean	.....	− 52.8(5)	.....	+ 7.2(4)
	20. HD 151932		0c	6.3
Apr. 30	8:44	.....	+ 28.4(12)	− 0.7(1)
Apr. 30	11:23	.....	+ 56.8(3)	.....
May 1	8:53	.....	+ 30.4(12)	+14.1(1)
May 1	10:05	.....	+ 13.3(11)	+ 4.9(1)
May 2	8:26	.....	+ 23.7(12)	− 7.5(1)
May 2	8:35	.....	− 1.3(12)	− 7.5(1)
May 3	9:25	.....	+ 16.4(13)	−11.1(1)
May 5	9:55	.....	+ 16.9(12)	+ 3.4(1)
May 6	9:16	.....	+ 14.7(13)	−27.4(1)
May 7	7:34	.....	+ 36.2(13)	− 9.4(1)
May 8	8:12	.....	+ 23.0(13)	−19.1(1)
May 9	7:43	.....	+ 17.1(13)	−16.3(1)
May 10	9:36	.....	+ 30.9(13)	+ 7.4(1)
May 11	9:47	.....	+ 31.2(12)	+ 7.0(1)
May 12	8:36	.....	+ 7.8(13)	− 17.8(1)
May 13	9:48	.....	+ 22.9(11)	0.0(1)
May 14	9:33	.....	+ 28.2(13)	+ 2.6(1)
May 15	6:53	.....	+ 24.1(13)	− 9.8(1)
Mean	.....	.....	+ 23.4(18)	− 5.1(17)

Of particular interest are the large positive shift of *N* v 4603 and the large negative shift of *N* iv 4058. The former has the most conspicuous violet absorption of any line; the latter has no violet absorption whatever. Both lines are essentially unblended and are fairly narrow and strong. I believe there can be little doubt that in this star *N* iv 4058 does give the radial velocity of the cluster, while *N* v 4603 is shifted toward the red by the action of absorbing gases in the expanding shell. The positive shifts of *He* ii 4542 and *He* ii 4686 are probably caused in a similar manner. The former often shows conspicuous violet absorption.

The lines *N* iii 4639 and *Hδ* are seriously blended and therefore unreliable. The two *He* i lines seem to give negative shifts, which would, after applying the correction of +52.5 km/sec, make them almost independent of the red shift. The line *N* iii 4379.09 is weak and is perhaps incorrectly identified. It is usually a narrow line, without violet absorption. The line *Si* iv 4116 may be seriously blended.

TABLE 4

SYSTEMATIC SHIFTS OF INDIVIDUAL LINES FROM MEAN VELOCITIES IN HD 151932

Emission Line	Line − Mean (In Km/Sec)	M.E. (In Km/Sec)	Line − Mean (In A)
He i 4026.22....	− 35.4	± 8.8	−0.48
N iv 4057.80....	− 57.9	3.4	−0.78
Hδ 4101.74....	+ 33.6	9.2	+0.46
Si iv 4116.10....	− 57.7	7.1	−0.79
He ii 4199.87....	+ 4.0	6.0	+0.06
Hγ 4340.47....	+ 6.7	7.3	+0.10
N iii 4379.09....	− 67.6	7.8	−0.99
He i 4471.51....	− 48.4	6.7	−0.72
N iii 4513.06....	− 0.1	11.2	0.00
He ii 4541.63....	+ 81.3	5.2	+1.23
N v 4603.20....	+159.1	8.0	+2.44
N iii 4638.74....	− 71.9	9.7	−1.11
He ii 4685.81....	+ 27.8	± 6.4	+0.44

The nature of the self-absorption giving rise to the observed red shift is not yet obvious. In a thin, uniformly expanding envelope the occultation effect and the effect of absorption in front of the stellar disk exactly balance each other. But the phenomenon probably results from a more complicated mechanism of self-absorption in a thick shell with nonuniform expansion. It is of interest in this connection that O. C. Wilson[17] concluded from an examination of 14 WN stars that "the available data tend against the absorption explanation." He had found only 2 stars having violet absorption at *He* ii 4686 and 11 in which it was "definitely or probably absent." Similarly *N* v 4603 had violet absorption in 5 stars while in 2 it was absent. Wilson thought that "weak bands somewhat to the violet of λ 4603 . . . . may give the appearance of a weak absorption."

In HD 151932 the violet absorption at *N* v 4603 is unquestionably real. But in the other stars, where the absorption is not seen, it is still possible that a broad absorbing band cuts down the violet wing of the emission line to a greater extent than the occultation effect cuts down the red wing.

The McDonald series of plates of HD 151932 shows some interesting changes in the spectrum. These are almost certainly real, even though it is not possible from the limited amount of material to ascertain whether they are periodic. The most conspicuous of these changes occur in the ratio of the violet absorptions of *N* v 4603 and *He* ii 4542. Prob-

[17] *Op. cit.*, p. 401.

ably both are variable, but the latter changes more conspicuously than the former. Table 5 gives the estimated intensities of the violet absorptions on the best plates (Pl. X). There are almost certainly other changes in the violet absorptions. It is probable that, when the absorption of *He* II 4542 is strong, the absorption of *He* I 4472 is also strong. Another possible change occurs in the intensity and width of *N* III 4379. This emission line is very narrow and sharp, but quite intense on May 7. It is faint and diffuse on May 3. There is no visible violet absorption.

The emission lines attributed to $H\delta$ and $H\gamma$ are probably mostly due to hydrogen. The *He* II lines are relatively weak and are less diffuse. The spectral type of HD 151932 is WN7.

TABLE 5

ESTIMATED INTENSITIES OF VIOLET ABSORPTIONS

Date	*N* v 4603	*He* II 4542	Date	*N* v 4603	*He* II 4542
May 3.....	1	5	May 10....	7	1
May 5.....	3	1	May 11....	5	0
May 6.....	4	3	May 12....	5	3
May 7.....	6	1	May 13....	2	1
May 8.....	4	1	May 14....	4	2
May 9.....	5	2	May 15....	3	0

Star 19 (HD 152270).—This star is of the type WC6+, according to Swings. The radial velocities in Table 3 were obtained from the central absorptions of $H\delta$ and $H\gamma$. On a few plates I have also measured the central absorption of *He* II 4199.87. It agrees in velocity with the *H* lines, thereby confirming the attribution of the latter to hydrogen and not to *He* II. The radial velocity changes conspicuously, but it is not certain whether this change is caused by orbital motion or by changes in the structure of the lines. The observed range is 125 km/sec in five days. It is possible that there are slight changes in the intensities of these central absorptions. The strongest emission feature is a blend of *C* III 4650 and *C* IV 4658. Using the wave length of *C* IV 4658.64, I find the following velocities for the center of the emission:

April 30.....	−380 km/sec	May 5.....	−865 km/sec
May 1.....	−543	May 6.....	−690
May 2.....	−684		
		Mean.....	−632 km/sec or −9.8 A

This would suggest that the line is mostly due to *C* III 4647.40 (20), *C* III 4650.16 (19), and *C* III 4651.35 (18). It is not possible to ascertain whether the average value shows a shift from the blended wave length. On the red edge the broad *C* III emission band is blended with the weaker emission of *He* II 4686. There is, however, a fairly conspicuous "step" between the two features, and, uncertain though they are, the measurements show a definite shift between April 30 and May 5. This may be ascertained by comparing the enlargements in Plate XI. I am not certain whether these shifts are related to those of the central absorptions or whether the phenomenon represents binary motion. There is a very strong violet absorption at *C* III 4650, and that, too, may be variable in intensity, but the evidence is not conclusive.

At the present time it would seem that the central absorptions do not represent the motion of the cluster. It is impossible to ascertain whether the emission lines are systematically shifted.

Star 17 (HD 152408).—This spectrum has been fully described by Swings,[18] who has called attention to an unidentified emission line at λ 4503.3. I have again measured this

[18] *Ap. J.*, **95**, 123, 1942.

line on several plates. There is a strong and very strange absorption line at λ 3880.5. The line is stronger than $H\zeta$ and does not have a red emission component. I have been unable to identify this line. It is broad and somewhat diffuse, resembling the *H* lines rather than the lines of other elements. One or two plates suggest that it may be double. The average shifts of the individual lines from the plate averages are given in Table 6. The large differences in the values are due partly to blends and partly to real displacements. The inconsistent values for absorption and emission of $H\delta$ must be due to blending with *N* III 4103.37. The average for the emission lines gives a red shift of +41.4 km/sec with respect to the cluster. In this star *He* II 4686 is shifted less than most other lines. The absorption lines, whether accompanied by emissions or not, give large negative displace-

TABLE 6

SYSTEMATIC SHIFTS OF INDIVIDUAL LINES FROM MEAN VELOCITIES IN HD 152408

LINE	ABSORPTION		EMISSION	
	Line − Mean (In Km/Sec)	M.E. (In Km/Sec)	Line − Mean (In Km/Sec)	M.E. (In Km/Sec)
H 3797.90	[−18.8]			
He I 3819.69	[−32.8]			
H 3835.39	[+61.2]			
$H\zeta$ 3889.05	[−66.2]			
N III 3938.52			− 22.1	±14.9
He I 4026.22	+21.6	± 8.2	+ 32.2	2.8
Si IV 4088.86	− 3.8	12.4	+ 13.9	14.2
N III 4097.31	−84.4	12.0	− 26.1	18.2
$H\delta$ 4101.74	+53.2	12.2	+108.4	5.7
Si IV 4116.10	−42.5	5.7	− 27.5	7.6
He II 4199.87	+46.7	25.8		
$H\gamma$ 4340.47	−27.6	10.5	+ 13.6	18.1
He I 4471.51	−29.6	15.6	+ 32.8	11.0
He II 4541.63	+77.2	±13.4		
N III 4634.16			− 48.3	6.7
N III 4640.64			+ 4.9	11.6
He II 4686.81			− 36.5	±13.1

ments and must all originate in an expanding shell. I believe that this star is a typical P Cygni object and is of great interest because its ionization is considerably higher than that of P Cygni itself (Pl. XII, *a*).

The general conclusion is that those emission lines which, like *N* III 4634, *N* III 4641, and *He* II 4686, show no appreciable violet absorptions are shifted little from their normal wave lengths, while those lines which possess strong violet absorptions are shifted to the red by an appreciable amount. Disregarding lines which are poorly determined and those which are obviously influenced by blends, we form the following averages:

Lines with strong violet absorption give shift of emission = +23.4 km/sec (λλ 4026, 4089, 4340, 4472),

Lines without violet absorption give shift of emission = −26.6 km/sec (λλ 4634, 4641, 4687).

Star 18 (*HD 151804*).—This spectrum has also been described by Swings.[19] This is a P Cygni type star, although its emission lines are much weaker than those of HD 152408. (Pl. XII, *b*). Of interest is *O* III 3759.96, which has the typical P Cygni type structure.

[19] *Ibid.*

PLATE XI

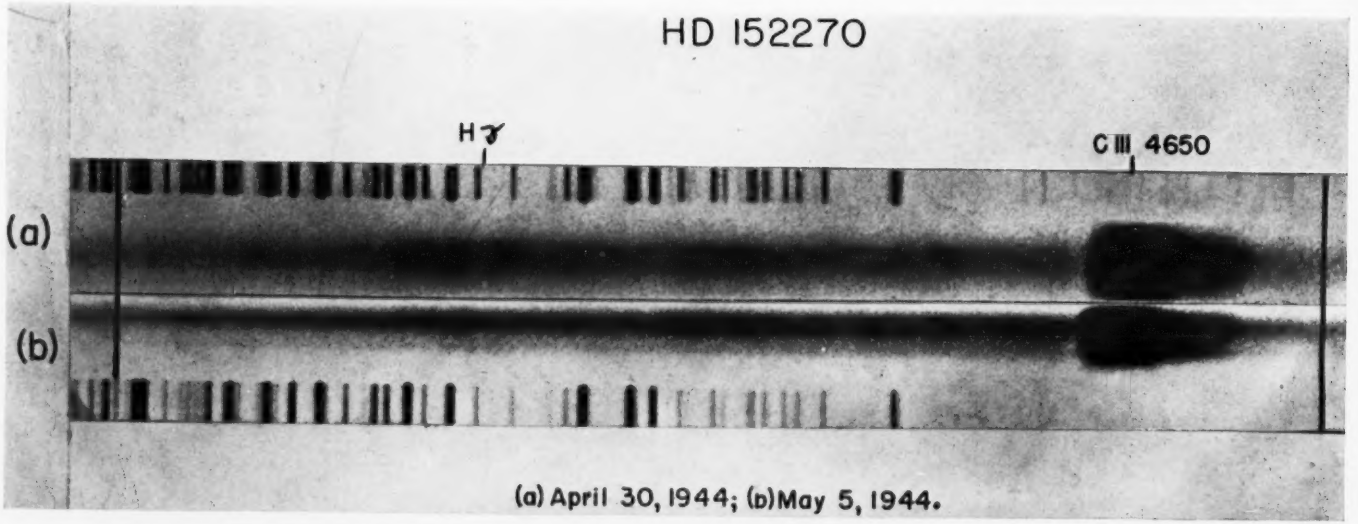

SPECTRUM OF HD 152270

PLATE XII

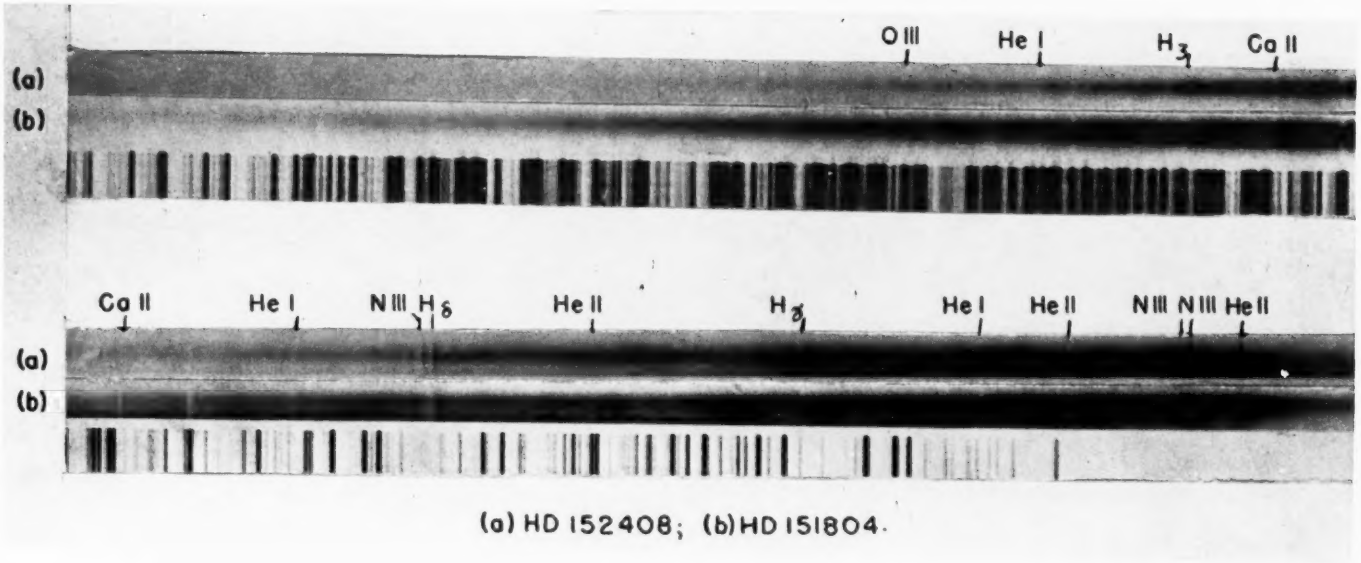

(a) HD 152408; (b) HD 151804.

The other emission lines are without violet absorptions. The unidentified emission line, λ 4503.3, is again present and has no absorption component. Table 7 lists the systematic shifts of the lines. We again infer that those emission lines which have no violet absorptions (*N* III 4634, 4641) display little or no red shift, while those with violet absorptions

TABLE 7

SYSTEMATIC SHIFTS OF INDIVIDUAL LINES FROM MEAN VELOCITIES IN HD 151804

LINE	ABSORPTION		EMISSION	
	Line − Mean (In Km/Sec)	M.E. (In Km/Sec)	Line − Mean (In Km/Sec)	M.E. (In Km/Sec)
H 3734.37	−15.0	± 9.7	.....	.....
H 3750.15	+ 6.4	11.7	.....	.....
O III 3759.96	− 5.1	21.5	+ 9.6	± 9.6
H 3770.63	+ 0.7	12.4	.....	.....
O III 3791.26	+62.5	10.6	.....	.....
H 3797.90	+ 9.3	6.4	.....	.....
He I 3819.64	+10.5	6.8	.....	.....
H 3835.39	+20.2	6.7	.....	.....
Hζ 3889.05	−14.1	9.3	.....	.....
He I 4026.22	− 0.1	13.7	.....	.....
Si IV 4088.86	− 7.4	10.4	.....	.....
N III 4097.31	−53.0	5.6	.....	.....
Hδ 4101.74	+32.6	7.4	.....	.....
He II 4199.87	−10.3	17.5	.....	.....
Hγ 4340.47	−36.8	3.8	.....	.....
He I 4471.51	+ 8.3	10.5	+ 91.3	± 8.4
Mg II 4481.23	.....	.....	+137.4	.....
He II 4541.63	+23.8	± 6.6	.....	.....
N III 4634.16	.....	.....	− 79.9	.....
N III 4640.64	.....	.....	− 24.9	.....

(*O* III 3760, *He* I 4472) are shifted quite considerably. Probably all absorption lines come from the expanding shell. The very large scatter in the individual plate velocities from the emission lines in Table 3 is due to the fact that on several plates the region of the lines of *N* III 4634 and *N* III 4641 was not measurable because of overexposure. On these plates the other lines gave large positive values. I am inclined to think that the identification of the emission line at λ 4481 may be wrong. Swings[20] mentions an unidentified line at λ 4485 in this star and also in 9 Sagittae. Probably this line is identical with the one I have measured at λ 4483.

[20] *Ibid.*

NOTE ON THE DOUBLE WHITE DWARF L 462-56 = LDS 275

W. J. LUYTEN
University of Minnesota
Received May 20, 1944

The star L 462–56, in position $\alpha = 9{:}32.9$, $\delta = -36{:}54$ (1900), with a proper motion of 0".35 in 299°, was announced as a wide double, LDS 275, with components of $13^m.7$ and $15^m.0$, photographic, and a separation of 9". During the systematic search for white dwarfs among southern proper motions undertaken by the writer with the 36-inch reflector of the Steward Observatory, it was found that the $15^m.0$ companion is optical; but not only did the $13^m.7$ primary turn out to be white but its image appeared elongated. A subsequent plate, taken with the 100-inch telescope by Dr. Baade and forwarded by him to Minnesota, shows conclusively that the star is double, with a separation of about 3" and a photographic magnitude difference of about 0.3. It would appear advisable, therefore, to continue the designation "LDS 275."

Further plates taken by the writer at Tucson were of such poor quality, owing to the star's southern declination, that it was impossible to ascertain the color index of the fainter component, although it appeared probable that it, too, was white. Recently Dr. Van Biesbroeck has taken two pairs of plates with the 82-inch McDonald telescope, in yellow and blue light, and forwarded them to Minnesota for measurement. These show conclusively that the two components have very nearly the same color index, the fainter star being perhaps the redder by 0.15 mag. The resulting magnitudes are now estimated to be

Primary.....	14.1 pg; 14.2 pv
Secondary.....	14.4 pg; 14.35 pv

From measures of the Mount Wilson and McDonald plates (Pl. XIII) and from visual measures made by Van Biesbroeck at McDonald, which I am permitted to quote here, we have the following values for the separation and position angle:

1942.29.....	3".4	34°	Mt. Wilson 100-inch
1944.24.....	3.2	38	McDonald 82-inch
1944.29.....	3.87	37.1	Van Biesbroeck visual

Owing to the well-known systematic differences between visual and photographic measures of separations of close double stars, not much can be deduced from the values of these separations; but, especially because the two components are virtually of the same color, the position angles should be more reliable. These would appear to indicate an orbital motion of the order of 3° in 2 years; hence a period of the order of 250 years. From the proper motion alone, a parallax of the order of 0".050 would appear probable; and hence, with normal masses, a period of the order of 500 years and an orbital motion of the order of 0".04 annually would appear reasonable. Such amounts should be verifiable within a very few years, and it is hoped that observers more favorably situated will undertake to determine both the parallax and the orbital motion.

For the sake of comparison, other binaries containing white dwarfs may be briefly discussed here. In addition to the classical systems of Sirius and o_2 Eridani BC for which reliable orbits are available, the system of Procyon, and the possible white dwarf—red giant system of Mira Ceti, six other systems are now known in which one of the components is a white dwarf. The present binary, however, is the only one in which both com-

PLATE XIII

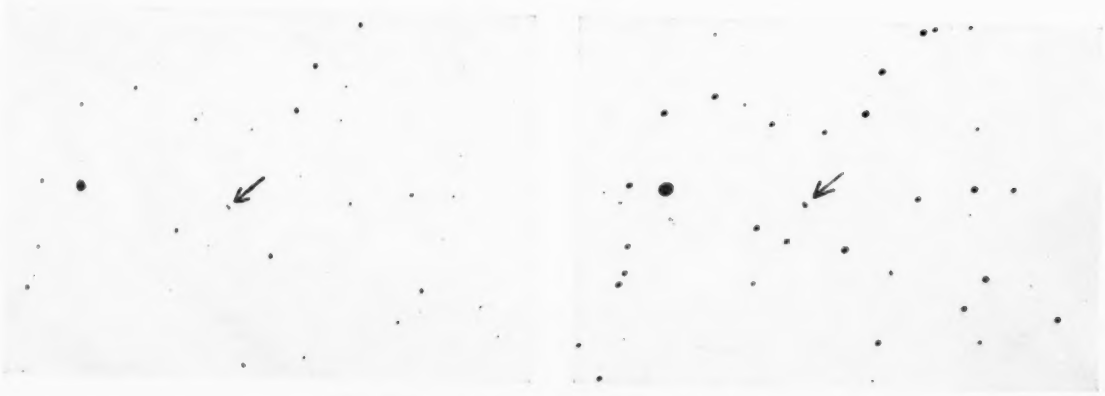

FIELD OF THE DOUBLE WHITE DWARF LDS 275

Left: Mount Wilson blue plate; *right:* Macdonald yellow plate. The color of the components may perhaps best be judged by comparing their images with that of the star south following it. The bright star following the double is CPD-36°3791; the double precedes this by 160″ and is south by 24″.

ponents are white dwarfs. In Table 1 data are given for these seven systems; it will be seen that the present binary holds out the greatest promise for an early determination of orbital motion and mass.

TABLE 1

LIST OF BINARIES CONTAINING WHITE DWARFS

Designation	α (1900)	δ (1900)	Mag.	Sp.	Mag.	Sp.	Sep.	μ
L 587-77.....	3^h24^m7	$-27°44'$	15.0	m	13.8	a	8″	0″81
CPD−37°6571..	15 41.0	−37 36	6.9	G0	13.5	A	.....	0.48
W 672.....	17 13.6	+ 2 04	14.3	M3	14.4	A	.....	0.56
LDS 749*.....	21 27.0	− 0 14	10.8	.....	14.4	con.	134	0.43
L 1512-34, 35...	23 38.9	+32 00	14.0	M3	14.1	A	174	0.22
L 577-71, 72....	23 48.9	−33 50	14.0	m	13.9	a	7	0.51
LDS 275.....	9 32.9	−36 54	14.1	b	14.4	a	4	0.35

* BD-0°4234.

In conclusion it is a pleasure to record my obligation not only to the Graduate School of the University of Minnesota, through whose financial assistance the work on the present star became possible, but likewise to Drs. Paul D. Jose at Steward Observatory, Walter Baade at Mount Wilson, and Georges Van Biesbroeck at McDonald Observatory for their splendid co-operation in obtaining observational material on this interesting object.

A STUDY OF THE WOLF-RAYET ECLIPSING BINARY HD 193576 = V 444 CYGNI

ZDENĚK KOPAL
Harvard College Observatory
Received July 14, 1944

ABSTRACT

An analysis of the Lick photoelectric light-curve of HD 193576, coupled with available spectroscopic evidence, leads to the following conclusions regarding the structure and absolute dimensions of this remarkable eclipsing system:

1. The Wolf-Rayet component of HD 193576 must possess an extended envelope capable of dimming light of the O star which passes through it at the time of primary minimum but whose own emission is so small a fraction of the total luminosity of the star that no appreciable loss of light results when the O star passes in front of it. This should explain the observed unequal durations of the alternate minima.

2. The radius of the effective core of the Wolf-Rayet component (which emits at least 90 per cent of its total light) cannot exceed approximately one-fourth the radius of the whole star. The envelope surrounding this core must be partially transparent to blue light of the O star and cannot be of the nature of a thin absorbing shell. Whether or not the transition between the luminous core and surrounding envelope is gradual or abrupt seems impossible to decide from the photometric evidence alone.

3. The bodily eclipses of the O component and of the effective core of the Wolf-Rayet star are partial, the orbital inclination being in the neighborhood of 77°. The radius of the O component is found to amount to approximately 27 per cent of the radius of the relative orbit, or about 10$\odot$, that of the opaque core of the Wolf-Rayet star being less determinate but apparently much smaller. The masses of the O and W stars are 27$\odot$ and 10.5$\odot$, respectively. This model of HD 193576 is in agreement with the small variation of light observed between minima.

4. Practically the entire photometric ellipticity of HD 193576 can be accounted for by the O component, leaving little or nothing to be explained by the W envelope. This shows again that this envelope must be relatively dark. Because of its great dimensions, its distortion is undoubtedly considerable; but, since it does not appear noticeably to affect the light-changes between minima, the contribution of the envelope to the combined light of the system must be insignificant.

5. The abnormal width of the primary minimum indicates that the envelope surrounding the W core extends to at least 14 solar radii in the direction of the line joining the centers of the two stars. An atmosphere of such dimensions must be at the limit of dynamical stability and is likely to suffer a continuous loss of matter streaming out of the conical end of the critical equipotential with velocities smaller than the ordinary velocity of escape. Atmospheric tides raised by the O component might explain the observed asymmetry of helium emission bands and its variation with the phase. This suggests, incidentally, that these bands are likely to originate in outer parts of the extended envelope rather than close to the photosphere of the W star, where tides are much less important.

6. Since, by hypothesis, even the uneclipsed part of the O component shines at mid-primary minimum through the whole extent of the W envelope, which may seriously reduce its light, the observed depth of the primary minimum, combined with that of the secondary, can yield only a lower limit for the surface brightness of the W star. On the basis of computations made in this paper—crude as they are—it appears certain that the true surface brightness, and consequently the effective temperature, of the W core is at least as high as that of the O component, and quite possibly higher. Our hypothesis removes, therefore, any conspicuous discrepancy between the effective and ionization temperature of the Wolf-Rayet star.

The system of HD 193576 = HV 11111 = V 444 Cygni, recognized as a spectroscopic binary by Wilson[1] and discovered as an eclipsing variable by S. Gaposchkin,[2] turned out to be one of unusual interest because it was found to consist of a Wolf-Rayet star of the type WN 5 attended by an early-type component whose spectrum was classified as B1 by Wilson and reclassified as O6 by Beals.[3] Since this is the first, and so far the best, observed eclipsing binary having a genuine Wolf-Rayet star as a component, its detailed study may be expected to throw considerable light on the structure and sev-

[1] *Pub. A.S.P.*, **51**, 55, 1939; *Ap. J.*, **91**, 379, 1940.

[2] *Pub. A.A.S.*, **10**, 52, 1940; *Ap. J.*, **93**, 202, 1941.

[3] *Pub. A.A.S.*, **10**, 304, 1943.

eral otherwise inaccessible properties of a representative of this rare class of peculiar stars. The object of the present paper will be to re-examine the available photometric evidence pertaining to HD 193576, together with an attempt to show how far an interpretation of the observed light-changes may contribute toward obtaining a definite picture of this intriguing binary system.

Following the discovery light-curve of Gaposchkin's, based on estimates from Harvard photographic plates, an unusually precise photoelectric light-curve of HD 193576 was recently published by Kron and Gordon[4] from the Lick Observatory. This light-curve, corresponding to a somewhat longer effective wave length than Gaposchkin's, has closely confirmed his amplitudes of both minima and the constancy of light between eclipses but has shown that the primary minimum is more than twice as wide as the secondary one[5]—a unique and puzzling feature for a system whose components, according to their radial-velocity curves, revolve in orbits that are practically circular.[6]

An orbital solution based on the preliminary Lick light-curve was already carried out by Wilson.[7] Wilson did not publish all details of his photometric solution. It seems, however, that his large relative dimensions of both components were obtained by confining the orbital analysis to the wide primary minimum. Now, after the definitive Lick curve has been published, it appears that Wilson's elements are at variance with it in two important respects: they are unable to account for the observed difference in widths of both minima, and, worse still, they seriously conflict with the constancy of light of HD 193576 between eclipses. In point of fact, this system as envisaged by Wilson strikingly resembles in its relative dimensions that of β Lyrae, and its light-changes due to shallow partial eclipses should be drowned entirely in a secondary variation invoked chiefly by the distortion of the W component, which, according to Wilson, was to be the larger, less massive, and (photoelectrically) more luminous of the two. A theoretical amplitude of light-changes due to the ellipticity alone in Wilson's model of HD 193576 should be in the neighborhood of half a magnitude—which has certainly not been observed. Wilson's failure to obtain genuine photometric elements of the system by so large a margin can undoubtedly be traced back to one fact, namely, that *the wide primary minimum cannot be interpreted as arising from an eclipse of two opaque stellar disks.* The situation is apparently more complex, and a reinvestigation of the existing photometric material seems desirable.

The salient facts which will have to guide us in our interpretation of HD 193576 are, first, the greatly unequal widths of the primary and secondary minima and, second, the apparent constancy of combined light of the system between eclipses. Spectroscopic observations demonstrate that during the primary minimum the O star undergoes eclipse by the W component, and the light-curve shows that this minimum is the wider of the two. It is known, furthermore, that stars of the Wolf-Rayet type are likely to possess extended atmospheres. We shall, therefore, base our interpretation of HD 193576 on a working hypothesis that *the envelope of its W component is capable of absorbing light of the O star which passes through it at the time of primary minimum but that the surface brightness of outer parts of this envelope is so low as to produce no appreciable loss of light when the O star passes in front of it.*[8] In other words, we shall picture the W star as consisting of an

[4] *Ap. J.*, **97**, 311, 1943.

[5] This feature is also borne out, although to a lesser degree, by a plot of Gaposchkin's original observations.

[6] A slight displacement of the secondary minimum by -0.011 day, observed by Kron and Gordon, would correspond to $e \cos \omega = -0.0012$. An orbital eccentricity of this order of magnitude is not inconsistent with the spectroscopic data and would have no further observable consequences.

[7] *Ap. J.*, **95**, 402, 1942.

[8] A suggestion that "the presence of some type of envelope around one or both components" could be invoked to explain peculiarities of the light-curve of HD 193576 has been advanced by Kron and Gordon (*op. cit.*, p. 322).

"effective" core which emits most of its light and is surrounded by an extended atmosphere whose contribution to the total luminosity of the star we shall ignore. Our aim will be to investigate how well this model will stand up in quantitative comparison with the observed facts and which conclusions can be drawn from the photometric evidence as to the relative dimensions of the core and its envelope.

The foregoing hypothesis leads us logically to begin with an analysis of the secondary minimum, owing to the eclipse of the W core by the O component. This secondary minimum is, unfortunately, shallow; and it is sufficiently known from the theory of light-curves that, in such cases, the ratio of radii of the components may become an almost indeterminate quantity.[9] In our present case the photometric evidence may, fortunately, be supplemented by a spectrophotometric determination of the ratio of luminosities of the two components. According to Wilson's interpretation of certain spectral features, the W star appeared to be the brighter of the two. On the other hand, the Victoria spectrograms as interpreted by Beals[10] indicated that the W star was by 1.75 mag. fainter than the O component, with an uncertainty of two- or three-tenths of a magnitude. Since Beals's approach to the problem was much less sensitive to observational errors than Wilson's[11] and leads, moreover, to luminosities which are in a close agreement with properties of the respective stars as a class, in what follows we are going to adopt his results and base our photometric solution upon it.

In more precise terms, the outcome of Beals's study indicates that

$$\frac{L_W}{L_O} = \left(\frac{r_W}{r_O}\right)^2 \frac{J_W}{J_O} = 0.20 \pm 0.04 , \tag{1}$$

where L, r, and J stand for the luminosity, radius, and mean surface brightness of the respective component. If HD 193576 were an ordinary eclipsing system, the ratio of surface brightnesses, J_O/J_W, could be obtained directly from the fractional intensities of light, λ, observed at the bottom of the primary and secondary minimum by means of the well-known formula

$$\frac{J_O}{J_W} = \frac{1 - \lambda_1}{1 - \lambda_2} , \tag{2}$$

and a combination of equation (1) and equation (2) should specify the ratio of the radii, $r_W/r_O = k$. Now, according to Kron and Gordon, the observed depths of the primary and secondary minima of HD 193576 are 0.297 and 0.141 mag., respectively, which, translated in intensity units, give $1 - \lambda_1 = 0.2393$ and $1 - \lambda_2 = 0.1218$. These values inserted in equation (2) yielded $J_O/J_W = 1.96$ at the effective wave length of a potassium hydride cell (4500 A). The fact that the eclipse of the O star by the W component gives rise to a minimum which is, in the blue, about three times as deep as when the O star is in front led Gaposchkin and, following him, Wilson to conclude that the surface brightness, and so the effective temperature, of the W star should be approximately by one-third lower than that of the O component. The presence of an extended absorbing envelope around the W star would, however, completely change the picture. The fractional intensities λ in equation (2) refer, by definition, to bodily eclipses (i.e., to eclipses of completely opaque disks). According to our above hypothesis providing that the envelope of the W star is dark or emits but faintly, the secondary minimum of HD 193576 should essentially be such a bodily eclipse. The wide primary minimum may, however, be largely atmospheric; that is, apart from eclipse by the opaque W core, the light of uneclipsed portion of the O star gets further dimmed by a passage through the atmosphere

[9] Cf. Kopal, *Ap. J.*, **94**, 145, 1941 (secs. 8–10).

[10] Private communication.

[11] According to Wilson, the less massive Wolf-Rayet component was to be the brighter of the two.

surrounding the W core. Since the true proportion of light lost during primary minimum by "atmospheric" and "bodily" eclipse is not known a priori, we are compelled, at this stage, to resort to a black-body approximation and evaluate the ratios of surface brightnesses of the two components by means of Planck's formula for certain plausible temperatures of both components.

The effective temperature of an O6 star should, according to Kuiper,[12] be roughly 60,000°. The ionization temperature of the Wolf-Rayet core was estimated by Beals[10] and by Menzel[10] to be probably between 80,000° and 100,000°. This ionization temperature need not necessarily be identical with the effective temperature of the W core. For the sake of simplicity we shall, however, in what follows, assume this to be the case; and, if so, the Planck's formula (for the effective wave length of 4500 A) readily yields the results given in Table 1. The third column in Table 1 contains the theoretical losses of light, at mid-primary minimum, owing to a bodily eclipse alone and computed from equation (2); while the ratios of the radii, k, as given in the last column, were then obtained from equation (1). The first alternative (A) would correspond to a purely transparent envelope and can therefore be regarded only as a limiting case; the alternative (B)

TABLE 1

	T	J_O/J_W	$1-\lambda_1$	r_W/r_O
A	37,000°	1.96	0.239	0.63
B	60,000	1.00	.122	.45
C	80,000	0.70	.085	.37
D	100,000	0.54	0.065	0.33

is likewise based on the assumption that the surface brightnesses of both components are equal. If the ionization temperatures are of any guidance, the reality should lie somewhere between alternatives (C) and (D). Whether or not such a high effective temperature of the W core is compatible with all other observational evidence can be verified only at a later stage of our analysis. For the present we notice that, if effective temperature of the W core is to be as high as 100,000°, three-fourths of the fractional loss of light observed during primary minimum must be due to atmospheric eclipse. We also notice that, regardless of the uncertainty in temperature, *the radius of the W core must be considerably smaller than that of the O star.*

Before we proceed with a solution for photometric elements of HD 193576, another consideration should be pointed out. The absence of any definite stillstand at the bottom of the secondary minimum indicates that eclipses of the W core by the O component are most likely partial; and it has long been recognized that, to the degree of accuracy attained by any existing photometric measures, the problem of arriving at the elements of a partially eclipsing system solely from its light-curve in one minimum is practically indeterminate.[13] In order to solve this problem, another independent relation between the elements of the eclipse must be sought for. Such a relation is ordinarily provided by the well-known equation[14]

$$a_0 = 1 - \lambda_2 + \frac{1-\lambda_1}{k^2}, \qquad (3)$$

[12] *Ap. J.*, **88**, 429, 1938.

[13] Cf., e.g., Russell, *Ap. J.*, **35**, 315, 1912.

[14] This equation is true provided that both stars appear as uniformly bright disks. As far as the O component is concerned, this assumption is probably justified. In extending it also to the core of the W star we do so not because we believe this to be actually the case but rather because a uniform distribution of intensity provides just as good an approximation to reality as any other simple distribution would give.

where a_0 stands for the maximum fractional loss of light of the smaller star. In using this equation it is, however, necessary to remember that the $1 - \lambda$'s of both minima refer again, by definition, to fractional losses of light due to bodily eclipses; and hence, for HD 193576, the values of $1 - \lambda_1$ should be taken from the third column of the above tabulation rather than directly from the observations.

With these precautions duly considered, a solution of the light-curve of HD 193576 within secondary minimum for photometric elements of the system should present no difficulties. In order to obtain them, we employ a method, recently proposed by the writer,[15] which makes direct use of observed normal points rather than of a free-hand curve, on which most of the older methods were based. Its application yields the results shown in Table 2, where i denotes the inclination of orbital plane to the celestial sphere and θ', the theoretical angle of first contact during secondary minimum, the radius of the relative orbit of both components being taken as the unit of length. The maximum obscuration of the W core attained at the moment of mid-secondary minimum is the same for either alternative and equal to $a_0 = 0.73$. The reader will, furthermore, notice

TABLE 2

	r_O	r_W	i	θ'
A	0.215	0.135	81.3°	18.6°
B	.249	.112	78.5	17.9
C	.266	.098	77.1	17.1
D	0.274	0.091	76.5	16.8

that the sum of the fractional radii $r_O + r_W$ is influenced but little by the uncertainty of their ratio and is sensibly equal to 0.36.

The orbital inclination, once known, offers a clue to the absolute dimensions of HD 193576. According to Wilson,[1] the spectroscopic masses of both components are

$$m_W \sin i = 9.74\odot ,$$
$$m_O \sin i = 24.8\odot ,$$

and the sum of projected semimajor axes of their absolute orbits is

$$(a_W + a_O) \sin i = 35.8\odot .$$

Inserting the above values for i, we obtain the values given in Table 3. The mean density of the O component should amount to 0.027 ⊙, while that of the luminous core of the W star should be 0.23 ⊙. These figures differ greatly from the absolute dimensions deduced by Wilson.[7] The dimensions derived earlier by Gaposchkin[2] appear to have approximated much more closely the properties of the O star.

The light curve of HD 193576 within primary minimum does not lend itself readily for orbital analysis. Since Wilson's attempt to interpret the primary minimum as an eclipse of two opaque stellar disks led to contradictory results, we conclude that this eclipse must be partly atmospheric. A rigorous analysis on this basis is naturally impossible as long as we are in the dark concerning the law which relates absorption with the dip, but at least the extension of the envelope surrounding the W core may be estimated from the width of the primary minimum. An inspection of the light-curve re-

[15] *Ap. J.*, **94**, 145, 1941. For fuller details of the photometric solution compare the orbital analysis by Professor H. N. Russell appearing in this *Journal*, p. 213. It should, however, be pointed out that the fractional radii of both components as defined by Russell and in the present paper are not strictly the same, owing to the peculiarities of the system under consideration, and that no close agreement should be expected between them.

veals that a loss of light begins to be noticeable at least 11 hours before the moment of mid-primary minimum, or at a phase-angle of approximately 40°. The fractional mean radius r'_W of the envelope may then be approximated from the equation

$$\sin^2 \theta' \sin^2 i + \cos^2 i = (r_O + r'_W)^2 . \qquad (4)$$

Since an analysis of the secondary minimum gave $i = 77°$ and $r_O = 0.27$, equation (4) yields $r'_W = 0.40$. The last digit of this figure is admittedly uncertain; but, even so, this shows that *the envelope surrounding the W star must be at least four times as large as its luminous core.*

The great extension of atmosphere of the W star leads to two immediate consequences. First, *this atmosphere cannot be wholly opaque to the radiation (around 4500 A) of the O star passing through it during primary minimum,* for, if it were, the minimum would have to exhibit a phase of constant light of appreciable duration. The evidence for a partial transparency of the atmosphere is further strengthened by the fact that the O spectrum remains visible throughout the whole cycle. Second, *the envelope cannot be of the nature of a thin absorbing shell,* for, in this case also we should have to expect a discontinuity at the transition from atmospheric to bodily eclipse, of which there seems to be no trace in the

TABLE 3

	r_O	r_W	m_O	m_W
A	7.8	4.9	25.7	10.1
B	9.1	4.1	26.4	10.4
C	9.8	3.6	26.8	10.5
D	10.1	3.3	27.0	10.5

light-curve. The form of the observed curve would suggest that the atmospheric absorption increases gradually from the limb toward the center. Whether or not the transition between the luminous core and absorbing atmosphere of the W star is gradual or abrupt —i.e., whether the O component sinks into partial obscurity during primary minimum behind the envelope of the W star, like the sun setting in a smoky terrestrial atmosphere, or whether the core of the W star represents a distinct horizon—seems impossible to decide on the basis of available photometric evidence. We may, however, approximate at least the lower limit of absorbing power of the envelope from the following consideration. Since the relative orbit of both components is circular or very nearly so, the durations of bodily eclipses in either minimum should naturally be the same. This implies that the eclipse should still be purely atmospheric 0.20 day before or after the mid-primary minimum. The light-curve shows, however, that by then the loss of light has already reached more than one-half of its maximum value. It should be stressed that this represents only the lower limit of absorbing power of the envelope, because the absorption is likely to increase as the O star merges behind deeper atmospheric layers. Until the theory of absorption processes in extended envelopes of Wolf-Rayet stars offer us more guidance as to the quantitative relation between absorption and dip, the depths of both minima observed at any particular frequency of light will not lend themselves to a direct determination of the ratio of surface brightnesses or effective temperatures of central portions of the two components. Since the upper limit of absorbing capacity of the envelope is as yet impossible to estimate, we may reconcile the observed data with almost any temperature of the W core. *There is nothing in the available photometric evidence that should demand for the luminous core of the W star an effective temperature lower than that of its O-type companion.* On the other hand, it is quite possible that the W star is the hotter of the two.

Let us further insure whether or not our above model of HD 193576, in addition to

giving rise to two minima of unequal durations, will also render its light between minima approximately constant. As is well known, the combined light (l) of a close eclipsing system out of eclipses is usually found to vary with the phase θ as

$$l = 1 - c_1 \cos\theta - c_2 \cos^2\theta - \ldots\ , \tag{5}$$

where c_2, the first-order ellipticity effect, is in turn essentially equal to

$$c_2 = z_O L_O + z_W L_W\ , \tag{6}$$

where the z's are individual photometric ellipticities of the two components and the L's stand for their respective fractional luminosities. The theory shows[16] that, very approximately,

$$z_i = \frac{3(15+u)}{10(3-u)}\{1+\tau\}\frac{m_j}{m_i}\, r_i^3 \sin^2 i + \ldots\ , \tag{7}$$

where u and τ stand for coefficients of limb and gravity darkening of the distorted star, respectively. Now it is reasonable to assume that for stars as hot as both components of HD 193576 the limb darkening at $\lambda = 4500$ A is small, if any; and, furthermore, it is unlikely that the W component should exhibit any gravity darkening,[17] while for the O star the gravity darkening is probably close to full (i.e., $\tau = 1$). Under these conditions the elements corresponding to our alternatives (B), (C), and (D), coupled with Wilson's mass-ratio of $m_W/m_O = 0.39$ and Beals's spectrophotometric determination of fractional luminosities $L_O = 0.83$ and $L_W = 0.17$, yield

$$B \ldots . \ c_2 = 0.015\ ,$$
$$C \ldots . \ c_2 = 0.018\ ,$$
$$D \ldots . \ c_2 = 0.020\ .$$

On the other hand, a harmonic analysis of Kron and Gordon's observations between minima (normals Nos. 11–26 and 38–57; all attributed equal weights) gives[18]

$$\begin{aligned} l = \ & 0.9995 - \ 0.0104\cos\theta - \ 0.0109\cos^2\theta - \ldots\ , \\ & \pm 0.0009 \quad \pm 0.0021 \qquad \pm 0.0033\,(\text{p.e.}) \end{aligned} \tag{5.1}$$

and therefore the observed $c_2 = 0.011 \pm 0.003$ (p.e.). This is somewhat less than the above theoretical values. A direct comparison of the observed and computed c_2's is, however, still inadmissible, because the observed value of effective ellipticity is known to be partly masked by the reflection effect. The term, due to reflection and varying as $\cos^2\theta$, is rather difficult to evaluate; in terms of a theory recently proposed by the writer,[19] it should, in the present case, amount to 0.007 or more. This should be added to the observed c_2 in order to obtain the pure ellipticity constant. The latter should therefore not be smaller than 0.018 ± 0.003, which brings it to an almost exact agreement with theoretical expectation.

The fact that the O component, together with the core of the W star, can thus account for the entire observed ellipticity proves again that the extended atmosphere surrounding the W core must be almost devoid of light—proper or diffused. Because of its great dimensions its distortion is undoubtedly considerable; but, since it does not appear to affect the combined light of the system between minima to any appreciable degree, its own fractional luminosity must evidently be insignificant.

[16] Cf. Kopal, *Ap. J.*, **96**, 20, 1942, or *Proc. Amer. Phil. Soc.*, **85**, 399 (sec. 14), 1942.

[17] The existence of gravity darkening presumes an absence of any appreciable convection currents in or beneath the star's photosphere—a condition not likely to be met in Wolf-Rayet stars.

[18] The probable error of a single such normal results ± 0.0037 mag., in substantial agreement with an estimate by Kron and Gordon.

[19] *Proc. Amer. Phil. Soc.*, **86**, 351, 1943.

The first-order reflection effect in HD 193576 represents a difficult object for theoretical interpretation. The bolometric reflection in a system specified by the elements (*C*) or (*D*) should not exceed 0.002, which is significantly less than the observed coefficient of cos θ in equation (5.1). This discrepancy may partly arise from our inability to translate the total reflected light into its observable amount; or it may indicate that a certain fraction of light of the O component gets absorbed and re-emitted in the extended atmosphere of the W star before reaching its core;[20] or it may be due to still another and rather interesting cause. The envelope surrounding the Wolf-Rayet star must naturally dim to a certain extent the light of the core which is imbedded in it. If the envelope were symmetrical, this dimming would remain constant and independent of time. The tides raised by the O star will, however, distort the envelope from a spherical form. The tidal bulge must always remain pointed to the center of mass of the disturbing body; and hence the optical depth of the envelope as viewed by a distant observer should vary as the O star revolves: at the time of primary minimum the W core should appear brighter, because of the "low tide" of absorbing matter over the visible hemisphere, and vice versa.[21] A variation of light arising from this cause will evidently simulate an exaggerated reflection of light of the W star from the O component and thus counteract the reflection of O light from the W core; hence the net effect may come out so small. This phenomenon might, in principle, enable us to estimate the absorbing power of the envelope independently of the eclipses, but existing photometric observations are still insufficiently accurate for this purpose.

The great extension of envelope surrounding the core of the W star should have one more interesting consequence. So tenuous an atmosphere cannot fail to yield to the tidal forces exerted upon it by the massive O star, and its external form should be closely approximated by an equipotential corresponding to Roche's model.[22] If the envelope is to be stable, its extension (x) in the direction of the center of mass of the system should, however, not exceed the root of the equation

$$\left(\frac{R}{x}\right)^2 - \frac{x}{R} = \frac{m_O}{m_W}\left\{\left(\frac{R}{R-x}\right)^2 - \frac{R-x}{R}\right\} \qquad (8)$$

between 0 and 1, where R denotes the separation of the components. This equation represents the last equipotential capable of containing the whole mass of the distorted body within a closed volume. Since, according to Wilson, $m_W/m_O = 0.39$, the critical root of equation (8) is found to be $x/R = 0.405$. A coincidence of this root with the mean radius, r'_W, of the envelope found from equation (4) above is too good to be wholly true but is doubtless significant. It shows that *the atmosphere surrounding the W core must be at the limit of stability*, for, should its volume exceed that of the corresponding branch of the equipotential (8), dynamical motion would occur, and this motion would consist of matter streaming out of the conical end of the critical equipotential.[23] Certain spectroscopic evidence reported recently by Beals[3] suggests that this is, indeed, the case.

[20] It seems, however, certain that incident light of the O star must penetrate fairly deeply in the extended atmosphere of the Wolf-Rayet star before being absorbed and re-emitted (possibly at a temperature quite different from that at which it was emitted originally); because, should re-emission occur in its outer layers, the amount of reflected light would have to be much larger than that actually observed.

[21] It may be of historical interest to recall that precisely this mechanism, on a greater scale, was invoked years ago by Duncan (*Lick Bull.*, No. 151, 1908) to explain the light changes of Cepheid variables.

[22] Cf. Jeans, *Problems of Cosmogony and Stellar Dynamics*, sec. 163, Cambridge, 1919.

[23] This presumes, in other words, that outer parts of the W envelope of HD 193576 (or, more precisely, those of its constituents responsible for the dimming of light which passes through it) are in dynamical equilibrium. Although the problem of detailed equilibrium of such envelopes is still far from being well understood, the cyclic variations in profiles of lines of the Wolf-Rayet spectrum, discovered by Wilson and Beals, lend, by implications, rather strong empirical support to the view that at least outer parts of the W envelope do approach dynamical equilibrium.

The aim of the present paper is, in brief, to point out that the two outstanding features of the light-curve of HD 193576—namely, unequal widths of both minima and the constancy of light between eclipses—may be logically explained if we assume the W star to consist of a relatively small luminous core surrounded by an absorbing but dark extended atmosphere. This model was found to account quantitatively for all observed features of the light-curve and, in particular, made it clear that the effective temperature of the W core, as resulting from the photometric evidence, need not differ greatly from its ionization temperature. Our model seems, furthermore, to offer a natural explanation for several observed particularities of the Wolf-Rayet spectrum—such as the asymmetry of profiles of helium emission lines and its variation with the phase, where an action of atmospheric tides suggests itself. A fuller discussion of these and other spectral features would, however, widely exceed the scope of this paper and will be included in a forthcoming study by Dr. Beals, now in manuscript, which the present writer was fortunate enough to see in advance of publication.

The outcome of this study should in no way imply that further photometric investigations can contribute no more significant facts toward obtaining the complete solution of our problem. In point of fact, the system of HD 193576 should, more than ever, provide a fascinating subject for heterochromatic photometry. For instance, the dominating feature of the entire blue-violet region of its spectrum, He II λ 4686, falls well within the range of effective wave lengths of both Harvard and Lick light-curves. It would be highly interesting to know whether or not the relative widths of both minima or their depths would change if the light of this emission band were cut off by a suitable filter; or whether at some effective wave length the photometric ellipticity of the system would become more conspicuous. Such investigations could reveal a great deal concerning the structure of outer layers of the Wolf-Rayet stars. They should, in principle, enable us to distinguish between pure absorption and scattering of light in semitransparent envelopes surrounding the luminous cores or to conclude on the density of these envelopes as well as the kind of particles constituting them—and thus contribute greatly to our fuller understanding of these peculiar objects.

In conclusion, the writer considers it a pleasure to express his sincere thanks to Dr. C. S. Beals for the privilege of seeing the results of his spectrophotometric investigation of HD 193576 in advance of publication and for permission to quote them in the present paper and to Professors H. N. Russell and D. H. Menzel for stimulating discussions of certain aspects of the subject.

PROVISIONAL ELEMENTS OF THE ECLIPSING BINARY V444 CYGNI

HENRY NORRIS RUSSELL
Princeton University Observatory
Received July 7, 1944

ABSTRACT

The precise photoelectric light-curve can be well represented by the assumption that the effective diameter of the Wolf-Rayet component with its envelope is much greater when acting as an obscuring body than as a luminous one—except for deviation in the wings of the curves, which indicate that the body is actually very diffuse.

The relative luminosity of the components cannot be found from the light-curve but has been determined spectroscopically by Beals.

Widely different assumed values of this ratio lead to practically identical light-curves and to almost the same values of the radius of the O star, the orbital inclination, and the masses of the components. The effective surface brightness of the W-component is more than twice that of its companion. The envelope must be wholly gaseous and highly ionized.

Dr. Kopal's discussion of this remarkable system (which he has kindly shown to the writer) may be amplified by making the substitution of a sharp-edged disk for the diffuse Wolf-Rayet component, W, not only when it undergoes eclipse but when it partially obscures the other component, O. In the absence of an adequate theory it is uncertain in which case the actual diffuseness is the greater; in both cases this representation should lead to some sort of effective mean radius for the diffuse body. The exact nature of each mean will depend not only on the law of diffuseness but on the radius of O and other details of the eclipse.

The light-curves for both eclipses will have wider wings than those calculated for the disk, since beyond its edge there will be outer luminosity to be eclipsed, or obscuring matter to cut off light, where the simplified theory predicts no effect.

The following schematic model is therefore suggested. The components present uniformly bright circular disks of fixed luminosities, L_1 and $L_2 = 1 - L_1$. The radius r_1 of O (in terms of that of the orbit) is fixed, but the values r_2' and r_2'' adopted for W are different for the two eclipses. The system is then defined by the five parameters L_1, r_1, r_2', r_2'' and i (the inclination of the orbit).

1. Let $r_2' = k'r_1$ and $r_2'' = k''r_1$ and let a_0' and a_0'' be the fractions of the area of the disk of W involved at mid-eclipse. The depths of the minima then are

$$1 - \lambda_1 = k'^2 a_0' L_1 , \qquad 1 - \lambda_2 = a_0'' L_2 . \tag{1}$$

(It is here supposed that r_2' and r_2'' are less than r_1, as turns out to be true in the present case. The changes in other cases are easily made if required.)

2. If the value of L_1/L_2 is known (or assumed), a solution may be made as follows:

a) Equation (1) gives a_0'' and $k'^2 a_0'$.

b) The distance of centers at mid-eclipse is given by

$$\cos i = r_1\{1 + k'p(k', a_0')\} = r_1\{1 + k''p(k'', a_0'')\}, \tag{2}$$

whence

$$k'p(k', a_0') = k''p(k'', a_0'') . \tag{3}$$

These are functions of k' and k'', which may readily be calculated and plotted. The values of k' and a_0' corresponding to any assumed value of k'' are thus determined.

c) From the general equation

$$\sin^2 \theta(n) = r_1^2 \operatorname{cosec}^2 i\,[\{1 + kp(k\ \ na_0)\}^2 - \{1 + kp(k, a_0)\}^2] \tag{4}$$

the values of $\sin^2 \theta/r_1^2 \operatorname{cosec}^2 i$ may be calculated for comparable depths (e.g., $n = \frac{1}{2}$) in the two eclipses, and the ratio $\sin^2 \theta''(n)/\sin^2 \theta(n)$ may be determined for any assumed value of k'' and for the corresponding values of k' and α_0'.

d) The observed value of $\sin^2 \theta''(n)/\sin^2 \theta'(n)$ may be found from freehand light-curves. Comparison with (*c*) determines the k's and α_0'. Then $r_1^2 \operatorname{cosec}^2 i$ follows from equation (4) and cot i from equation (2), and all the elements are determined.

e) More than one pair of values of n may be used to get a mean value of k'', etc.; but it is more profitable to compute the theoretical light-curves corresponding to the first provisional set of elements from equation (4) and to plot these with the observations. Changes to improve the general fit can then be made by any intelligent computer.

In the present case, where this observed curve is not expected to be of the theoretical form, there is no excuse for employing the least-square methods.

f) The resulting elements and light-curves correspond, of course, to the schematic model and not to the actual system. Their principal merit is probably that they correspond to eclipses in which the luminosity or observation is arranged isotropically (circularly) about a point moving in a specified orbit, the same for both eclipses. This should make them a good starting-point for further approximation. If the law of diffuseness can be predicted—even approximately—by theory, progress can be made by the method of "false position."

To find this law itself from the residual discordances of the observations would probably be difficult.

3. The only nonuniform distribution for which tabulated functions exist is that corresponding to darkening at the limb according to the cosine law. This still gives a far sharper boundary than is to be expected in the actual object, but it is worth trying. Only one modification need be made in the preceding analysis. When W is smaller than O and behind it, α_0'' is now to be taken as the fraction of the light of the limb-darkened disk representing W which is cut off by O. But, when W is in front, it must be supposed to exert an absorption which diminishes the surface brightness of the part of O seen through it by 100 per cent at its center, but elsewhere by smaller amounts, following the cosine law. If W is completely projected upon O, it will obscure the fraction k'^2 of its area but will cut off only $\frac{2}{3}k'^2$ of its light. If α_0' represents the fraction of this which is cut off at any partial mid-eclipse, the loss of light will be $1 - \lambda_1 = \frac{2}{3}k'^2\alpha_0'$. Equation (1) then becomes

$$k'^2\alpha_0' L_1 = \tfrac{3}{2}(1 - \lambda_1); \qquad \alpha_0'' L_2 = 1 - \lambda_2 .$$

In *both* cases the relation between k_1, α_0, and p is that which holds good for occultation, when the smaller body is behind the larger.

4. In the foregoing analysis, only the function $p(k, \alpha)$ is required. Extensive tables of this function for uniform disks, computed by J. E. Merrill, are being prepared for publication at this observatory, and also tables of $\chi(k, \alpha_0, n)$ for various values of n from 0.0 to 0.95. When these are at hand, the computation of the light-curve may be much abbreviated by using the equation

$$\sin^2 \theta(n) = \chi(k, \alpha_0, n) \sin^2 \theta(\tfrac{1}{2}). \qquad (5)$$

5. The discussion which follows is based on the photoelectric observations of Kron and Gordon.[1] These were rectified[2] by subtracting from them corrections corresponding to Kopal's solution[3] for the light outside eclipse.

$$l = 0.9995 - 0.0104 \cos \theta - 0.0109 \cos 2\theta ,$$

[1] *Ap. J.*, **97**, 311, 1943.

[2] The equations for elliptical components should, in general, be used with a rectified curve. But in this system it is doubtful to what degree, if any, the ordinary concepts of ellipticity and reflection may be applied to the diffuse envelope of W, which is probably composed of rapidly moving expelled matter. The "rectification" may be regarded as the removal of a small empirical term, probably leading to improved values of the depths of the minima.

[3] *Ap. J.*, **100**, 204, 1944.

converted into intensities, as illustrated in Figure 1. From freehand curves, drawn to represent these, the depths of minima were adopted as

$$1 - \lambda_1 = 0.222 , \qquad 1 - \lambda_2 = 0.128$$

(with the middle of principal minima 0.005 days and of secondary 0.003 days earlier than Kron's values). These curves give $\sin^2 \theta''(\frac{1}{2}) = 0.0296$ and $\sin^2 \theta'(\frac{1}{2}) = 0.0687$, with the ratio 0.432.

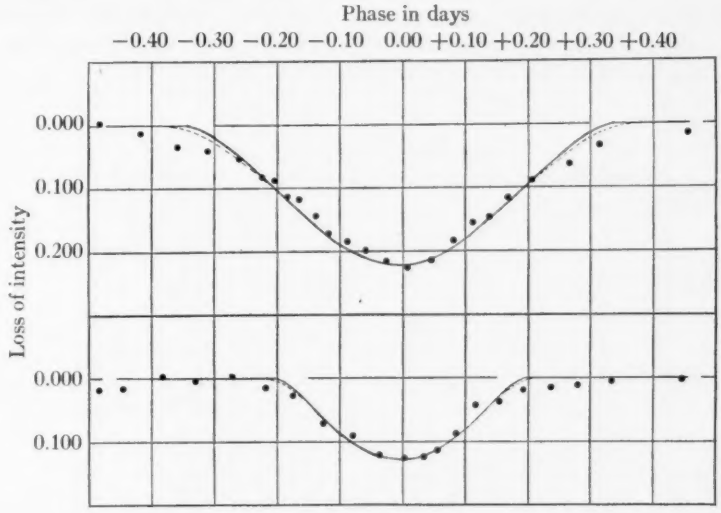

FIG. 1.—Rectified minima of V 444 Cygni

The shallowness of the eclipse indicates that L_1/L_2 can hardly be obtained, if at all, from purely photometric data. Fortunately, Beals[4] has made a careful spectrophotometric study and has concluded that $L_1/L_2 = 5$. Adopting $L_1 = 0.833$ and $L_2 = 0.167$, equation (1) gives $a_0'' = 0.768$ and $k'^2 a_0' = 0.267$. The principal steps of the solution are shown in Table 1. First come corresponding values of k', a_0', and $k'p(k', a_0')$; then independently chosen values of k'', etc. The second half gives the values of k' and a_0' which, for these values of k'', satisfy equation (3), and finally the data leading to $\sin^2 \theta''/\sin^2 \theta'$.

TABLE 1

SOLUTION FOR $L_1 = 5L_2$

k'	+0.750	+0.700	+0.650	k''	+0.300	+0.250	+0.200
a_0'	+ .474	+ .545	+ .632	k'	+ .696	+ .713	+ .732
$k'p(k', a_0')$	−0.069	−0.138	−0.211	a_0'	+0.550	+0.525	+0.499
k''	+0.300	+0.250	+0.200	$\text{Sin}^2 \theta''(\frac{1}{2})/r_1^2 \text{ cosec}^2 i$	+0.349	+0.295	+0.238
a_0''	+ .768	+ .768	+ .768	$\text{Sin}^2 \theta'(\frac{1}{2})/r_1^2 \text{ cosec}^2 i$	+ .661	+ .669	+ .678
$k''p\ (k'', a_0'')$	−0.143	−0.118	−0.093	$\text{Sin}^2 \theta''(\frac{1}{2})/\sin^2 \theta'(\frac{1}{2})$	+0.528	+0.442	+0.352

To the observed value $\sin^2 \theta''(\frac{1}{2})/\sin^2 \theta'(\frac{1}{2}) = 0.432$ corresponds $k'' = 0.245$. A change of 0.01 in the former corresponds to 0.012 in the latter, so that the determination is sharp. The elements for this value of k'' were found by interpolation. The light-curves computed from them are decidedly too narrow to fit the outer observations, and a much better fit

[4] The writer has been privileged to see Dr. Beals's results in manuscript.

can be obtained by increasing the freehand values of $\sin^2\theta'(\frac{1}{2})$ and $\sin^2\theta'(\frac{1}{2})$ by 9 per cent—which does not affect Table 1, since their ratio is unchanged. With the resulting values, $\sin^2\theta'(\frac{1}{2}) = 0.0748$, and $\sin^2\theta''(\frac{1}{2}) = 0.0322$, the elements given in Table 2 for $L_1/L_2 = 5$ and the light-curves shown as solid lines in Figure 1 were obtained. The representation is satisfactory except for the wings, where there are considerable deviations of the anticipated type.

6. It is of interest to know to what extent the deduced elements depend upon the adopted value of L_1/L_2. Calculations have therefore been made for the values 2, 3, and 6.81 of L_1/L_2 (the last corresponding to a grazing total eclipse of W). The resulting elements are given in Table 2, and also those derived on the assumption of a distribution of light corresponding to cosine-law darkening (§ 3) with $L_1 = 5L_2$.

TABLE 2

ELEMENTS OF THE SYSTEM ON VARIOUS HYPOTHESES

	Uniform Disks				Darkened
L_1/L_2	2.0	3.0	5.0	6.81	5.0
k'	0.954	0.829	0.715	0.666	0.886
a_0'	0.366	0.431	0.522	0.573	0.510
k''	0.469	0.364	0.245	0.155	0.302
a_0''	0.384	0.512	0.768	1.000	0.768
i	72°50′	72°59′	73°32′	73°56′	74°03′
$\cos i$	0.298	0.292	0.282	0.276	0.274
r_1	0.283	0.302	0.318	0.326	0.314
r_2'	0.270	0.250	0.228	0.217	0.278
r_2''	0.133	0.110	0.078	0.050	0.094
J_2''/J_1	2.26	2.50	3.33	6.11	2.19
J_2'/J_1'	0.55	0.49	0.39	0.33	0.25
$m_1/\odot$	28.6	28.3	28.1	28.0	28.0
$m_2/\odot$	11.2	11.1	11.0	11.0	11.0
$r_1/\odot$	10.6	11.3	11.9	12.2	11.7
$r_2''/\odot$	5.0	4.1	3.0	1.9	3.5
$\rho_1/\rho\odot$	0.024	0.020	0.017	0.016	0.018
$\rho_2''/\rho\odot$	0.09	0.16	0.45	1.28	0.24

Most of the elements of the system are remarkably stable with respect to the uncertainty of L_1/L_2, which is probably much less than the tabular range. The five values of i have a range of $1\frac{1}{4}°$; and those of r_1, the radius of the O star, range only 14 per cent on each side of the mean.

The effective radius r_2'' of the Wolf-Rayet star, regarded as a bright body, diminishes steadily with its assumed brightness, while the ratio J_2''/J_1 of its average apparent surface brightness to that of the O star changes little (except for the extreme case of grazing eclipse). It appears to be well established that the apparent surface brightness of the central core of this object is at least double that of the O star, although it shines through about half the thickness of the envelope which seriously obscures the latter when in front of it.

The "uniform" and "darkened" solutions for $L_1 = 5L_2$ are almost identical except that the effective radius of W is increased by 21 per cent for emission and 22 per cent for absorption. The calculated surface brightness of the center of the luminous disk differs by only 1 per cent on the two hypotheses. It is probable that the outer limits of the actual diffuse distributions are much more extensive.

The masses and radii of the components follow from Wilson's data.[5] The results for the O star appear to be well established. With Kuiper's effective temperature[6] (60,000° for O6) the bolometric absolute magnitude should be −8.2 and the photometric −3.3. The observed visual magnitude corresponds to 8.2 for this component, making the distance 1900 parsecs if there is no space absorption. These values are rough, mainly because of the uncertainty of the spectral class and temperature; but they suffice to show that it is among the brightest stars for which a good determination of mass is available. Its density appears to be normal.

The densities computed for the W star are formal. It appears probable that the radius of the actual core is smaller than r_2'', in which case its density is considerable. There is probably very little mass between the radii r_2'' and r_2'.

TABLE 3

VALUES OF χ (k, a_0, n)

n	L_1/L_2				
	2.0	3.0	5.0	6.81	5.0*D*
	Primary Minimum				
0.0	3.208	3.212	3.212	3.206	3.95
0.2	1.927	1.936	1.936	1.934	2.13
0.4	1.268	1.269	1.269	1.269	1.31
0.6	0.759	0.759	0.759	0.760	0.75
0.8	0.344	0.345	0.345	0.346	0.36
0.9	0.165	0.165	0.165	0.165	0.16
	Secondary Minimum				
0.0	2.893	2.835	2.658	2.231	3.04
0.2	1.836	1.816	1.753	1.575	1.80
0.4	1.247	1.243	1.228	1.179	1.23
0.6	0.773	0.775	0.787	0.827	0.79
0.8	0.363	0.368	0.386	0.480	0.40
0.9	0.177	0.180	0.193	0.289	0.20

The tabular values of J_2'/J_1 are also formal, except that they represent the ratio of the outward flux of light through the surface of the "obscuring" sphere surrounding W to that at the surface of O. The lowest value 0.25 corresponds, according to Kuiper's data, to about the effective temperature of a star of class B0. The whole of this envelope must therefore be exceedingly hot, and not merely free from dust and solid or liquid particles of any sort, but highly ionized.

7. Table 3 gives values of enough of the χ-functions for the various computed eclipses to illustrate the course of the light-curve.

For uniform disks the entire course of the light-curve at principal minimum is identical for all the solutions, within the utmost accuracy now to be hoped for. Slight but perceptible differences are present for the secondary, and large ones for the artificial case of grazing eclipse, where the uniform-disk approximation should break down.

All these data were derived very rapidly from Merrill's tables. More work had to be

[5] *Ap. J.*, **91**, 379, 1940.

[6] *Ap. J.*, **88**, 429, 1938.

put on the darkened case, as no extensive χ-tables were available and the function had to be computed from first principles. The concise tables of 1912 were used, since high precision is not essential in the present illustrative case. For the same value of L_1/L_2 the differences in the χ-functions are very small except at the beginning and end of eclipse, where the computed duration of the primary minimum is 11 per cent, and of the secondary minimum 7 per cent, greater for the darkened case. This is a good illustration of the way in which the adjustment of light-curves to fit the observations tends to conceal differences in the model on which they are based. Although the calculated values of r'_2 and r''_2 are more than 20 per cent greater, the small corresponding changes in r_1 and cos i reduce the effect on the duration of eclipse to about half this. The "darkened" light-curves are shown by the dotted lines in Figure 1. The deviation from the uniform curves is perceptible only in the wings. Much greater diffuseness in the distribution both of emitting and obscuring intensity is indicated by the observations.

NOTES

NOTE ON THE LATITUDE VARIATION OF THE SUNSPOT BELTS

During each sunspot cycle the belts in which spots appear, in both northern and southern hemispheres, shift continuously toward the sun's equator according to what is known as Spoerer's law. Again, it is known that the speed of solar rotation depends on the heliographic latitude. The purpose of the present note is to show that possibly a relation exists between these two phenomena.

For the form of Spoerer's law to be used we can take Waldmeier's diagram,[1] in which the average heliographic latitudes of the sunspots are plotted against the time reckoned from the epoch of the maximum. Let us consider, in Waldmeier's diagram, the curve representing the latitude variation for a cycle of which the maximum is of medium height.[2] From this curve we can easily determine the time Δt during which the average heliographic latitude of the spots decreases by 1°. The unit of time is one synodic rotation period (27.27 days) as in Waldmeier's diagram. These values of Δt are given in the second horizontal row of Table 1 for different values of heliographic latitude φ from 26° to 10°. It may be noticed that intervals smaller than half a rotation period cannot be read from Waldmeier's diagram.

TABLE 1

φ	26°	24°	22°	20°	18°	16°	14°	12°	10°
Δt	3.5	4.0	4.0	4.5	5.0	5.5	6.5	7.5	9.0
sin 2φ	0.79	0.74	0.69	0.64	0.59	0.53	0.47	0.41	0.34
Δt sin 2φ	2.77	2.96	2.76	2.88	2.95	2.92	3.06	3.08	3.06

Observations of long-lived sunspots made in Greenwich during the years 1878–1933 led to the result[3] that the dependence of the sun's sidereal angular daily motion ξ on heliographic latitude φ can be represented by a formula of the form $\xi = a - b \sin^2 \varphi$, where a and b are positive constants. Hence the variation of ξ per one degree of latitude is proportional to sin 2φ. Values of sin 2φ are given in the third horizontal row of the table, and its fourth row contains the products Δt sin 2φ. As the table shows, this product is found to be nearly constant for all sunspot latitudes.

Since Δt is the reciprocal value of the variation of the mean latitude of sunspots per unit of time and sin 2φ, as mentioned above, is proportional to the variation of the angular motion with latitude, the approximate constancy of the product Δt sin 2φ means that the speed of the shifting of the sunspot belts toward the equator is nearly proportional to the gradient of the rotational velocity. The approximately constant value for Δt sin 2φ may be merely accidental, but it is also possible that there is a real significance to the relationship between the drift of the sunspot zones and the equatorial acceleration of rotation, the cause of which is not known. Thus the variation of the rotational velocity may possibly exercise some influence upon the drift of the sunspot belts toward the sun's equator.

[1] M. Waldmeier, *Ergebnisse und Probleme der Sonnenforschung*, p. 127, Leipzig: Akademische Verlagsgesellschaft, 1941.

[2] The other curves of the diagram yield similar results.

[3] H. W. Newton, *M.N.*, 95, 60, 1935.

Professor Royds was kind enough to call my attention to the fact that from the constancy of $\Delta t \sin 2\varphi$ a simple mathematical expression for Spoerer's law can be derived, provided that Δt is proportional to the differential quotient, $dt/d\varphi$. For we have in this case

$$\frac{dt}{d\varphi} \sin 2\varphi = \text{constant} ;$$

hence, by integration,

$$\log \tan \varphi = -ct - \tfrac{1}{2} \log 3 ,$$

where φ denotes the average latitude of the sunspot zone, t the time reckoned from the moment when $\varphi = 30°$, and c a positive constant. If $\Delta t \sin 2\varphi$ is put equal to 3 and if logarithms to base 10 are used, the value of c is 0.005, the unit of t being one synodic rotation period.

W. GLEISSBERG

ISTANBUL UNIVERSITY OBSERVATORY
March 1944